E.O. Paton Electric Welding Institute of the National Academy of Science of Ukraine
International Association “Welding”

The Paton Welding Journal

03
2024

International Scientific-Technical and Production Journal ◊ Founded in January 2000 (12 Issues Per Year)

Address of Editorial Board
E.O. Paton Electric Welding Institute, 11 Kazymyr Malevych Str., 03150, Kyiv, Ukraine
Tel./Fax: (38044) 205 23 90, E-mail: journal@paton.kiev.ua, patonpublishinghouse@gmail.com
https://patonpublishinghouse.com/eng/journals/tpwj

State Registration Certificate 24933-14873 ПР from 13.08.2021
ISSN 0957-798X, DOI: http://dx.doi.org/10.37434/tpwj

Subscriptions, 12 issues per year:
$384 — annual subscription for the printed (hard copy) version, air postage and packaging included;
$312 — annual subscription for the electronic version (sending issues in pdf format or providing access to IP addresses).

Representative Office of “The Paton Welding Journal” in China:
China-Ukraine Institute of Welding, Guangdong Academy of Sciences
Address: Room 210, No. 363 Changxing Road, Tianhe, Guangzhou, 510650, China.
Zhang Yupeng, Tel: +86-20-61086791, E-mail: patonjournal@gwi.gd.cn

The content of the Journal includes articles received from authors from around the world in the field of welding, cutting, cladding, soldering, brazing, coating, 3D additive technologies, electrometallurgy, material science, NDT and selectively includes translations into English of articles from the following journals, published in Ukrainian:
- Automatic Welding (https://patonpublishinghouse.com/eng/journals/as);
- Electrometallurgy Today (https://patonpublishinghouse.com/eng/journals/sem);
- Technical Diagnostics & Nondestructive Testing (https://patonpublishinghouse.com/eng/journals/tdnk).

CONTENTS

ORIGINAL ARTICLES

INFORMATION

*Translated Article(s) from “Automatic Welding”, No. 1, 2024.

**Translated Article(s) from “Electrometallurgy Today”, No. 1, 2024.

***Translated Article(s) from “Technical Diagnostics & Nondestructive Testing”, No. 1, 2024.

DOI: https://doi.org/10.37434/tpwj2024.03.01

INFLUENCE OF ARC WELDING TECHNOLOGY ON RESISTANCE OF WELDED JOINTS OF 06G2BDP STEEL TO COLD AND HOT CRACKING, FATIGUE AND BRITTLE FRACTURE

O.A. Haivoronskyi[1], V.D. Poznyakov[1], S.L. Zhdanov[1], A.M. Gerasymenko[1], V.D. Ryabokon[1], A.O. Maksymenko[1], Jianxin Wang[2]

[1]E.O. Paton Electric Welding Institute of the NASU
11 Kazymyr Malevych Str., 03150, Kyiv, Ukraine
[2]Jiangsu University of Science and Technology, No. 666, Changhui Road, Dantu District, Zhenjiang, Jiangsu, China

ABSTRACT

The paper studies the influence of arc welding technological processes on the resistance of welded joints of sparcely-alloyed weathering 06G2BDP steel to cold and hot cracking and brittle and fatigue fracture. With the help of the Implant method and using the technological Tekken sample, the conditions for cold cracking were evaluated and the methods of their elimination were recommended. It is shown that with the use of mechanized welding in shielding gases, solid-section and flux-cored wires provide high technological strength of welded joints in terms of hot cracking in a wide range of welding modes. On the other hand, when using coated electrodes, this range is narrowed, and at $V_{def} \geq 20$ mm/min, joints are prone to the formation of this defect. The results of studies on the evaluation of welded joint resistance to brittle fracture indicate high values of the stress intensity factor K_Q for both the weld and HAZ metal. The endurance limit of T-joints when tested by cyclic loading was determined, which is $[\sigma]_{-1} = 35$ MPa.

KEYWORDS: weathering steel, welded joints, cold cracks, hot cracks, brittle fracture, cyclic loading, fatigue fracture

INTRODUCTION

Publications of recent years indicate an increase in the use of weathering sparcely-alloyed steels in metal structures of bridges and other building structures [1–3]. Such trends are characteristic of developed countries, such as the USA, Japan, Italy and Great Britain [4–7]. In view of the interest of domestic bridge builders in the use of weathering rolled steel for span structures of bridges in Ukraine, sparcely-alloyed weathering 06G2BDP steel with an increased phosphorus content of up to 0.05 % is proposed [3]. The conducted studies of the impact of thermal welding cycles on the change in the structure and mechanical properties of the HAZ metal of welded joints of the mentioned steel made it possible to establish a range of optimal cooling rates, at which static strength and impact toughness grow due to the formation of a bainitic-martensitic structure in this area of a joint [3, 8]. In [9], based on the carried out studies of the influence of mechanized arc welding in shielding gases and automatic submerged arc welding methods on the mechanical properties and structure of welded joints of 06G2BDP steel of C390 and C500 strength classes, welding consumables are proposed that provide the required set of mechanical properties of the weld metal at the level of the base metal of the abovementioned strength classes. At the same time, it is known that an increased content of phosphorus in steel can deteriorate its weldability.

The main difficulties in welding low-carbon steels are related to the need in preventing the probability of cold cracking in the HAZ and weld metal, as well as structures that sharply reduce the resistance of welded joints to brittle and fatigue fracture. Hardening structures in the HAZ and weld metal, hydrogen in these areas of a welded joint and stresses of the first kind caused by the welding process and the rigidity of joint fixation have a decisive impact on cold cracking [10–14].

The most common defects in welded joints, in addition to cold cracks, include intercrystalline fracture — hot cracking. Hot cracks are one of the types of high-temperature fracture. They can arise with an unfavorable combination of factors associated with a deterioration in the deformation capacity of the metal due to the appearance of low-melting eutectics, defects in the crystalline structure, precipitations of brittle phases in the structure, as well as under the effect of external and internal stresses. Hot, or crystallization cracks represent micro- and macroscopic discontinuities originating in the crystallization interval of the metal. The temperature at which they are formed depends on the chemical composition of the weld metal. In welding of carbon steels, hot cracks are

formed, as a rule, in the temperature range from 1200 to 1350 °C. Hot cracks are an unacceptable defect of a welded joint, which can be the cause of fracture of structures during manufacture or operation.

The ability of weld metal to perceive elastic-plastic deformations at high temperatures in the welding process without hot cracks determines its technological strength. The high probability of defects in welded joints of metal structures made it necessary to assess the probability of brittle fracturing of welded structures depending on their load conditions, location of a defect, its shape and size in order to ensure the reliability of their operation. It became possible to solve this problem due to the use of criteria and methods of fracture mechanics. They are based on tests of specimens with artificial defects, the sizes of which are stable during manufacture and are subjected to analytical interpretation, in contrast to natural technological defects, the stable sizes of which are very difficult to predict.

Therefore, the aim of the work was to study the influence of welding technological processes on the resistance of welded joints of 06G2BDP steel to delayed, intercrystalline, brittle and fatigue fracture. To achieve the set aim, the following research tasks were solved in the work based on the use of specialized research methods:

- the influence of the technological parameters of arc welding (preheating temperature, welding input energy, etc.) and the content of diffusible hydrogen in the deposited metal on the resistance of welded joints of 06G2BDP steel to cold cracking (delayed fracture) was determined;
- the resistance of welded joints of the studied steel to hot cracking (intercrystalline fracture) was evaluated;

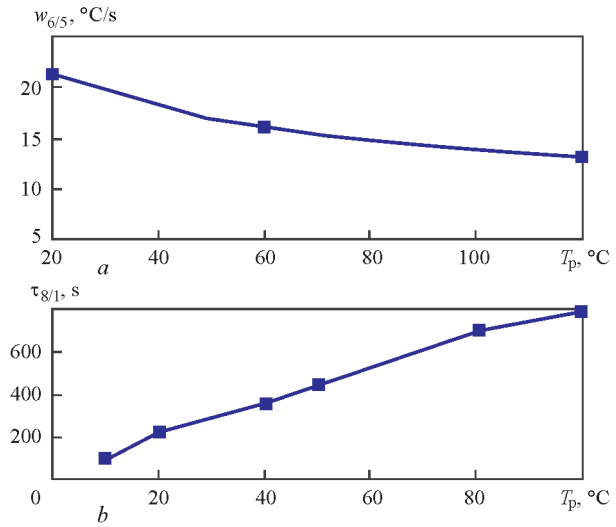

Figure 1. Influence of preheating temperature on cooling rate of specimens in the temperature range of 600–500 °C (*a*) and their period of stay in the temperature range of 800–100 °C (*b*)

- the influence of arc welding parameters on the resistance of welded joints to brittle and fatigue fracture under the cyclic load was studied.

RESEARCH PROCEDURE

Studies of the tendency of the HAZ metal of welded joints of 06G2BDP steel to delayed fracture depending on the content of diffusible hydrogen in the weld metal and the value of critical stresses were carried out using the Implant method [10]. Cylindrical specimens-inserts manufactured of 13 mm thick 06G2BDP steel with the following chemical composition in %: 0.07 C; 1.36 Mn; 0.08 Si; 0.3 Cr; 0.03 Nb; 0.47 Cu; 0.011 S; 0.053 P were subjected to tests. The same steel was used in manufacturing technological plates of 300×250 mm, into which specimens-inserts were inserted.

Manual arc welding was performed with ANP-10 electrodes of 4.0 mm diameter, which provided the indices of yield strength of the weld metal approximately at the level of this steel and were 539–550 MPa. The following mode was used for welding: I_w = 160–180 A, U_a = 26–27 V, V_w = 7.5 m/h. The cooling rate of the HAZ metal was regulated due to preheating. At the same time, the initial temperature of the plates varied from 20 to 90 °C, and the cooling rate of welded joints in the temperature interval of 600–500 °C ($w_{6/5}$) varied in the range from 21 to 14 °C/s. Dependencies characterizing the effect of the preheating temperature on the cooling rate of the specimens and the period of their stay in the temperature range of 800–100 °C ($\tau_{8/1}$) are shown in Figure 1 [11]. The content of diffusible hydrogen in the deposited metal, which was determined by the method of pencil samples using a mixture of glycerin and distilled water in a ratio of 1:4 as a blocking substance, was changed due to electrodes with different coating humidity. For this purpose, the electrodes were moistened or calcinated at different temperatures.

Resistance to cold cracking of welded joints was evaluated using the well-known Tekken technological sample [12].

The presence of cold cracks in it was detected within 24 h after welding by an external inspection of the weld surface and on the macrosections, if they occurred in depth without exit to the surface of a joint. The critical cooling rate of welded joints or the concentration of diffusible hydrogen in the deposited metal was used as a test criterion, at which the total length of cracks in the root, on the surface, and in the weld or HAZ section did not exceed 50 %.

Manual arc welding of Tekken technological samples was performed with coated ANP-10 electrodes of 4.0 mm diameter in the same mode as in weld-

ing by the Implant method. Mechanized welding in shielding gases was performed with the solid-section NiMo1-IG wire and the flux-cored Filarc PZ 6114S wire of 1.2 mm diameter. Welding with the flux-cored wire was performed in CO_2, and with the solid-section wire — in shielding gases 82 % Ar + 18 % CO_2. The modes of mechanized welding were the following: I_w = 180–200 A, U_a = 26–28 V, V_w = 14–16 m/h. Both manual arc and mechanized welding were performed without preheating.

The succeptibility of the weld metal to hot cracking was evaluated by the method of tests during static bending of welded joints in the process of their welding. At the same time, the critical deformation rate V_{def}, which leads to hot cracking, was determined. The welding modes are indicated above, only the welding speed was a variable. In manual arc welding, it was changed in the range of 9.5–12 m/h and in mechanized welding — in the range of 15–20 m/h.

Standard specimens of 120×20×10 mm were used to evaluate the resistance of welded joints to brittle fracture, which were tested in three-point bending according to the methods of fracture mechanics.

For comparison, one series of specimens was manufactured from the base metal and other — from butt joints produced by mechanized welding in a gas mixture of 82 % Ar + 18 % CO_2 with the solid-section NiMo1-IG wire and the flux-cored Filarc PZ 6114S wire in CO_2.

The notch and the tip of a fatigue crack in the specimens were located in the weld or in the HAZ metal. The specimens were loaded in the Friedland installation, while the loading rate was 4–18 mm/min.

In order to evaluate the resistance of welded joints to fatigue fracture [15], the studies were conducted using T-specimens with a one 50 mm height transverse stiffener, which was welded-on to a 13 mm thick plate in two fillet welds with full penetration (Figure 2).

Mechanized welding of T-specimens was performed with the solid-section BOEHLER NiMo1-IG wire of 1.2 mm diameter in a gas mixture of 82 % Ar + 18 % CO_2. After welding, the specimens were subjected to the cyclic bending load (UMP-02 installation) with a frequency of 14 Hz at different symmetrical cycle stresses of 45, 40 and 35 MPa. During the fatigue tests, a number of load cycles was recorded, during which fatigue cracking of a critical size (3 mm) occurred.

RESULTS OF THE WORK AND THEIR DISCUSSION

Using the Implant method, it was shown that the stress, at which delayed fracture of 06G2BDP steel specimens is not observed is 440 MPa. At higher

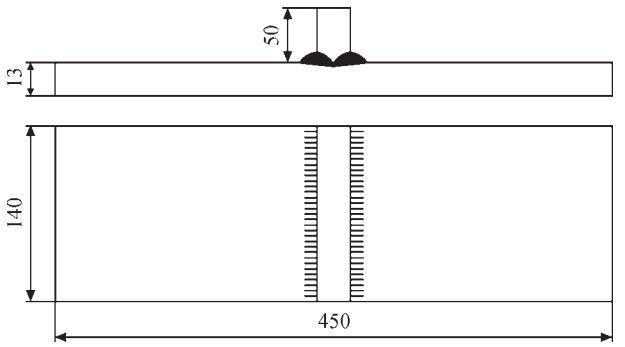

Figure 2. Schematic representation of T-specimen for fatigue tests

values of loads, flowability of the specimens was observed. As was shown by the results of previously conducted metallographic examinations, under the given cooling conditions, in the HAZ metal, a bainitic structure is formed. Based on that, it can be assumed that with a limited amount of diffusible hydrogen in the deposited metal of up to 0.8 ml/100 g, the HAZ metal with this structure does not undergo hydrogen embrittlement and has a high resistance to cold cracking. Using the same method, it was established that the critical stresses, at which delayed fracture does not occur, decrease to 220 MPa when $[H]_{diff}$ is increased to 3.8 ml/100 g, and increase to 340 MPa when its value is reduced to 1.8 ml/100 g (Figure 3).

With an increase in the content of diffusible hydrogen in the deposited metal from 0.8 to 3.8 ml/100 g, the risk of cold cracking in the HAZ metal of welded joints grows. To exclude the probability of cracking in such joints, the level of residual stresses should not exceed 440 and 360 MPa. It is possible to improve the resistance of the HAZ metal of welded joints to delayed fracture thanks to the use of preheating. Thus, it was established that at $[H]_{diff}$ = 3.8 ml/100 g, preheating (T_p) to a temperature of 60 °C makes it possible to increase the level of critical stresses to 380 MPa, and at T_p = 90 °C, to σ = 420 MPa.

Therefore, with a limited content of diffusible hydrogen in the weld, the HAZ metal is not prone to delayed fracture. According to these conditions, welded

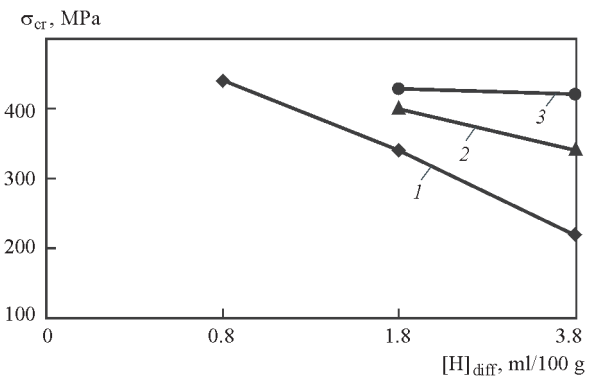

Figure 3. Influence of diffusion hydrogen on resistance to delayed fracture of HAZ metal of 06G2BDP steel: *1* — without heating; *2* — T_p = 60 °C; *3* — T_p = 90 °C

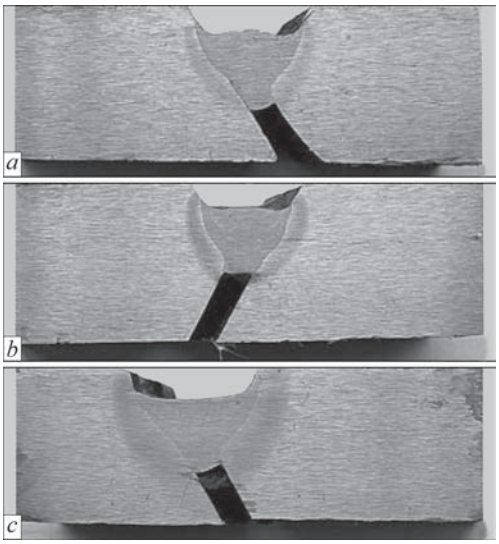

Figure 4. Macrosections of welded joints of Tekken samples of 06G2BDP steel, produced: *a* — with the solid-section NiMo1-IG wire in a gas mixture of 82 % Ar + 18 % CO_2; *b* — with the flux-cored Filarc PZ 6114S wire in CO_2; *c* — with coated ANP-10 electrodes

joints of this steel have sufficient resistance to cold cracking.

The analysis of macrosections cut out from Tekken samples within 24 h after making the reference welds showed that in welding without preheating, all the abovementioned welding methods and welding consumables provide sufficiently high resistance of welded joints to cold cracking, regardless of the alloying weld metal (Figure 4).

It was established that sparcely-alloyed welding consumables, namely ANP-10 electrodes and the flux-cored Filarc PZ 6114S wire, as well as the solid-section NiMo1-IG wire alloyed with nickel and molybdenum under the conditions of manual arc and mechanized welding in shielding gases, provide high resistance of welded joints of 06G2BDP steel to cold cracking.

The obtained data on the resistance of welded joints of 06G2BDP steel to hot cracking show (Table 1) that during mechanized welding in shielding gases with both flux-cored as well as solid-section wire, sufficient technological strength is provided in a wide range of loading rates. On the other hand, under the conditions of using ANP-10 coated electrodes at a deformation rate $V_{def} \leq 20$ mm/min, welded joints of 06G2BDP steel have a margin of technological strength. An increase in the deformation rate to the values higher than 20 mm/min leads to hot cracking, the resistance to which deteriorates.

The conducted studies using the criterion of fracture mechanics established that the highest K_Q indices are typical for the base metal. Their values depend on the test temperature of the specimens and decrease from 103.8 MPa√m (test temperature of 20 °C) to 90.7 and 86.0 MPa√m at (–20 and –40 °C), respectively. Somewhat lower, but still rather high K_Q values were obtained from the results of tests of the specimens, in which the tip of the fatigue crack was located both in the center of the weld metal, as well as in the HAZ metal of welded joints.

Regardless of the welding method, the studied welding consumables and applied welding modes provide fairly close K_Q indices both for the welds as well as for HAZ of welded joints. Thus, for the weld metal, produced by the flux-cored Filarc PZ 6114S wire at test temperatures of –40, –20 °C and 20 °C, the average K_Q values are, respectively: 82.2; 84.9 and 96.2 MPa√m, and for the weld metal produced by the solid-section NiMo1-IG wire, at similar test temperatures, the average K_Q values are 81.6; 84.4 and 94.9 MPa√m, respectively (Figure 5, *a*).

A similar dependence of K_Q indices on the temperature of specimen tests, namely, a decrease in their values as the temperature drops, was also observed in the specimens where the tip of the notch fell on

Table 1. Technological strength of welded joints of 06G2BDP steel

Number	Welding variant	Deformation rate V_{def}, mm/min	Presence of hot cracks
1	Mechanized with the flux-cored Filarc PZ 6114S wire of 1.2 mm diameter in CO_2	10.3	Absent
		15	
		28.6	
2	Mechanized with the solid-section NiMo1-IG wire of 1.2 mm diameter in a mixture of 82 % Ar + 18 % CO_2	28.2	
		37.1	
3	Manual arc with coated ANP-10 electrodes of 4.0 mm diameter	18.3	
		25.5	
		32.7	
		52	

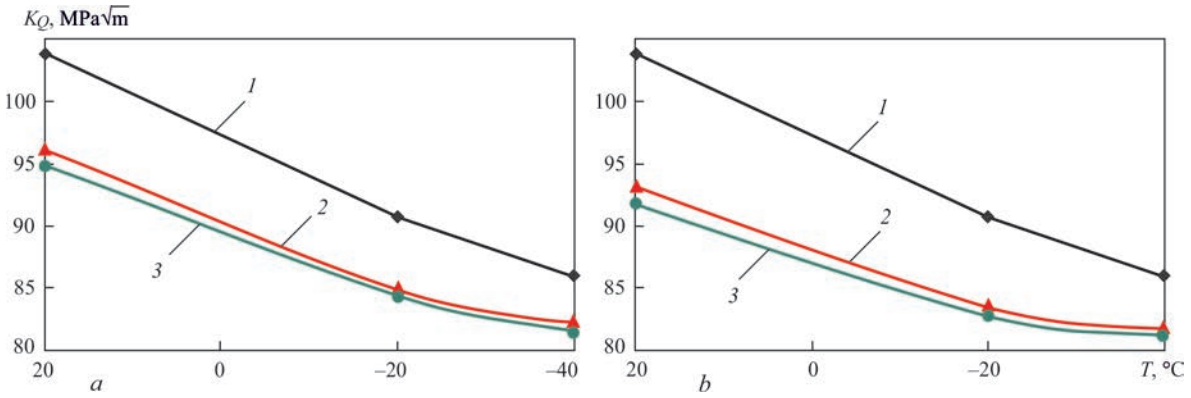

Figure 5. Dependence of values of critical stress intensity factor K_Q on test temperature for the base metal of 06G2VDGI steel (*a*, *b* — *1*) of weld (*a*) and HAZ metal (*b*) of welded joints produced with the solid-section NiMo1-IG wire in a gas mixture of 82 % Ar + 18 % CO_2 (*2*) and Filarc PZ 6114S in CO_2 (*3*)

the HAZ metal of welded joints. In terms of the value, they are somewhat lower compared to K_Q indices of the weld metal, but they are also at a high level and in welding with the flux-cored Filarc PZ 6114S wire they were 81.7; 83.5 and 93.1 MPa√m, and in welding with the solid-section wire — 81.2; 82.8 and 91.7 MPa√m at test temperatures of –40, –20 and 20 °C, respectively (Figure 5, *b*).

The results of fatigue resistance studies showed that at symmetrical cycle stresses of 45 and 40 MPa, cracks of critical length were formed in the T-specimens along the fusion line. Namely: at σ_{-1} = 45 MPa, a fatigue crack formed after N = 999,000 load cycles, at σ_{-1} = 40 MPa, it was observed after N = 1,670,000 load cycles.

Under the test conditions at the symmetric cycle stress of σ_{-1} = 35 MPa, the T-joint of 06G2BDP steel remained non-destructive after $N = 2.1 \cdot 10^6$ load cycles. Thus, it can be assumed that for welded joints of 06G2BDP steel, the endurance limit is at the level of σ_{-1} = 35 MPa.

CONCLUSIONS

Studies of the influence of arc welding technological processes on the resistance of welded joints of corrosion-resistant 06G2BDP steel to cold and hot cracking as well as brittle and fatigue fracture established the following:

- the use of sparcely-alloyed ANP-10 electrodes with a content of diffusible hydrogen in the deposited metal limited to $[H]_{diff}$ = 0.8 ml/100 g in manual arc welding, flux-cored Filarc PZ 6114S wire, as well as solid-section NiMo1-IG wire alloyed with nickel and molybdenum in mechanized welding provide high resistance to cold cracking in the HAZ and weld metal of welded joints. With an increase in the content of diffusible hydrogen to $[H]_{diff}$ to 3.8 ml/100 g, it is necessary to apply preheating to T_p = 90 °C;
- the abovementioned welding consumables during mechanized welding in shielding gases provide sufficient technological strength in a wide range of loading rates. On the other hand, in manual arc welding with the coated ANP-10 electrodes, the margin of technological strength is ensured under the conditions of the deformation rate of $V_{def} \leq 20$ mm/min;
- high resistance of both weld and HAZ metal to brittle fracture is ensured also when using mechanized welding in shielding gases with the flux-cored Filarc PZ 6114S wire and solid-section NiMo1-IG wire. Indices of the stress intensity factor reach the values of K_Q = 96 MPa√m. A reduction in the test temperature to –40 °C leads to a decrease in the stress intensity factor by 15 %, K_Q = 82 MPa√m;
- cyclic load tests show that the endurance limit of welded joints of 06G2BDP steel is symmetrical cycle stresses of σ_{-1} = 35 MPa.

The authors express their gratitude to V.A. Yashchuk, head of the group, and senior research associate Zavdoveev A.V for carrying out tests of welded joints on resistance to brittle and fatigue fracture.

REFERENCES

1. Kovtunenko, V.A., Gerasimenko, A.M., Gotsulyak, A.A. (2006) Selection of steel for critical building welded structures. *The Paton Welding J.,* **11**, 27–31.
2. Poznyakov, V.D., Zhdanov, S.L., Maksimenko, A.A. et al. (2013) Weldability of sparcely-alloyed steels 06GBD, 06G2BD. *The Paton Welding J.,* **4**, 8–14.
3. Zavdoveev, A.V., Poznyakov, V.D., Zhdanov, S.L. et al. (2020) Impact of thermal cycles of welding on formation of the structure and properties of corrosion-resistant steel 06G2BDP. *The Paton Welding J.,* **9**, 14–10. DOI: https://doi.org/10.37434/tpwj2020.09.02
4. Morcillo, M., Díaz, I., Cano, H. et al. (2019) Atmospheric corrosion of weathering steels. Over view for engineers. Pt II: Testing, inspection, maintenance. *Construction and Building Materials*, **222**, 750–765.
5. Miki, C., Homma, K., Tominaga, T. (2002) High strength and high performance steels and their use in bridge structures. *J. of Constructional Steel Research*, 58(**1**), 3–20.
6. Bjorhovde, R. (2004) Development and use of high performance steel. *J. of Constructional Steel Research*, 60(**3–5**), 393–400.

7. Albrecht, P., HallJr, T.T. (2003) Atmospheric corrosion resistance of structural steels. *J. of Materials in Civil Engineering*, 15(**1**), 2–24.
8. Berdnikova, O.M., Poznyakov, V.D., Kostin, V.A. et al. (2021) Structure and fracture mode of HAZ metal corrosion-resistant 06G2BDP steel. *Suchasna Elektrometal.,* **3**, 35–41 [in Ukrainian].
9. Zhdanov, S.L., Poznyakov, V.D., Zavdoveyev, A.V., et al. (2023) Structure and properties of welded joints of 06G2BDP steel. *The Paton Welding J.,* **9**, 11–16. DOI: https://doi.org/10.37434/tpwj2023.09.02
10. Sterenbogen, Yu.A. (1986) Some factors determining the resistance of HAZ metal of martensitic steels to cold cracking. *Avtomatich. Svarka,* **6**, 5–8 [in Russian].
11. Poznyakov, V.D. (2023) *Welding technologies for repair of metal structures*. Kyiv, PWI [in Ukrainian].
12. Hrivnak, I. (1984) *Weldability of steels*. Moscow, Mashinostroenie [in Russian].
13. Lobanov, L.M., Poznyakov, V.D., Mikhoduj, O.L. (2004) Effect of residual stresses on technological strength of welded joints of high-strength steel 14KhGN2MDAFB. *The Paton Welding J.,* **8**, 30–34.
14. Tsaryuk, A.K., Skulsky, V.Yu., Nimko, M.A. et al. (2016) Improvement of the technology of welding high-temperature diaphragms in steam turbine flow section. *The Paton Welding J.* **3**, 28–36. DOI: doi.org/10.15407/tpwj2016.03.05
15. Trufyakov, V.I. (1973) *Fatigue of welded joints*. Kyiv, Naukova Dumka [in Russian].

ORCID

O.A. Haivoronskyi: 0000-0002-5922-5541,
V.D. Poznyakov: 0000-0001-8581-3526,
S.L. Zhdanov: 0000-0003-3570-895X

CONFLICT OF INTEREST

The Authors declare no conflict of interest

CORRESPONDING AUTHOR

O.A. Haivoronskyi
E.O. Paton Electric Welding Institute of the NASU
11 Kazymyr Malevych Str., 03150, Kyiv, Ukraine.
E-mail: paton39@ukr.net

SUGGESTED CITATION

O.A. Haivoronskyi, V.D. Poznyakov, S.L. Zhdanov, A.M. Gerasymenko, V.D. Ryabokon, A.O. Maksymenko, Jianxin Wang (2024) Influence of arc welding technology on resistance of welded joints of 06G2BDP steel to cold and hot cracking, fatigue and brittle fracture. *The Paton Welding J*., **3**, 3–8.

JOURNAL HOME PAGE

https://patonpublishinghouse.com/eng/journals/tpwj

Received: 13.11.2023
Received in revised form: 27.12.2023
Accepted: 19.03.2024

DOI: https://doi.org/10.37434/tpwj2024.03.02

THERMAL CYCLES AND MICROSTRUCTURE OF THE FL ASH BUTT WELDED JOINTS OF 110G13L AND K76F STEEL RAILS THROUGH 08Xh18N10T STEEL INSERT

O.V. Kavunichenko[1], I.V. Ziakhor[1], Yu.A. Shylo[1], A.M. Levchuk[1], Ye.V. Antipin[1], Andrew Fong[2]

[1]E.O. Paton Electric Welding Institute of the NASU
11 Kazymyr Malevych Str., 03150, Kyiv, Ukraine
[2]Yardway Railquip Limited, Unit A5, 29/F., TML Tower, 3 Hoi Shing Road, Tsuen Wan, N.T., Hong Kong

ABSTRACT

The article presents the results of studying the choice of temperature-time and energy-force parameters in flash butt welding (FBW) of the railway crosspiece core (110G13L steel) with rail (K76F steel) through an intermediate chrome-nickel austenitic insert (08Kh18N10T steel). Using an algorithm of numerical solution of the three-dimensional heat conduction equation under the initial and boundary conditions corresponding to the real conditions of welding of the specimens, thermal cycles in FBW of K76F steel with austenitic 08Khl8N10T steel and 110G13L steel with austenitic 08Khl8N10T steel and temperature distribution in welded joints (in the heat-affected zone for both steels) were obtained. Ranges of varying the main technological parameters of the FBW process have been determined, in which during flashing of rails from K76F, 110G13L and 08Khl8N10T steels, their uniform heating across the cross-section and length is provided, sufficient for achieving deformation to the specified extent during upsetting.

KEYWORDS: flash butt welding, railway crosses, rail steel, pulsating flashing

INTRODUCTION

The development of various welding methods made it possible to solve many problems typical for manufacturing products from metal materials. One cannot imagine modern mechanical engineering without welding technologies and other processes accompanied by materials fusion. One of the most difficult problems is related to the formation of permanent combined structures, the elements of which are made of materials with different composition [1].

There are products of critical purpose that determine the safety of railway transport. One of the most typical examples in this field is welded crosses, in the formation of which three types of steels are used [2–4].

The method of producing permanent joints, based on using the technology of flash butt welding of crosses from 110G13L steel with railway rails, largely eliminates the drawbacks characteristic of detachable structures. This technology is used by European and Ukrainian manufacturers of switches. The technological process consists in successive welding of elements from high-manganese and chrome-nickel steels, and then rail steel. Without using intermediate inserts from 08Kh18N10T steel, the quality of joining 110G13L steel and rail steel, which differ sharply in chemical composition and belong to different structural classes, does not meet the operating conditions of switches.

Replacing open-hearth steel with converter steel requires the improvement in the technology for flash butt welding (FBW) of the railway crosspiece core from 110G13L steel with rail ends of K76F steel. In Ukraine, railway rails from oxygen-converter steel — non-heat-strengthened (R260), surface-hardened (R350NT) and surface-hardened, additionally microalloyed with transition metals, in particular vanadium (K76F) and titanium (K76T) are used.

At present, one of the most important parts of the track upper structure used in the railway industry, are crosses. High-manganese austenitic 110G13L steel is successfully used in mechanical engineering. Due to the ability of the operating surface to cold working, 110G13L steel even now is practically irreplaceable for manufacturing products operating under the influence of shock, shock-abrasive loads and high specific static pressures, as for example, tractor caterpillar tracks, rail frogs, switches. Along with its unique properties, the steel has a fairly low cost, so its use has undeniable advantages.

High-manganese 110G13L steel contains 11–13 % Mn and is unique for the reason that it combines high toughness and ductility with a high ability to hardening. Wear resistance depends on the level of intensity of surface hardening and the hardening process during operation [5–8]. Railway rails are made of pearlitic steel, which contains 0.72–0.82% of carbon, up to 1.5 % of manganese and up to 0.5 % of silicon. The physical properties of these two materials create a problem during

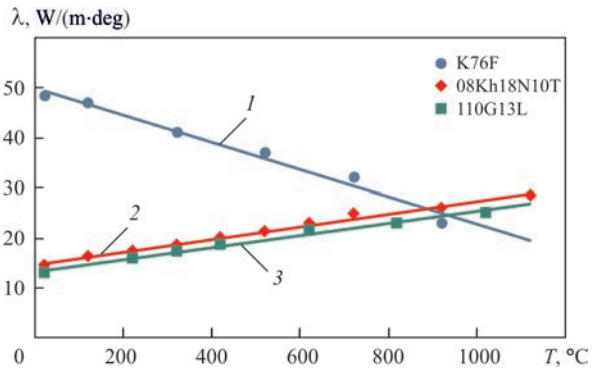

Figure 1. Dependence of coefficient of heat conductivity of welded steels on temperature: *1* — linear (K76F); *2* — linear (08Kh18N10T); *3* — linear (110G13L)

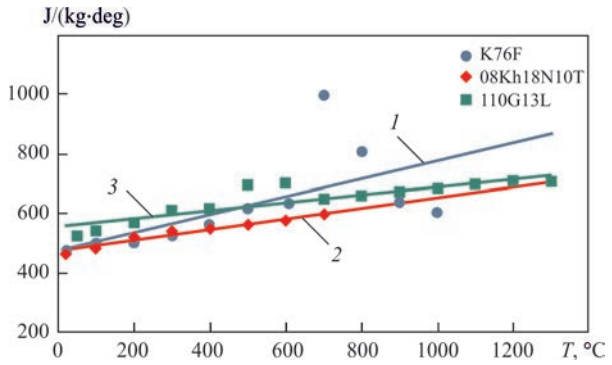

Figure 2. Dependence of specific heat capacity of welded steels on temperature: *1* — linear (K76F); *2* — linear (08Kh18N10T); *3* — linear (110G13L)

Table 1. Mechanical properties of studied steels

Steel grade	σ_t, MPa	σ_y, MPa	δ, %	ψ, %	Hardness, HV_{30}
K76F	485–575	1311–1368	13.5	31	370–380
110G13L	400	800	25	35	205–230
08Kh18N10T	205	510	43	45	140–150

Notes. σ_y — yield strength; σ_t — tensile strength; δ — relative elongation after rupture; ψ — reduction in area after rupture.

welding due to different thermophysical (Figures 1, 2) and mechanical properties (Table 1) [9].

The aim of the work is to establish the influence of temperature-time and energy-force parameters in flash butt welding (FBW) on the formation of structure and phase composition, mechanical characteristics of solid-phase joints of wear-resistant high-manganese 110G13L steel with rail steels through an austenitic chrome-nickel steel insert.

MATERIALS, RESEARCH PROCEDURES AND EQUIPMENT

For research, steels were used, the chemical composition of which is given in Table 2.

Welding was carried out in the K924M machine designed at the PWI. The machine is designed for flash butt welding of railway crosspiece elements from special steel with corresponding parts from rail steel in stationary conditions or for welding rails of 140–195 mm height, with a cross-sectional area from 5000 to 15000 mm^2 with flash removal immediately after welding. The produced welded joints were used to make sections to study their structural features. The strength and ductility of welded butts, elements of railroad crosspieces, were determined by static 3-point bending in the MSP-300 hydraulic press. To evaluate structural features of welded joints, the methods of light (Neophot-32), scanning electron microscopy (JAMP-9500F Auger-microprobe, JEOL with an installed OXFORD EDS INCA Energy 350 spectrometer) were used. The hardness of metal in the HAZ of the welded joint was measured by Vickers in a stationary hardness tester NOVOTEST TS-BRV at a load of P = 300 N.

Prediction of the phase state kinetics of the metal of the joint zone of K76F + 08Kh18N10T and 08Kh18N10T + 110G13L steels in the process of welding and cooling of the welded rail butt was performed on the basis of numerical analysis of temperature cycles under the specific modes of thermal effect, chemical composition of ingot steels and anisotropic austenite decomposition (AAD) diagrams. Such diagrams, taking into account the duration of holding above the corresponding temperatures (austenite grain size number), have now been developed for many steels. With the help of AAD diagrams, it is possible to evaluate the mass fraction Vn of a particular nth structural component (n = A, F, P, B, M, respectively, austenitic, ferritic, pearlitic, bainitic, martensitic) in the areas of both pure as well as mixed phases: austenitic (A), austenitic-ferritic (A + F), pearlitic (A + F + C), where C is carbides adjacent to the zone limited by the temperature of the beginning of martensitic transformation and above by temperatures be-

Table 2. Chemical composition of studied steels

Steel grade	Mass fraction of chemical elements, %							
	C	Cr	Ni	Ti	Mn	Si	S	P
K76F	0.8	–	–	–	1.3	0.35	0.004	0.035
110G13L	1.2	1	1	–	14.5	0.8	0.05	0.12
08Kh18N10T	0.07	17.2	11.8	0.4	1.82	0.6	0.001	0.025

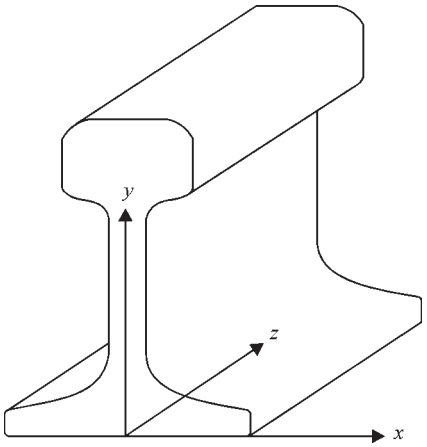

Figure 3. Product to be welded in a rectangular coordinate system

low 600 °C. Accordingly, the points of intersection of the temperature cycle curves $T(t)$, characterized by an average cooling rate in the zone of 800–500 °C determine the temperature of the beginning and end of the corresponding structural transformations of austenite into the n-th phase.

RESEARCH RESULTS AND DISCUSSION

To study the thermal cycles occurring during FBW, a mathematical model of continuous rail heating was developed in cooperation with the Department No. 34 "Mathematical methods for studying physical and chemical processes in welding and special electrometallurgy" of the PWI.

The kinetics of the thermal field in welded rails was described by the equation (1) of heat conductivity with variable thermokinetic characteristics of the material in a three-dimensional coordinate system, shown in Figure 3 [10–12].

$$C\rho(x,y,z,T)\cdot\frac{\partial T(x,y,z)}{\partial t}= \\ =\frac{\partial T(x,y,z)}{\partial x}\cdot\left[\lambda(x,y,z)\cdot\frac{\partial T(x,y,z)}{\partial x}\right]+ \\ +\frac{\partial T(x,y,z)}{\partial y}\cdot\left[\lambda(x,y,z)\cdot\frac{\partial T(x,y,z)}{\partial y}\right]+ \\ +\frac{\partial T(x,y,z)}{\partial z}\cdot\left[\lambda(x,y,z)\cdot\frac{\partial T(x,y,z)}{\partial z}\right]. \quad (1)$$

Taking into account different mechanisms of heat dissipation (convective, infrared radiation), the boundary conditions were described.

$$-\lambda(T)\frac{\partial T(t)}{\partial n}=\alpha(T-T_C)+\varepsilon\cdot\sigma\cdot\left(T^4-T_C^4\right). \quad (2)$$

The heat source in FBW is thermal energy, described by setting boundary conditions in the following form (3), where η is the efficiency coefficient, which takes into account active and reactive losses due to the characteristics of the secondary circuit of the machine; I is the welding current; U is the welding voltage.

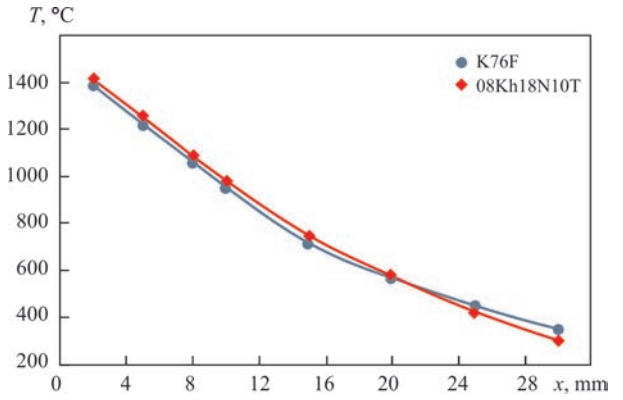

Figure 4. Temperature distribution along the axis of the rails before upsetting at FBW of K76F and 08Kh18N10T steels (calculation)

$$\lambda(T)\frac{\partial T(t)}{\partial n}\bigg|_{z=0}=0{,}5\cdot\eta\cdot U\cdot I. \quad (3)$$

Using a mathematical model of three-dimensional tracing of temperature fields, the temperature distribution over the thickness of the welded joint before upsetting in FBW of K76F with 08Kh18N10T steel was obtained (Figure 4).

To obtain the necessary thermal cycles, the PWI developed a welding technology called pulsating flashing.

Due to the multifactor control of the spark gap between the contacting parts during the flashing process, as well as instantaneous voltage values, intensification of contact heating is ensured, which reduces metal losses during flashing and improves the efficiency coefficient compared to conventional processes of continuous flashing or resistance preheating. The heating period and flashing tolerances are reduced by 1.5 to 2.0 times. High-quality joints are produced with a smaller HAZ width.

The use of pulsating flashing (PF) makes it possible to provide the necessary heating of the rail and austenitic steels, which differ significantly in their thermal properties [13].

Experimental studies of thermal cycles were carried out according to the following scheme. Thermocouples were welded to the rail head at a distance of 5 mm from

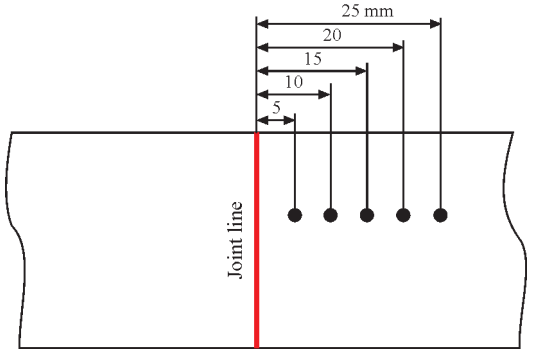

Figure 5. Layout of thermocouples

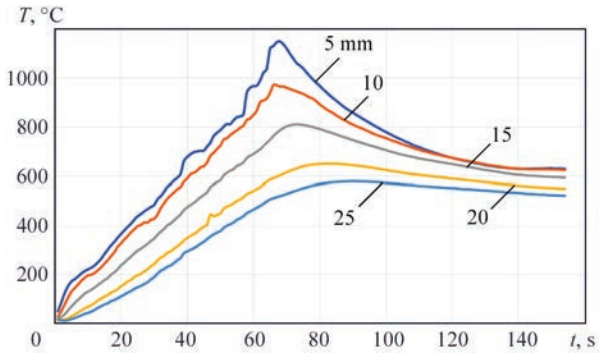

Figure 6. Thermal cycles of FBW at different distance from the joint line of K76F and 08Kh18N10T steels

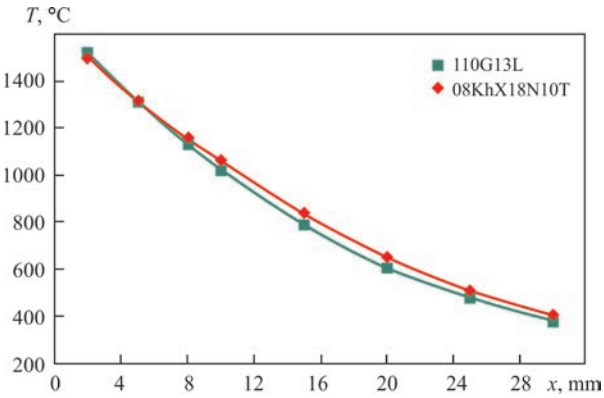

Figure 7. Temperature distribution along the axis of the rails before upsetting at FBW of 08Kh18N10T and 110G13L steels (calculation)

each other (Figure 5). The distance to the first thermocouple was calculated in such a way that after a complete welding cycle, it was 5 mm from the joint line.

The calculated results of thermal cycles coincide with the experimental studies with a small error (Figure 6).

Using a similar procedure, the temperature distribution over the thickness of the welded joint before upsetting in FBW of 08Kh18N10T steel with 110G13L steel was determined by calculation (Figure 7).

In FBW of austenitic (08Kh18N10T + 110G13L) steels, it is necessary to combine more intensive heating with the depth of metal heating. During the experiments, the heating duration at its different intensity, tolerances for flashing and upsetting were varied.

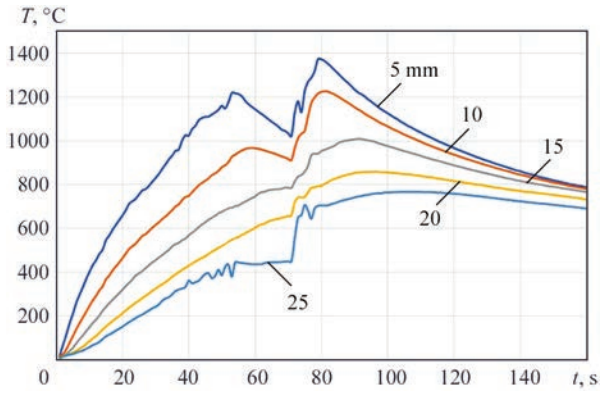

Figure 8. Thermal cycles of FBW at different distance from the joint line of 08Kh18N10T and 110G13L steels

Table 3. Mode for FBW of K76F rail steel with 08Kh18N10T steel

Welding parameters	
Welding tolerance S, mm	30
Voltage U_1, V	280–380
Upsetting, mm	12
End flashing rate V_f, mm/s	1.6–1.8

Table 4. Mode for FBW of 08Kh18N10T with 110G13L steel

Welding parameters	
Welding tolerance S, mm	30
Voltage U_1, V	255–380
Upsetting, mm	13
End flashing rate V_f, mm/s	1.8–2.0

When using the combined heating method (mode), experimental thermal cycles were obtained, shown in Figure 8.

Reducing the voltage at a certain stage of the welding process made it possible to ensure the heating of steels necessary for the thermo-deformation process.

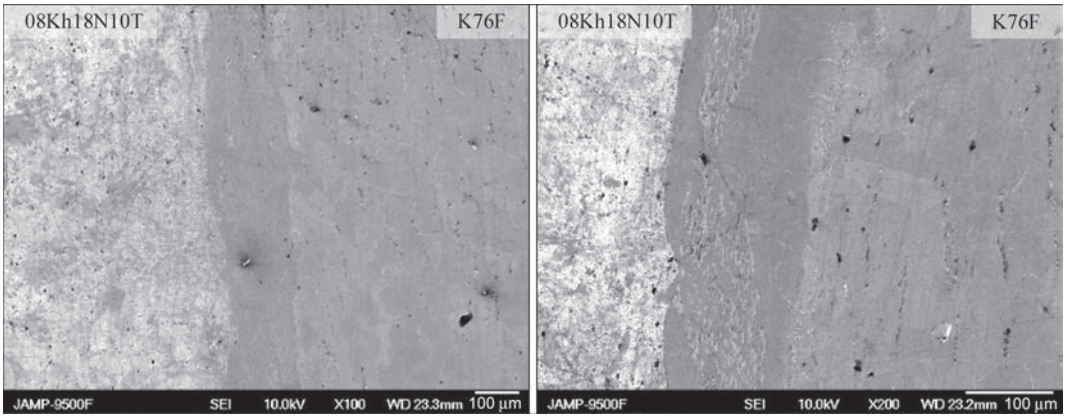

Figure 9. SEM-image of metal microstructure in the transition zone of the joint K76F + 08Kh18N10T steels

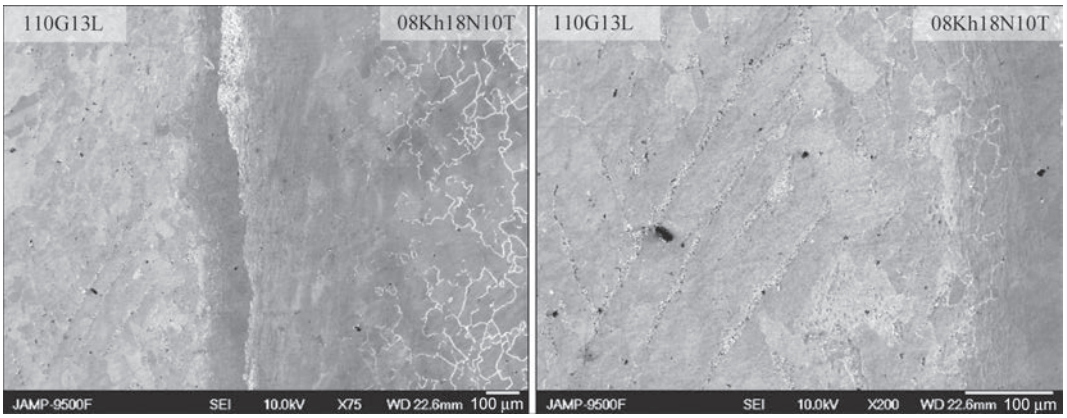

Figure 10. SEM-image of metal microstructure in the transition zone of the joint 110G13L + 08Kh18N10T steels

In the course of the experiments, the duration of heating at different intensities, tolerances for flashing and upsetting values were varied. To ensure the required energy input, a welding mode for K76F rail steel with 08Kh18N10T (Table 3) and 08Kh18N10T with 110G13L steel (Table 4) was selected.

Changing the primary voltage in the range of U_1 = 255–380 V and the displacement velocity V_d = 0.8–2.4 mm/s in the FBW process ensures equalization of temperature gradients in austenitic and pearlitic steels, which allows optimizing the deformation conditions of both steels during the upsetting process and ensuring that the mechanical properties of joints meet regulatory requirements.

The transition zone of the joint K76F + 08Kh18N10T steel (Figure 9) is formed as a result of fusion of subgrain boundaries of the rail steel and heterodiffusion processes. The microstructure of the transition zone is characterized by regions with an acicular structure against a light field. The flashed areas formed in the transition zone correspond to the chemical composition of low-alloy steels. Depending on the cooling rate, the products of the eutectoid austenite transformation in such steels can be pearlite, bainite, or martensite.

The transition zone of the joint 110G13L + 08Kh18N10T steel (Figure 10) has a stable austenitic structure. The joint area with a variable concentration of chemical elements has a width of about 200 µm. At the same time, the transition zone with an almost constant concentration of alloying elements Cr, Mn, and Ni has a width of about 50 µm, which indicates that the welded joint in this zone was formed in a liquid state. The width of diffusion zones in the joint is up to 50 µm in the direction of 08Kh18N10T steel and up to 100 µm in the direction of 110G13L steel (Figure 11).

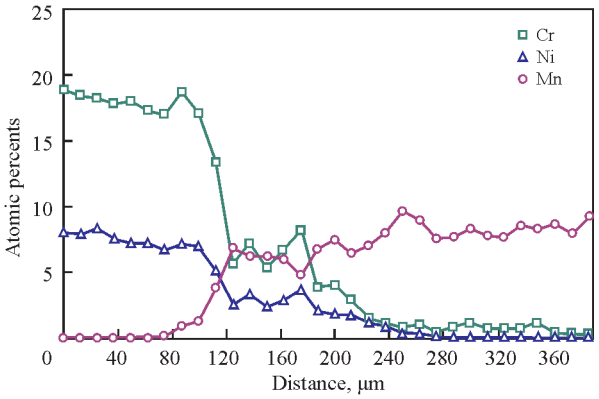

Figure 11. Distribution of chemical elements concentration in the transition zone of the joint 110G13L + 08Kh18N10T steels (at.%)

CONCLUSIONS

1. The influence of temperature-time and energy-force parameters was established and the ranges of changes in the main technological parameters of the FBW process were determined, at which, in the process of flashing rails from K76F, 110G13L and 08Kh18N10T steels, their uniform heating over the cross-section and length is ensured, sufficient to perform deformation at a specified value during upsetting.

2. Using the algorithm for numerical solution of the three-dimensional heat conductivity equation under the initial and boundary conditions corresponding to the actual welding conditions of the specimens, thermal cycles were obtained in FBW of K76F steel with austenitic 08Kh18N10T steel and high-manganese 110G13L with austenitic 08Kh18N10T steel and the temperature distribution in the welded butts (in the heat-affected zone for both steels) was determined.

3. The thermal cycles in FBW of K76F and 110G13L steels with an intermediate insert of 08Kh18N10T steel at different values of the main technological parameters of the welding process were determined, and the influence of the FBW process on structural changes in the zone of joining the 1st and 2nd butts was established.

4. The range of changes in the primary voltage U_1 and the displacement velocity V_d (U_1 = 255–380 V and V_d = 0.8–2.4 mm/s) in the process of flash butt welding, at which the equalization of temperature gradients in austenitic and pearlite steels is provided,

which allows optimizing the deformation conditions of both steels in the process of upsetting and ensuring the compliance of mechanical properties of the joint with regulatory requirements, has been established.

REFERENCES

1. Gotalsky, Yu.N. (1981) *Welding of dissimilar steels*. Kyiv: Tekhnika [in Russian].
2. Kuchuk-Yatsenko, S.I., Kavunichenko, O.V., Ma, Ping et al. (2017) Technology and equipment for flash butt welding of railway frogs with rail ends through austenitic insert. *Railway Eng. China*, **12**, 102–105.
3. Kuchuk-Yatsenko, S.I., Shvets, Yu.V., Kavunichenko, O.V. et al. (2015) Flash butt welding of railway frogs through cast austenitic insert. *The Paton Welding J.*, **8**, 5–7. DOI: https://doi.org/10.15407/tpwj2015.08.01
4. Kavunichenko O.V., Shvets V.I. and Antipin E.V. (2018) Peculiarities of flash-butt welding of rail frogs with rail ends. *The Paton Welding J.*, **4**, 19–24. DOI: https://doi.org/10.15407/tpwj2018.04.04
5. Karaman, I., Sehitoglu, H., Chumlyakov, Y. et al. (2001) Extrinsic stacking faults and twinning in Hadfield manganese steel single crystals. *Scripta Mater.*, **44**, 337–443.
6. Efstathiou, C. (2009) Strengthening Hadfield steel welds by nitrogen alloying. *Materials Sci. and Eng.*, **506**, 174–179.
7. Efstathiou C., Sehitoglu H. (2010) Strain hardening and heterogeneous deformation during twinning in Hadfield steel. *Acta Materialia*, **58**, 1479–1488.
8. Mohyla, P. (2004) Affect of tempering temperatures on mechanical properties of weld joints in low-alloyed creep-resistant steels. *Acta Metallurgica Slovaca*, **10**, 193–200.
9. (2003) *Grades of steels and alloys*: Refer. Book. Ed. by A.S. Zubchenko. Mockow, Mashinostroenie.
10. Olivares, R., Garcia, C., DeArdo, A. et al. (2011) Advanced metallurgical alloy design and thermo mechanical processing for rails sleels for North American heavy use. *Wear*, **271**, 364–373.
11. Sahay, S., Mohapatra, G., Totten, G. (2009) Overview of Pearlitic Rail Steel: accelerated cooling, quenching, microstructure, and mechanical properties. *J. ASTM Int.*, **7**, 1–26.
12. Alves, L., Lagares, M., Filho, R. et al. (2019) Predictive mathematical modeling of the flash-butt welding process to optimize the properties of welds of premium and super premium rails. In: *Proc. of Inter. Heavy Haul STS Conf., 10–14 June, Narvik, Norway, 2019*.
13. Kuchuk-Yatsenko, S.I. et al. (2001) *Method of flash-butt welding*. Pat. US6294752B1. 219.100.

ORCID

O.V. Kavunichenko: 0000-0002-5164-9796,
I.V. Ziakhor: 0000-0001-7780-0688,
Yu.A. Shylo: 0000-0002-6174-5925,
A.M. Levchuk: 0000-0002-0361-7394,
Ye.V. Antipin: 0000-0003-3297-5382,
Andrew Fong: 0009-0000-3996-4403

CONFLICT OF INTEREST

The Authors declare no conflict of interest

CORRESPONDING AUTHOR

O.V. Kavunichenko
E.O. Paton Electric Welding Institute of the NASU
11 Kazymyr Malevych Str., 03150, Kyiv, Ukraine.
E-mail: avkava@gmail.com

SUGGESTED CITATION

O.V. Kavunichenko, I.V. Ziakhor, Yu.A. Shylo, A.M. Levchuk, Ye.V. Antipin, Andrew Fong (2024) Thermal cycles and microstructure of the flash butt welded joints of 110G13L and K76F steel rails through 08Xh18N10T steel insert. *The Paton Welding J.*, **3**, 9–14.

JOURNAL HOME PAGE

https://patonpublishinghouse.com/eng/journals/tpwj

Received: 17.10.2023
Received in revised form: 05.12.2023
Accepted: 04.04.2024

DOI: https://doi.org/10.37434/tpwj2024.03.03

ANALYSIS OF THE PROPERTIES AND FEATURES OF HIGH-STRENGTH DEFORMABLE ALUMINIUM ALLOYS OF Al–Li, Al–Cu–Mn SYSTEMS USED IN THE AEROSPACE INDUSTRY IN MANUFACTURE OF WELDED STRUCTURES (REVIEW)

V.I. Zagornikov

E.O. Paton Electric Welding Institute of the NASU
11 Kazymyr Malevych Str., 03150, Kyiv, Ukraine

ABSTRACT

The paper presents the main directions of development in the field of promising aluminium alloys. New generation alloys with improved chemical composition, technologies of manufacture and heat treatment of semi-finished products are considered. The question of the relationship between the structure of the alloys and their operational properties, the influence of heat treatment modes and alloying on mechanical properties and weldability of aluminium alloys in order to obtain the specified predicted operational properties is highlighted. The results of the use of aluminium alloys in aviation and space technology are described. A review of commercial deformable alloys of Al–Li and Al–Cu–Mn system, and comparative characteristics of weldability of various promising aluminium alloys (1460, V-1469, 1201 and their analogues 2090, 2195, 2219) is conducted.

KEY WORDS: heat treatment, weld alloying, weldability assessment, measures to prevent porosity, promising methods of producing welded joints, electron beam welding (EBW)

INTRODUCTION

The growth rate of commercial aircraft and rocket construction in Ukraine and in the world dictates the pace of introduction of modern and innovative technologies and materials. One of the most important tasks currently facing the aerospace industry is improving the equipment weight efficiency and its strength, which will allow increasing the weight of the orbited payload.

Modern requirements to materials are becoming ever more stringent. However, deformable aluminium alloys remain the basic structural materials for advanced aerospace products due to their low density, set of service properties, good adaptability-to-manufacture, weldability and mastering in the metallurgical production. In addition to a significant weight reduction, these alloys should have higher specific and service properties, which will allow application of more efficient design solutions, such as electron beam, laser, friction stir, and automatic argon-arc welding using new filler materials.

For flying vehicle structures not the absolute, but specific values of strength properties (σ_t/ρ, $\sigma_{0.2}/\rho$) are important. Therefore, owing to their high specific strenght the dispersion-hardening alloys of Al–Li and AL–Cu–Mn system are widely used in the structures of space and aviation technology products, in particular products for cryogenic applications, namely rocket fuel tanks, fuselage skins and load-carrying elements of aircraft design. Alloys not prone to delayed fracture and having a high ductility of base metal at liquid helium and hydrogen temperature are used for operation under the cryogenic conditions [1–3].

Despite all the advantages of the developed alloys, there is the task to improve the crack resistance characteristics at preservation of the high level of strength and corrosion resistance. Their composition, structure, modes of manufacture, in particular, of thermomechanical treatment, are constantly improved in keeping with the growing requirements to the structures. This task is solved through development and introduction of advanced superlight high-strength materials and their joining technologies.

The objective of this work consists in formulation of modern requirements to properties of semi-finished products from deformable aluminium alloys 1460, V-1469, 1201 and their analogs 2090, 2195, 2219, and substantiation of the priority of application of a deformable alloy of 1201(2219) type, when producing sound welded joints, using EBW in the structures of aerospace products.

DISCUSSION OF PROBLEMS IN THE FIELD OF THE TECHNOLOGY OF HEAT TREATMENT AND WELDING OF ALUMINIUM ALLOYS OF Al–Li AND Al–Cu–Mn SYSTEM FOR AEROSPACE PRODUCTS

With development of aerospace engineering, the following requirements are made to selection of the structural material:

● the alloy should have a sufficient level of strength and service life characteristics;

● high adaptability-to-manufacture and energy saving in metallurgical production;

● possibility of various kinds of semi-finished products;

● adaptability-to-manufacture in production of parts and assembly of various structure components, also with welding application;

● the alloy should not contain any highly toxic components (cadmium, lead, mercury, beryllium) — elements which evaporate during welding.

The aluminium alloy properties can be improved both when changing their composition, and a result of application of new technologies of their production and treatment. To ensure optimal mechanical properties, depending on operating conditions (normal — cryogenic temperature) there is a certain mode of aging at heat treatment for each type of semi-finished products. Here, a certain phase composition forms in the metal structure. Precisely regulated deformation after quenching in combination with a certain mode of final aging should ensure the required set of physicomechanical properties.

The considered deformable structural aluminium alloys, mainly, are aluminium alloys with four components: Cu, Mn, Mg, Zn. Li, Sc, Zr and Ag were relatively recently added to them (Table 1).

All the abovementioned components were selected by one feature: they have the highest solubility in solid aluminium, compared to other known elements. It abruptly decreases with temperature lowering, resulting in intermetallic phase precipitation at cooling of alloys with these components from the solid solution, and their dissolution at heating. This phase transformation (the only one in solid aluminium alloys) opened up the possibility of significantly influencing the alloy structure and properties through heat treatment. The alloys have a high level of properties after strengthening heat treatment (quenching and aging), when the alloy matrix is a solid solution strengthened by dispersed particles of the intermetallic phases, precipitating from the solid solution at aging. This applies to alloys of all the systems, i.e. the strengthening mechanisms of all the alloys are the same: solid solution treatment + dispersion hardening. The difference between the considered alloys is determined by the composition, crystalline structure and properties of the dispersed particles of intermetallics, precipitating from an oversaturated solid solution, on which the strengthening effect depends. The main property of these particles is a very high hardness, compared to the matrix. Secondary dispersed precipitates of these intermetallic phases determined the high level of strength characteristics, achieved for aluminium alloys and the level of their applicability for critical structures [4].

As natural aging does not cause any changes, after quenching the semi-finished products are subjected to artificial aging. It eliminated the need to regulate the time interval between quenching and aging [5].

The purpose of aluminium alloy aging usually consists in an additional increase of the quenched alloy strength. To achieve maximal strength of the heat-hardenable alloys, it is necessary to obtain by regulated heating a certain intermediate structure corresponding to initial stages of decomposition of the oversaturated solid solution.

A structure, which combines clusters (Guinier–Preston zones) corresponds to the initial stages of decomposition of the oversaturated solid solution. These clusters have the appearance of platelike precipitates from the solid solution uniformly distributed over the grain as fine acicular inclusions, as well as along grain boundaries in the form of large flakes. At this stage, no processes of coagulation (coarsening) of strengthening phase particles are observed.

Aging of commercial aluminium alloys is conditionally divided into low-temperature (20–140 °C) and high-temperature (140–220 °C) modes. The products of decomposition of the oversaturated solid solution at low-temperature aging usually are coherent dispersed or partially coherent precipitates, homogeneously distributed in the grain volume. In some aluminium alloys (Al–Cu–Mn) preparation to decomposition and initial decomposition stages occur only at heating of the

Table 1. Chemical composition of alloys of Al–Cu–Li and Al–Cu systems (1460, V-1469, 1201 and their analogs 2090, 2195, 2219)

Alloy grade	Weight fraction of elements, %										
	Cu	Li	Zr	V	Ti	Mn	Sc	Mg	Ag	Si	Fe
1460 (USSR)	2.6–3.3	1.9–2.3	0.1	–	0.1	0.05–0.1	0.06–0.1	0.06–0.1	–	–	–
2090 (USA)	2.4–3.0	1.9–2.6	0.1	–	0.15	0.05	–	0.25	–	–	–
V-1469 (Russia)	3.2–4.5	1.0–1.7	0.02–0.26	–	0.05–0.07	0.05–0.08	0.02–0.28	0.01–0.5	0.45	–	–
2195 (USA)	3.7–4.3	0.8–1.2	0.12	–	0.1	0.25	–	0.25–0.8	0.25–0.6	–	–
1201 (USSR)	5.8–6.8	–	0.1–0.25	–	0.02–0.1	0.20–0.40	–	0.02	–	0.20	0.30
2219 (USA)	5.8–6.8	–	0.1–0.25	0.05–0.1	0.02–0.1	0.20–0.40	–	0.02	–	0.20	0.30

quenched alloy up to temperatures, usually in the range of 100–200 °C. The purpose of this heating is thermal activation of the diffusion processes.

This is the stage, which ensures the maximal strength properties (T1), or artificial aging modes with regulated softening, compared to T1 mode – T2 and T3 modes, compared to the aging stage, which provides maximal strengthening (achieving maximal yield limit). States T2 and T3 are usually realized through two-step aging. In aging modes, corresponding to the ascending branch of the strengthening curve, an abrupt lowering of the corrosion cracking resistance is possible. Such a phenomenon is observed, in particular, in alloys of Al–Cu and Al–Cu–Mg systems [6].

Without experiments it is impossible to predict the specific structure, providing maximal strengthening, which a particular alloy should have. The answer depends on the decomposition stages, which can occur in this alloy at the given aging temperature, on the precipitate structure, density of each type of precipitates and other factors.

Two main ways to produce an optimal set of properties required for reliable service of high-strength heat-hardenable aluminium alloys have emerged:

1. Increase of the alloy purity as to the main metal impurities (Fe and Si), i.e. lowering the admissible level of iron and silicon impurities in the alloys. In the majority of aluminium alloys up to 0.5 % Fe and up to 0.5 % Si are allowed to GOST 4784–74. Lowering the admissible content of iron and silicon to 0.1–0.3 % and even better to hundredths of a percent leads to an abrupt reduction of the volume fraction of insoluble intermetallic phases [Al_3Fe, α(Al–Fe–Si), α(Al–Fe–Si–Mn), etc.] and considerable increase of fracture toughness. The alloy other properties (σ_t, $\sigma_{0.2}$, δ and σ_{cr}, exfoliating corrosion) change only slightly. In this connection, higher-purity alloys began to be used recently.

2. Application of aging modes, causing a certain overaging of the metal. Such modes are called “softening” aging modes and for deformable alloys they are designated by numbers T2 and T3 (aging to maximal strength is denoted as T1 and quenching with subsequent natural aging as T); T3 corresponds to stronger overaging than T2. Compared to aging to maximal strength, softening aging, while leading to partial or complete violation of the coherence of strengthening phase precipitates and the matrix, and to their more homogeneous distribution, causes a certain lowering of the strength, but an essential increase of fracture toughness, resistance to stress corrosion and exfoliating corrosion [7].

Heat treatment allows achieving a great diversity of structures also in alloys, having no phase transformations in the solid state, but only in the case, when the initial nonequilibrium state was produced either during casting (during nonequilibrium crystallization), or by deformation. To achieve maximal strength, the following three kinds of heat treatment became widely accepted for aluminium alloys: annealing, quenching and aging, which allow implementing a balanced set of mechanical properties and heat resistance.

The following system of designations of the states of deformable aluminium alloys after strengthening treatment was accepted:

T1 — artificial aging in its pure form. It allows increasing the mechanical strength of the semi-finished products and finished products, particularly, if their machining is planned furtheron. Such a kind of treatment has a negative impact on duraluminium corrosion resistance and mechanical strength, and it is seldom used for it.

T2 — annealing. It allows relieving the casting and thermal stresses in the material, and improves its ductility, and it is used in the case, when the billet will be subjected to cold pressure processing.

T3 — quenching. It is applied for improvement of the alloy strength properties and for ensuring the required corrosion cracking resistance.

T8 — a state, in which the solution heat treatment is followed by cold working, and then by artificial aging. It is applied for products subjected to cold working, straightening or leveling to increase the strength.

T81 — it is applied for products, artificially aged after solution heat treatment, here the strength rises by approximately 1% of cold working deformation.

T87 — applied for products with approximately 7 % cold working deformation to increase the strength after solution heat treatment and further artificial aging.

T62 — it is applied for artificially aged products after solution heat treatment in O or F state. It is also used for products, the mechanical properties of which reach T62 state after heat treatment of products treated to any state.

Not less promising is the route of further improvement of strength, high-temperature strength, corrosion resistance and other service and technological characteristics through application of aluminium alloy doping by metals, which are poorly soluble or practically insoluble in solid aluminium, but which form various intermetallic compounds with aluminium [8].

ADVANTAGES OF 2219 ALLOY

Let us consider 2219 aluminium alloy. The advantages of 2219 alloy are improved mechanical properties of base metal and welded structures at temperatures well below zero (to –253 °C). The alloy has good values

of tensile and yield strength, as well as good fatigue and creep fracture properties (to –315 °C). It can be easily worked by pressure. These properties remain unchanged after heat treatment. In George S.Marshall Center it was proved experimentally that structural 2219 aluminium alloy is sufficiently hardened so that the defects caused by nuclear and space radiation did not significantly affect its mechanical and physical properties, either at room ambient temperature and at elevated temperatures, below the accumulated doses of approximately 10^{22} particles s/cm^2 [9]. The possibility of receiving a dose of this order is extremely small, except for cases of pulsar action in immediate vicinity. The high resistance to elevated temperatures, hard vacuum, high-energy radiation and micrometeorites, which influence the characteristics of 2219 alloy surface through desorption and erosion processes, makes such an alloy highly promising for application as space vehicle skin.

The disadvantages of the abovementioned metal are as follows. Heating above 300 °C leads to strong softening, because of coarsening of the main phase of Al_2Cu strengthening agent. Moreover, the method of manufacturing wrought semi-finished products from ingots requires a complicated technology, which includes high-temperature homogenizing annealing, pressure treatment, heating of the semi-finished products above 500 °C for quenching in water and aging, which significantly increases the cost of the final product.

The wide range of possibilities for joining structural elements made from such an alloy should be noted. The 2219 alloy demonstrates the best weldability among aluminium alloys of 2xxx series, which is related to absence of magnesium and silicon as alloying elements in it. These elements form the ternary and quaternary eutectics with low melting temperatures and thus widen the alloy melting range. It is known that the wide range of melting temperatures, as the presence of phases with a low melting temperature, leads to weld cracking, but 2219 alloy does not have this drawback.

Considering the high value of the linear expansion coefficient and significant shrinkage of the crystallizing metal, alongside its low mechanical properties already at the temperature of 236.85–246.85 °C, the technology of aluminium alloy assembly and welding should envisage minimal welding strains and stresses. The process of welding and postweld heat treatment affects the deformational properties of 2219 alloy sheets [10, 11]. Minimal welding strains and stresses (2–4 times lower than in argon-arc welding) are achieved at single-pass electron beam welding of a large-sized structure, performed with a certain sequence of weld deposition [12]. In those situations, when quenching of the entire large-sized structure is not always admissible, because of the structure overall dimensions and deformations arising at heat treatment, application of narrow electron beam welds is indispensable.

These results show that 2219 is the most readily weldable and the least sensitive to changes in the welding procedures of all the heat-treatable high-strength aluminium alloys. At repeated heat treatment after welding the alloy steadily develops its strength, which is equal to tensile strength of the base metal. T81 and T87 annealing modes are recommended for components which remain in "as-welded" state. For components which are to be heat treated after welding, quenched alloys (without any additional treatment after manufacture) are recommended, due to their lower cost. Other characteristics, however, are also satisfactory. The recommended postweld practice is T62 for maximal strength and reducing distortions [13, 14].

THIRD GENERATION ALUMINIUM-LITHIUM ALLOYS

Over the recent years a decisive transition to aluminium-lithium alloys has been made in world cosmonautics. Compared to regular aluminium alloys, such as 2219, which is widely used in cryogenic tanks of space vehicles, as well as in unsealed structures, the aluminium-lithium alloys are characterized by a good combination of lower density with higher modulus of elasticity, good weldability, as well as mechanical properties superior to those of aluminium alloys without lithium.

Various factors influence the commercial alloy properties. The serviceability of aluminium-lithium alloys is determined chiefly by such service life characteristics as fatigue crack growth rate, coefficient of stress intensity in the crack tip (K_c, K_{ic}), low-cycle fatigue life, corrosion cracking resistance, and intercrystalline corrosion.

The most important factors having a great influence on the level of the abovementioned properties include:

- type of grain structure: degree of recrystallization, grain shape anisotropy, presence and density of precipitates on the boundaries of grains and subgrains, presence of near-boundary zones free from precipitates;
- cold tensile deformation between quenching and aging of the semi-finished products;
- artificial aging mode.

INFLUENCE OF GRAIN STRUCTURE ON THE ALLOY PROPERTIES

Semi-finished products with a predominantly recrystallized structure have higher characteristics of frac-

ture toughness and crack resistance at somewhat lower strength properties, compared to nonrecrystallized structure. The main mechanism of fine-grained structure formation is recrystallization.

INFLUENCE OF COLD DEFORMATION BETWEEN QUENCHING AND AGING

A considerable effect of improvement of the strength properties, characteristics of fracture toughness and crack resistance, as well as corrosion resistance is observed in alloys of Al–Cu–Li and Al–Li–Mg–Cu systems at application of regulated cold tensile deformation of quenched semi-finished products before artificial aging. Such treatment results in increase of the density and dispersity of precipitates of heterogeneously strengthening phases, reduction of the width of near-weld zones, free from precipitates, and of the dimensions and number of stable phases on the boundaries.

INFLUENCE OF AGING MODES

Aluminium-lithium alloys can be aged to three states: underaged (soft mode), to maximal strength (aging "peak") and overaged. The optimal aging modes were developed to ensure the required combination of strength, ductility, toughness and corrosion resistance. It was found that for the majority of the alloys the high ductility and fracture toughness, combined with an average level of strength properties are achieved after low-temperature aging in the soft mode — underaged state. However, the best corrosion resistance is ensured as a result of overaging or aging to maximal strength. The best set of properties (mechanical properties at tension — fracture toughness) was achieved at a combination of high deformation (2–8 %) after quenching with low-temperature aging.

The enumerated features are taken into account together with the economic considerations at selection of the temperature-time modes, which ensure the maximal strength and hardness in commercial semi-finished products. When establishing the commercial modes, preference is given to those, which ensure an extended maximum on the aging curves [15]. As follows from the obtained results, the best level of mechanical properties is found in sheets after artificial aging at the temperature of 160 °C — ultimate strength and proof strength are not less than 25–35 MPa higher, compared to other studied modes.

Aluminium-lithium alloys have a special position among other aging aluminium systems. However, they have the disadvantage of a low ductility in the state of maximal strength. In order to overcome it, many studies of the influence of different factors on ductility and fracture characteristics of aluminium-lithium alloys have been performed. It was clarified that the causes for lower ductility and fracture toughness are the deformation heterogeneity; presence of zones free from the strengthening phase precipitates, appearance of pores near large particles and presence of natural admixtures such as K, Na, S, H_2, Fe, Si, forming low-melting eutectics on the grain boundaries, or precipitation of phases on them. Let us enumerate the main measures proposed for solving this problem (ductility increase). This is primarily aluminium-lithium alloy doping by copper and manganese, forming ternary phases with lithium and causing solid-solution strengthening. These phases, alongside the intermediate one, promote alloy strengthening at aging and its more homogeneous deformation. Doping aluminium-lithium alloys by zirconium and scandium serves the same purpose, which allows refining the microstructure and ensuring additional structural strengthening due to formation of ultrafine intermetallic particles. The forming phases effectively block the dislocation movement due to formation of Al_3Sc type phase, having a rather high discrepancy between the lattice and matrix parameters [16]. Modern aluminium alloys are multicomponent, so in case of their alloying by scandium one should take into account the strengthening influence of other elements, and essentially correct the modes of thermomechanical treatment of the alloys. There is also the method of two-step aging. Such aging causes a more homogeneous distribution of the precipitating phases and stabilization of the dispersed structure.

The possibilities of improvement of aluminium alloy strength by the traditional methods through alloying and aging have almost been exhausted. It should be noted, however, that not all the possible methods to improve the ductility of Al–Li alloys have been used. A combination of high characteristics of strength and fracture toughness in these alloys is due to minimal content of impurities, introducing a small quantity of rare-earth modifiers and addition of silver, and lower lithium content. The 2195 alloy containing silver is used to manufacture TSV fuel tanks, ensuring approximately 13 % weight reduction, compared to earlier applied 2219 alloy [17]. On the other hand, it was found that auxiliary additives of small quantities of lithium to aluminium alloys having controlled quantities of copper and magnesium ensure a high crack resistance and high strength of the material, which also has equivalent or improved resistance to fatigue crack propagation, compared to aluminium-copper-magnesium alloys. Increase of lithium content leads to improvement of aluminium strength properties. At up to 2 % lithium content the alloy strength is increased without ductility lowering, at further increase of lithium content the ductility drops abruptly. At up to 0.8 %

concentrations, lithium provides higher corrosion resistance of aluminium alloys, higher than that of pure aluminium. More over, lithium additives ensure an improvement of impact toughness at an increased level of strength. Thus, the combination of crack resistance and strength properties is significantly improved. This effect is unexpected, as lithium additives are known to lower the crack resistance in the traditional aluminium-copper-magnesium-lithium alloys [18].

In technical literature it was reported more than once that scandium is the most effective alloying component of aluminium alloys. The main obstacle in the path of expansion of its application is the high cost of scandium, which is added to the alloys in the form of Al–2 % Sc master alloy. At scandium application, its addition to aluminium alloys increases their cost 5–10 times, which results in lowering of their compatibility compared to aluminium alloys of other alloying systems, widely used in aviation. Considering the deficit and high cost of Al–Sc master alloy, it is recommended to dope the aluminium alloys by small additives of scandium together with zirconium in equal quantities, in order to save deficit scandium and improve their properties [19]. Doping of aluminium-lithium alloys by scandium should be performed with caution, considering that this additive promotes the alloy embrittlement and lowering of fracture resistance characteristics.

Among the disadvantages it should be noted that the extravagant alloying elements of this alloy series make them unsuitable for processing into other alloys. The high cost of lithium makes it necessary to process lithium-containing alloys only from their wastes [20]. Application of lithium alloys is complicated by many production and metallurgical factors. At plastic deformation, formation and development of shear bands occurs, and their transformation into cracks is possible, which eventually causes fracture. Fracture along the shear bands is a feature of aluminium-lithium alloys [21].

When defining the area of Al–Li alloy application, it is necessary to take into account the data on solid solution stability and baking. The most widespread error is application of an alloy with low solid solution stability for manufacturing thick-walled semi-finished products, for instance complex-shaped stampings. In this case, “dark spots” appear on the massive element surface, and zones of incomplete quenching form in the central part, which lower the characteristics of static and cyclic crack resistance.

DISCUSSION OF PROBLEMS IN THE FIELD OF ALUMINIUM ALLOY WELDING

Introduction of welding technologies is one of the most highly productive and cost-effective methods of making permanent joints, which allows fabrication of structural elements of the most rational shape and dimensions, making them maintainable. Let us consider the current problems in welding aluminium alloy structures. The constraints for application of the considered aluminium alloys in welded joints are as follows:

- considerable softening (up to 50 %) under the impact of the thermal cycle of fusion welding;
- low hot cracking resistance;
- lower values of ductility and fracture toughness in the direction of the height;
- multistep procedure of manufacturing the semi-finished products and/or finished products;
- need for alloying the filler materials by deficit and expensive master alloys to form welds with higher values of hot cracking resistance, as well as mechanical properties (particularly, LCF) of welded joints;
- and tendency to embrittlement developing at a high degree of deformation.

The following technological solutions are used to prevent cracking or other defects in the welds during welding of the alloys:

- producing such a structure, which enables a significant grain refinement (in particular, with application of electron beam technologies);
- limiting penetration of harmful impurities such as hydrogen (H) into the weld;
- regulation of the crystallization process at application of welding processes, characterized by minimal energy input;
- weld alloying.

The common regularity of all the aluminium alloys is formation of a softening zone, the size of which depends on the alloy type, its chemical composition and welding heat input. When producing a welded joint with the required parameters of weld depth and width, usually the requirement of minimizing the HAZ is also made, in order to ensure minimal deterioration of the physicomechanical properties as a result of recrystallization [22]. At heating in welding, a wide range of structural and phase transformations usually take place, including further decomposition of the solid solution and its repeated formation. It leads to different HAZ subzones being in the state of recovery, artificial aging, partial annealing and repeated quenching. The welded joint properties, as well as the possibility of strengthening at repeated artificial aging and the level of properties relative to the initial state, respectively, depend on the extent of development of this or that process [23].

Metallographic studies show that fracture of the metal of the weld and near-weld zones occurs as a result of the change in the initial structure of the semi-fin-

ished products. Such changes are less pronounced at EBW and, possibly, in laser welding, which ensures a higher level of the studied characteristics of welded joints. The advantages of electron beam process of aluminium alloy welding include the possibility of making a metallurgical impact on the weld pool with minimal weld alloying. Due to that, the welded joints turn out to be close to the base metal by their thermophysical properties. The weld structure is characterized by 4–5 times finer grain compared to base metal, and this is exactly the main difference between them. In addition to the fine equiaxed grain structure, a homogeneous distribution of copper in the matrix is also observed. A high density and dispersity of excess phases is also found, which is due to high rates of weld metal crystallization. Increase of the degree of deformation prior to quenching leads to reduction of the dimensions of recrystallized grains forming as a result of subsequent quenching, which ensures high mechanical properties.

In welding the process of formation of a weld of a homogeneous composition is important, which provides the high quality of welded joints, required mechanical properties and minimal residual stresses. To ensure the correspondence of the characteristics of the material being welded and the weld metal, it is most often recommended to use filler material of the same composition, as the base metal, or close to it. For alloys of Al–Cu–Li system such an approach is not rational, because of the low resistance to hot cracking. Therefore, for this class of alloys FSUE "VIAM" developed filler materials based on an alloy of Al–Cu system with additives of effective modifiers, including those with rare-earth metals (REM) [24]. Investigations with optimization of the quantity of modifiers, added to the alloy, are conducted under the conditions of commercial production, where the ingot crystallization rates are low and they are furtheron subjected to pressure treatment (pressing, extrusion, rolling). In the case of weld metal the situation is somewhat different. The weld has a cast structure which is not subjected to further pressure treatment, and melt crystallization rates are by 1–2 orders of magnitude higher than in commercial production of the alloys. In work [25] it is reported that application of high energy density sources, such as the electron beam, will allow optimizing the quantity of modifiers (scandium) added to the alloy. It is stated that in this case increase of mechanical properties of the metal of welds will be due to grain refinement and solid solution strengthening of the cast metal.

Porosity in EB welded joints in a number of cases can be a serious obstacle for effective application of this welding process in industry. The main cause for porosity is believed to be a jumplike lowering of hydrogen solubility in the weld metal at solidification (crystallization). Appearance of such porosity usually is the consequence of a severe violation of optimal welding conditions, including preparation of base metal and welding wires, as well as high content of gases in the metal being welded. Elimination of such porosity is complicated even at multiple remelting of the weld.

Much less difficulties arise during welding with subsequent strengthening heat treatment, which ensures equal strength of the welded joint metal and base metal. Alloy welding can be performed in the hot-deformed state or after quenching with performance of repeated thermal-strengthening treatment. Here, the welded joint strength is increased, but its ductility is decreased.

The advantages of this process compared to arc welding are especially noticeable at EBW of heat-hardenable aluminium alloys. Producing tight welds is largely ensured when alloying the weld pool by elements lowering the gas solubility in the liquid metal or binding them into stable compounds. Here, alloying element addition to the weld pool is performed by different methods: through filler wire fed under the electron beam during welding, or through metal foil or plates, which are preliminarily inserted into the butt, as well as spraying alloying elements on the edges being welded, or deposition of a metal-organic compound [26].

It is characteristic that due to a combination of high specific strength and specific modulus of elasticity, the aluminium-lithium alloys, while ensuring production of strong welds, usually do not meet the requirements to equal strength of welded joints. It is known that the strength coefficient of such materials after argon-arc welding is usually equal to 0.5–0.65 % of tensile strength of the base material. Equal strength of the base metal and welded joint can be achieved through reinforcement of the welding zones, or additional work hardening. To compensate for the loss of strength and ensure equal strength of the welded joints and base metal the butt joint is located in a region of thicker welded edges. Thickening is usually equal up to 100 % of the thickness of the welded metal, and the width of the thicker region should always be greater than that of the HAZ. It means a significant increase of welded structure weight. Now the EBW joints have tensile strength 15–25 % higher, and HAZ width 2–3 times smaller than with the arc methods. It allows greatly reducing the weight characteristics of welded structures. Welding aluminium alloys by the electron beam can be performed in the unsupported position and in different positions in space without application of substrate or

forming devices, as the weld pool has a small volume of liquid metal due to a high heat conductivity of these alloys. It is important in welding structures, requiring a guaranteed penetration of the butt through its entire thickness in the absence of access to the butt joint reverse side. The impact toughness of the metal of the weld on aluminium alloys is always higher than that of the base metal, and the proof strength practically remains on the level of these properties of the base metal. With increase of the number of passes, the tensile strength decreases by 10–30 MPa, irrespective of the initial state of the material before welding, even on annealed material [12].

The influence of initial tempering before welding and postweld treatment on the strength and elongation of welded joints also depends on their thickness [27–30]. Both base metal and weld strength increase with reduction of elongation. Fracture runs in the weld HAZ prior to any significant elongation occurring in the base metal.

To sum up, we can note that three main kinds of heat treatment became widely accepted for aluminium alloys: annealing, quenching, thermomechanical treatment and aging as a means to improve the functional properties. Application of postweld heat treatment (quenching + artificial aging) ensures equalizing of the grain structure of the welded joint at recrystallization and change of the morphology of precipitates on the grain boundaries, which improves the strength of welded joints to 0.9 of base metal strength. Despite a certain lowering of ductility values, significant advantages of the new alloys as to rigidity and tensile strength are obvious. However, at application of lithium-containing alloys it was found that achievement of high strength properties of aluminium alloys most often is detrimental to their adaptability-to-manufacture.

Furtheron, development and introduction of alloys, having significantly higher strength characteristics at preservation of adaptability-to-manufacture, will allow even further improvement of the reliability and residual life of structures, and lowering of their weight and metal intensity.

Thus, fabrication of high-tech welded structures from aluminium alloys involves two interconnected directions of investigations: creation of new high-tech alloys, as well as development of different technological processes of joining them with application of modern welding technologies that, eventually, determines the possibility of creation of advanced aerospace products.

CONCLUSIONS

1. On the whole, weldable aluminium alloys remain to be the main structural materials for aerospace industry. Their application ensures higher weight effectiveness, and an increase of the structure strength and reliability at a significant weight reduction. On the other hand, increase of the abovementioned characteristics is based on a complication of the chemical composition, heat treatment modes and other technological measures, leading to lowering of the material ductility properties.

2. Results of the conducted literature review indicate that at present materials scientists have created original compositions of complex aluminium alloys of different alloying systems with microadditives of effective modifiers of REM type, which feature higher characteristics of adaptability-to-manufacture and strength.

3. Despite a range of technological difficulties, third generation alloys of Al–Mg–Li–Zr and Al–Cu–Li–Zr systems are promising materials in aircraft construction. However, despite the high adaptability-to-manufacture of aluminium-lithium alloys at application in the aerospace industry, we should not forget about the high toxicity of welding these alloys for humans.

4. Allowing for all the mentioned factors in their totality ensures achievement of not only higher level of heat resistance and strength of the alloys, their anisotropy, but also their good adaptability-to-manufacture. In manufacture of cryogenic welded products for flying vehicles, 2219 aluminium alloy remains the best choice at this moment among the dispersion-hardening alloys.

REFERENCES

1. Beletsky, V.M., Krivov, G.A. (2005) *Aluminium alloys (Composition, properties, technology, application):* Refer. Book. Ed. By I.N. Fridlyander. Kyiv, Komintekh [in Russian].
2. (2018*) Aviation maintenance technician handbook.* Airframe Vol. 1. U.S. Department of Transportation, Federal Aviation Administration Flight Standards Service, Oklahoma City-2018. http://www.faa.gov
3. Davis J.R. (1993) *Aluminum and aluminum alloys*. ASM Speciality Handbook, ASM International.
4. Stefanovich, V.A., Poznyak, I.G., Stefanovich, A.V. (2021) *Fundamentals of alloying structural materials.* Belarussian NTU, Minsk [in Russian].
5. Setyukov, O.A. (2013) Aluminuium alloy 1201 in the design of Buran spacecraft. *Aviats. Materialy i Tekhnologii.* Spec. Issue, 15–18 [in Russian].
6. Ber, L.B. (2013) On aging stages of aluminium alloys. *Tekhnologiya Lyogkikh Splavov,* **4**, 66–76 [in Russian].
7. Merkulova, G.A. (2008) *Metals science and heat treatment of nonferrous alloys:* Manual. Krasnoyarsk, SFU [in Russian].
8. Markashova, L.I., Grigorenko, G.M., Lozovskaya, A.V. et al. (2006) Effect of scandium additions on structure-phase state of weld metal in aluminium alloy joints after heat treatment. *The Paton Welding J.,* **6**, 7–11.
9. Ovchinnikov, V.V., Drits, A.M., Krymova, T.V. (1997) Technological features of the production of aircraft welded structures from aluminium-lithium alloy 1460. *Svarochn. Proizvodstvo,* **12**, 26–29 [in Russian].

10. Ishchenko, A.Ya., Labur, T.M., Bernadsky, V.N., Makovetskaya, O.K. (2006) *Aluminium and its alloys in modern welded structures.* Kyiv, Ekotekhnologiya [in Russian].
11. Rabkin, D.M., Ignatiev, V.G., Dovbishchenko, I.V. (1982) *Arc welding of aluminium and its alloys.* Mashinostroenie [in Russian].
12. Dudar, L.A. (1995) *Features of electron beam welding of aluminium alloys used in the production of aircrafts:* Manual. Samara Gos. Aerokosm. Un-t [in Russian].
13. Luts, A.R., Suslina, A.A. (2013) *Aluminium and its alloys:* Manual. Samara GTU [in Russian].
14. Dovbishchenko, I.V., Ishchenko, A.Ya., Mashin, V.S. (1997) The use of helium in consumable electrode welding of aluminium alloys. *Avtomatich. Svarka*, **2**, 14–19 [in Russian].
15. TALAT Lecture 1204: *Precipitation Hardening*. Ed. by M.H. Jacobs. Interdisciplinary Research Centre in Materials. The University of Birmingham, UKDate of Issue 1999. European Aluminium Association TALAT 1204.
16. Antipov, V.V., Klochkova, Yu.Yu., Romanenko, V.A. (2017) Modern aluminium and aluminium alloys. *Aviats. Materialy i Technologii,* 195–211 [in Russian]. DOI: https://doi.org/10.18577/2071-9140-2017-0-S-195-211
17. Teleshov, V.V., Golovlyova, A.P. (2011) Results of the investigations of high-strength aluminium alloys of conventional alloying system. *Tekhnologiya Lyogkikh Splavov,* **1**, 108–141 [in Russian].
18. Beibel Henry W., Sankaran Krishnan Dk., Owl, Brian J. (2012–2023) *Method for increasing the impact strength of aluminium-lithium alloys at cryogenic temperatures.* US Pat.
19. Zakharov, V.V., Fisenko, I.A. (2013) On saving scandium in its doping to aluminium alloys. *Tekhnologiya Lyogkikh Splavov,* **4**, 52–60 [in Russian].
20. Schmitz, C. (2014) *Mechanical preparation, metallurgical processing, heat treatment*: Handbook on aluminium recycling [in Russian].
21. Limarenko, A.L., Sitalo, V.G., Litvishko, T.N. (2002) Properties and structure of high-strength welded aluminium-lithium alloy 1460. *Kosmichna Nauka i Technologiya,* Dodatok, 8(**1**), 123–126 [in Russian].
22. Litvinov, V.V., Yarmilko, A.V. (2013) Multiparameter adaptive control of the technological process of electron beam welding. *Matematychni Mashyny i Systemy,* **2**, 130–138 [in Russian].
23. Gureeva, M.A., Grushko, O.E., Ovchinnikov, V.V., Shiganov, I.N. (2007) *Mechanical properties and structure of welded joints of aluminium alloy V-1341 depending on laser welding modes* [in Russian].
24. Skupov, A.A., Ioda, E.N., Panteleev, M.D. (2016) New filler materials for welding of high-strength aluminium-lithium alloys [in Russian].
25. Fedorchuk, V.E., Kushnaryova, O.S., Alekseenko, T.A., Falchenko, Yu.V. (2014) Peculiarities of alloying of weld metal of high-strength aluminium alloy welded joints with scandium. *The Paton Welding J.,* **5**, 28–32. DOI: https://doi.org/10.15407/tpwj2014.05.05
26. Krivtsun, I.V., Kvasnytskyi, V.V., Maksymov, S.Yu., Yermolaev, G.V. (2017) *Special methods of welding:* Manual. Ed. by B.E. Paton. Mykolaiv, NUK [in Russian].
27. Paton, B.E. (1995) Improvement of welding methods is one of the ways to improve the quality and efficiency of welded structures. *Avtomatich. Svarka,* **11**, 3–11 [in Russian].
28. Alieva, S.G., Altman, M.B., Ambartsumyan, S.M. et al. (1984) *Commercial aluminium alloys.* 2nd Ed. Moscow, Metallurgiya [in Russian].
29. Rabkin, D.M., Ignatiev, V.G., Dovbishchenko, I.V. (1975) *State-of-the art and prospects of application of aluminium alloys in welded structures.* Kyiv, Naukova Dumka [in Russian].
30. Kolobnev, N.I., Fridlyander, I.N. (1994) Aluminium-lithium alloys as a new stage for weight reducing of aircrafts. In: *Aviation Materials at the Threshold of 20–21 Centuries: Scientific and Technical Collection*, 89–92. Moscow, GP VIAM [in Russian].

ORCID

V.I. Zagornikov: 0000-0003-0456-173X

CORRESPONDING AUTHOR

V.I. Zagornikov
E.O. Paton Electric Welding Institute of the NASU
11 Kazymyr Malevych Str., 03150, Kyiv, Ukraine.
E-mail: zagornikov@technobeam.com.ua

SUGGESTED CITATION

V.I. Zagornikov (2024) Analysis of the properties and features of high-strength deformable aluminium alloys of Al–Li, Al–Cu–Mn systems used in the aerospace industry in manufacture of welded structures (Review). *The Paton Welding J.*, **3**, 15–23.

JOURNAL HOME PAGE

https://patonpublishinghouse.com/eng/journals/tpwj

Received: 01.11.2023
Received in revised form: 11.12.2023
Accepted: 19.03.2024

DOI: https://doi.org/10.37434/tpwj2024.03.04

THERMAL SPRAYING OF COATINGS, CONTAINING Cr_2AlC MAX PHASE (REVIEW)

N.V. Vihilianska[1], D.V. Filonenko[1], A.O. Yushchenko[1], C. Senderowski[2], J.-C. Grivel[3]

[1]E.O. Paton Electric Welding Institute of the NASU
11 Kazymyr Malevych Str., 03150, Kyiv, Ukraine
[2]Warsaw Polytechnic University
1 Polytechnic Sq., 00-661, Warsaw, Poland
[3]Technical University of Denmark
Anker Engelunds Vej, Building 301, Kongens Lyngby, Denmark, 2800

ABSTRACT

A review of research works is presented, devoted to formation of coatings, containing Cr_2AlC MAX-phase, under the conditions of the processes of thermal spraying. The main methods for producing coatings containing Cr_2AlC MAX-phase is plasma, high-velocity oxygen fuel and cold gas-dynamic spraying. As spraying materials, both powders with synthesized Cr_2AlC MAX-phase, obtained by the sintering method as well as powders of the mechanical mixture of initial components are used. To preserve the MAX-phase in a powder and prevent the oxidation of particles in the process of spraying, high-velocity spraying methods (high-velocity plasma, high-velocity oxygen fuel and cold gas-dynamic) are used. The velocity of particle flight during spraying by these methods is 500–900 m/s. Therefore, in these cases coatings are formed, the phase composition of which corresponds to the phase composition of sprayed powders, and the content of Cr_2AlC phase in such coatings amounts to 79–98 wt.%. In the case of using a mechanical mixture of components the plasma method is used in the spray process for running of synthesis of the MAX phase, resulting in the formation of coatings with MAX phase content of up to 42 wt.%. Studies of phase transformations in powder particles during spraying, mechanisms of decomposition and/or formation of the MAX phase, and the effects of spraying parameters on the structure and properties of coatings are shown. The prospect of further practical use of thermal coatings, containing Cr_2AlC MAX phase is described, which mainly consists in using them at elevated temperatures, in particular, in the structures of thermal barrier coatings.

KEYWORDS: Cr_2AlC MAX phase, thermal coatings, microstructure, mechanical properties, heat protection properties

INTRODUCTION

MAX phases belong to the class of ternary carbide and nitride compounds, which are united by a common structural formula $M_{n+1}AX_n$, where M is the early transition metal, A is an element of A-group (predominantly groups 13 and 14), and X is C and/or N [1]. MAX phases can be additionally classified by their n value as "211" for M_2AX (n = 1), "312" M_3AX_2 (n = 2), "413" for M_4AX_3 (n = 3), etc. They have a hexagonal crystalline structure, which consists of MX layers alternating with a layer of element A. M–X bonds are extremely strong due to mixed covalently ionic nature, whereas M–A metal bonds are relatively weak. This unique crystalline structure is responsible for the characteristic layered nanolaminated structure of MAX phases (Figure 1), and it ensures a unique set of properties, which consists in a combination of the properties of both ceramics and metal.

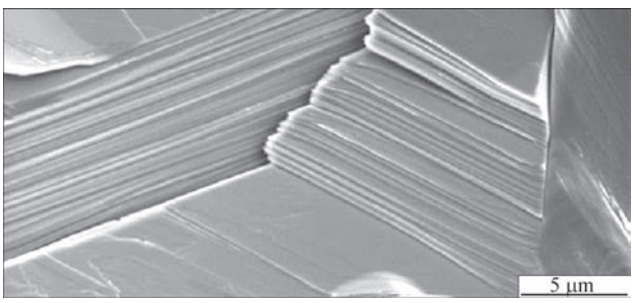

Figure 1. Typical nanolaminated structure of MAX phases [2]

At present more than 150 MAX phases have been identified and their number grows regularly due to a combination of experimental studies and theoretical calculations. Nonetheless, not all the possible combinations are thermodynamically stable. For instance, in Ti–Al–C system Ti_2AlC and Ti_3AlC_2 phases (n = 1 and 2, respectively) are stable in a broad temperature range, while in Cr–Al–C system the only stable phase is Cr_2AlC.

Ternary carbide Cr_2AlC is one of the most promising MAX phases for potential high-temperature application due to its resistance to high-temperature oxidation and hot corrosion [3]. At the same time, it demonstrates excellent mechanical properties, including relatively high hardness and Young's modulus, fracture resistance, bending strength and compressive strength, electric and heat conductivity properties.

Properties of ternary Cr_2AlC carbide [4–7]

Density, g/cm^3	5.21–5.24
Hardness, GPa	3.5–6.4
Modulus of elasticity, GPa	245–288
Shear modulus, GPa	102–116
Bending strength, GPa	305–513

Compressive strength, GPa 1159
Crack resistance characteristic, $MPa \cdot m^{1/2}$ 4.7–6.2
Heat conductivity, W/(m·K) (at 200 °C) 17.5
Coefficient of thermal expansion, K^{-1} . . . . . $1.33 \cdot 10^{-5}$
Specific heat, J(kg·K) 590
Electric conductivity, S/m . . . . . $1.4 \cdot 10^6$
Poisson's ratio 0.153

The traditional methods of producing samples of Cr_2AlC ceramics are as follows: hot pressing [8, 9], hot isostatic pressing [10], high-temperature sintering [11–14], self-propagating high-temperature synthesis [15], spark plasma sintering [16, 17], and other technologies of mechanical alloying and sintering [18]. Used as raw materials are different mixtures of elements or compounds, including Cr/Al/graphite (or soot), CrC_x/Al, $AlCr_2$/graphite, Cr/Al_4C_3/graphite and Cr_2O_3/Al/Al_4C_3. However, a mandatory requirement for synthesis of Cr_2AlC phase is conducting the above-listed processes at higher temperatures and high pressing pressures, that is why these processes are low-productive and energy consuming. These are exactly the factors limiting mass production of materials based on MAX phases.

Another direction of MAX phase application is their forming as protective coatings on product surface. Coatings based on Cr_2AlC MAX phase are formed using the following methods of vacuum deposition (PVD-methods): cathode-arc deposition [19-21], pulsed-laser deposition [22, 23] and magnetron sputtering. The most widely accepted is the magnetron sputtering method, which allows producing dense homogeneous coatings [24–27]. For application of Cr_2AlC coatings by deposition methods individual element targets (for instance, Cr, Al and graphite) or composite targets (for instance, $AlCr_2$, and Cr_2AlC) are usually used.

Coatings produced by the methods of vacuum deposition, have the thickness of just several microns and do not meet the requirements to operation under extreme conditions. That is why the methods of thermal spraying are used for deposition of coatings based on Cr_2AlC MAX phase.

The objective of this work is analysis of literature data on the conditions of formation and properties of thermal coatings containing Cr_2AlC MAX phase.

At present there exist just several dozens of works devoted to studying formation of coatings containing Cr_2AlC MAX phase under the conditions of plasma [28–31], High Velocity Oxygen Fuel (HVOF)) [32, 33] and cold gas-dynamic spraying [34, 35]. This is, obviously related to difficulties of spraying materials manufacture in the form of powder with a high MAX phase content.

The methods of plasma, high-velocity oxygen fuel and cold spraying differ primarily by the jet temperature and particle flight velocity, which is one of the most important parameters of thermal spraying processes, influencing the coating structure and properties. In plasma spraying, the plasma jet temperature is equal to 10000–15000 °C (maximal particle flight velocity is 400 m/s), leading to powder particle oxidation and decomposition of MAX phases, as in the case of deposition of Ti_2AlC powder [36]. MAX phase oxidation and degradation can be avoided using the methods of high-velocity oxygen fuel and cold spraying, where the jet temperature is equal to 2000–3000 °C and <1000 °C, respectively. Here, the particle flight velocity is equal to 500–900 m/s, which shortens time of particle interaction with oxygen and the high-temperature jet. At spraying of Ti_2AlC MAX phase powders by high-velocity methods it is possible to minimize particle oxidation and development of phase transformations in them [37, 38].

FORMATION OF COATINGS CONTAINING Cr_2AlC MAX phase UNDER PLASMA SPRAYING CONDITIONS

The method of high-velocity plasma spraying was used to produce coatings of up to 100 μm thickness from Cr_2AlC powder, manufactured by sintering Cr, Al element powders and graphite (molar ratio of 2:1:1:1, respectively) and further grinding to particle size d_{10} = 5.5 μm, d_{50} = 10.4 μm, d_{90} = 18.3 μm [28]. Spraying was performed with TriplexProTM-210 plasmatron (Oerlicon Metco). Optimization of spraying parameters showed that the spraying distance has the greatest influence on coating thickness, reduction of which from 100 to 60 mm leads to coating thickness increase from 30 to 90 μm. Formation of coatings of greater thickness at smaller spraying distances can

Table 1. Optimal modes of deposition of Cr_2AlC powder by the method of high-velocity plasma spraying

Process parameters						Coatings characteristics	
Q_1 (Ar), l/min	I, A	V, mm/s	L, mm	Q_{tr} (Al), l/min	Q_2 (He), l/min	Thickness, μm	Weight, mg
170	450	500	60	7.5	40	90	0.39
				8	40	100	0.34
				7.5	20	70	0.36

Note. Q_1 is the flow rate of primary plasma-forming gas; I is the current; V is the speed of plasmatron movement; L is the spraying distance; Q_{tr} is the transport gas flow rate; Q_2 is the flow rate of secondary plasma-forming gas. Deposition was performed in 5 passes.

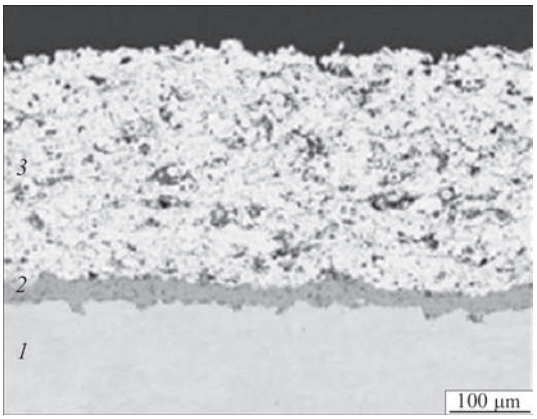

Figure 2. Microstructure of thermal barrier coating: *1* — Inconel 738 substrate; *2* — Cr_2AlC coating; *3* — ZrO_2–Y_2O_3 coating

be associated with a higher velocity and temperature of particles. The results of the conducted optimization of plasma spraying parameters were used to establish the modes, which ensure formation of Cr_2AlC coatings with the best values of sprayed coating thickness and weight (Table 1).

The sprayed coatings have a homogeneous dense structure with pore content on the level of 7–8 %. The content of Cr_2AlC MAX phase somewhat decreases relative to that in the powder (from 98 to 93 %), and difficult to indentify secondary phases are recorded in the coatings. The secondary phases can be chromium carbides (Cr_2C, $Cr_{23}C_6$, Cr_7C_3) and/or chromium aluminides (Al_3Cr_7, $Al_{84}Cr_{14}$, $AlCr_2$). These phases form as a result of decomposition of Cr_2AlC MAX phase, because of the high temperature of plasma spraying process.

In order to study the coating serviceability, a Cr_2AlC layer was deposited by the high-velocity plasma method on the high-temperature Inconel 738 nickel alloy as a bond coat in the system of thermal barrier coatings. A thermal barrier coating of zirconium dioxide, stabilized by yttrium oxide ZrO_2–8 wt.% Y_2O_3 was deposited over it by plasma spraying method. The thickness of Cr_2AlC bond coat was ~ 40 μm, that of the main ZrO_2–Y_2O_3 thermal barrier layer was ~ 400 μm. Adhesion between Inconel 738 substrate and Cr_2AlC coating, as well as Cr_2AlC coating and ZrO_2–Y_2O_3 was visually dense without any cracks or delaminations on the interface (Figure 2). Coating resistance was studied under the conditions of thermal cycling at heating of the coating surface by the torch up to 1400 °C (of the base up to 1050 °C) and cooling to 70 °C. The coating fails after 745 cycles. The main causes for fracture are open porosity and presence of secondary phases in Cr_2AlC bond coat, as well as interdiffusion between the bond coat and the substrate. Nonetheless, conducted investigations allow considering the possibility of application of coatings based on Cr_2AlC MAX phase as a bond coat in systems of thermal barrier coatings.

Table 2. Phase composition of coatings of Cr–Al–C system at different heat treatment temperatures

HT temperature, °C	Phase content, wt.%		
	Al	Cr_2AlC	Cr_7C_3
Without HT	9.3	4.6	89.1
400	6.7	2.7	90.6
500	5.1	4.5	90.4
600	–	8.2	91.8
700	–	14.8	85.2
800	–	23.7	76.3

A two-stage technology was proposed to produce coatings containing Cr_2AlC MAX phase, which consists of coating deposition by the plasma method and further heat treatment (HT) [29]. A mechanical mixture of powders of chromium (d_p = 40–70 μm), aluminium (d_p = 20–35 μm) and graphite (d_p = 1–5 μm) (2:1:1 molar ratio, respectively) produced by the method of mixing, conglomeration and spray-drying, was used for spraying. Heat treatment of the coated samples was conducted in an argon atmosphere at the temperature of 400, 500, 600, 700 and 800 °C for 1 h.

Sprayed coating (without HT) consists predominantly of Cr_7C_3 phase with residual Al; MAX phase content is equal to only 1.6 wt.% (Table 2). Heat treat-

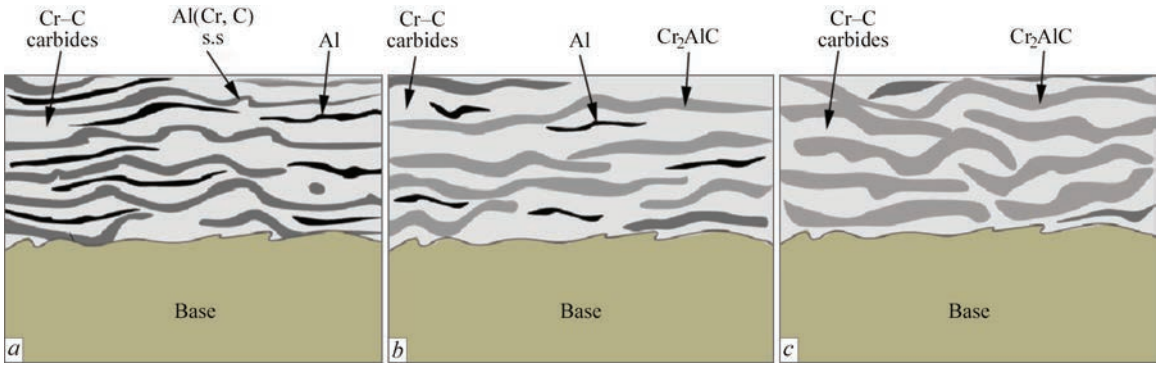

Figure 3. Schematic explanation of the influence of HT temperature on deposited coating of Cr–Al–C system: *a* — without HT; *b* — HT at the temperature of <660 °C; *c* — HT at the temperature of >660 °C

ment at the temperature of <600 °C does not lead to any significant changes in the phase composition of the coatings, but it changes considerably at the temperature of >600 °C. Aluminium disappears from the coatings and weight fraction of Cr_2AlC MAX phase increases up to 8.2 % after HT at 600 °C, up to 14.8 % after HT at 700 °C and up to 23.7 % after HT at 800 °C. It means that liquid Al promotes atom diffusion, thus accelerating nucleation and increase of the content of Cr_2AlC phase. Since Cr and C are homogeneously dispersed at the molar level in Cr–C carbides (Cr_7C_3 or $Cr_{23}C_6$), they can thus react with residual Al with Cr_2AlC formation. Influence of HT temperature on formation of composite coatings based on Cr_2AlC is schematically shown in Figure 3.

After spraying the coating has a dense lamellar structure, after heat treatment the coating structure does not essentially change and the structure lamellarity is preserved (Figure 4).

Figure 5 gives the microhardness and crack resistance values of coatings of Cr–Al–C system, produced by plasma spraying with subsequent HT.

Hardness of the produced coatings is equal from 544 up to 857 *HV*, and it mainly depends on chromium carbide content. The coating hardness is somewhat lower than that of chromium carbides, because of the presence of residual aluminium and porosity in them. At coating heat treatment the quantity of soft Al metal decreases, and that of the newly-formed Cr_2AlC phase increases, leading to an increase of hardness, which reaches the maximal value after HT at the temperature of 600 °C. After HT at 700 and 800 °C, the coating hardness somewhat decreases, because of an increase of the content of Cr_2AlC MAX phase, the hardness of which is equal to 350–640 *HV*.

Crack resistance value for a sprayed Cr_2AlC coating (without HT) is equal to 1.29 MPa·m$^{1/2}$, while after HT performance the crack resistance value increases, and it reaches the maximal value (2.02 MPa·m$^{1/2}$) after conducting HT at 700 °C. Increase of coating crack resistance after HT is attributable to formation of a more homogeneous microstructure and more uniform phase distribution in the coatings.

Possibility of producing plasma coatings with a higher content of Cr_2AlC MAX phase (up to ~ 43 %) without additional HT performance is demonstrated

Table 3. Phase content in plasma coatings of Cr_3C_2–Al–Cr system

Al content in the powder, mol.%	Phase content in the coating, wt.%	
	Cr_2AlC	Cr–C
0,5	22.41	77.59
1	28.02	71.98
2	42.78	57.22
3	30.25	69.75

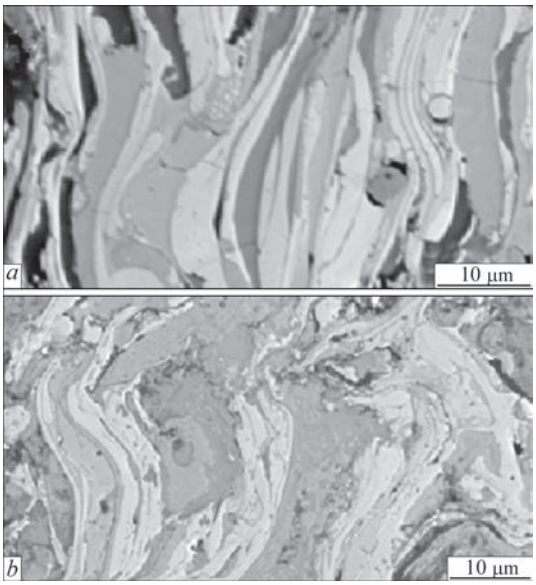

Figure 4. Microstructure of plasma coating of Cr–Al–C system: *a* — without HT; *b* — after HT at 800 °C

in the case of Cr_3C_2 chromium carbide application as a carbon source, instead of graphite [30]. The spraying powder was manufactured by the method of conglomeration with subsequent spray-drying in the mixture of initial powders of Cr_3C_2, Al and Cr in the molar ratio of 1:*x*:1, where *x* = 0.5, 1, 2, 3.

Investigations of the phase composition showed that all the coatings contain Cr_2AlC, Cr_7C_3 and $Cr_{23}C_6$ MAX phases, which is indicative of running of the process of interaction of the powder initial components during spraying with new phase formation. The content of the carbide component and MAX phase in the coatings is given in Table 3.

At deposition of powders with Al content of 0.5 and 1 %, initial Cr_3C_2 phase is recorded in the coatings, whereas at increase of Al content in the powders up to 2 and 3 % this phase disappears, which is indicative of a complete interaction of powder components. Formation of substable (Cr, Al)C_x carbide was also noted in the coatings, which arises as a result of Al

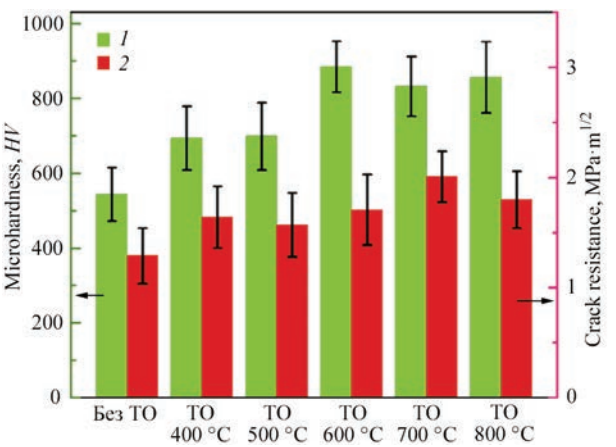

Figure 5. Microhardness (*1*) and crack resistance (*2*) of plasma coatings of Cr–Al–C system

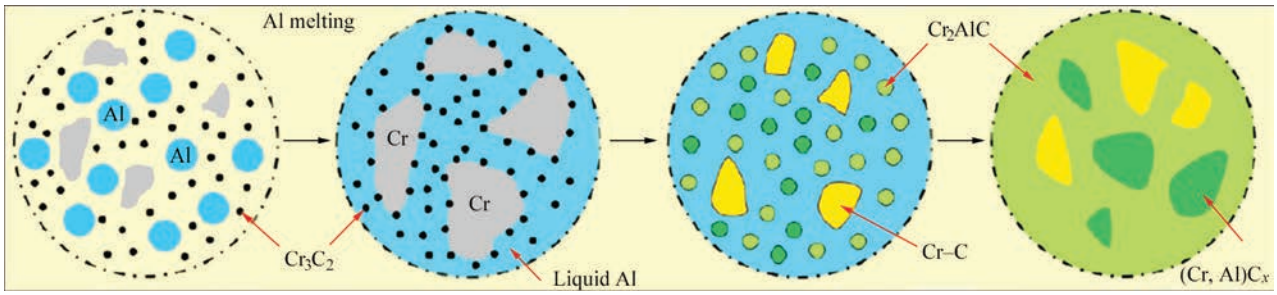

Figure 6. Scheme of phase transformations at plasma deposition of powder of Cr_3C_2–Al–Cr system

substitution in Cr–C lattice. At 2 % Al concentration in the powder, a more intensive interaction of liquid aluminium with Cr_3C_2 and Cr with formation of (Cr, Al)C_x and Cr_2AlC is in place, which results in MAX phase content in the coating reaching 42.78 %. At the same time, increase of Al content in the powder up to 3 % leads to increase of (Cr, Al)C_x phase content and decrease of the quantity of Cr_2AlC phase to 30.25 % in the coating. The mechanism of phase transformations at plasma deposition of powder of Cr_3C_2–Al–Cr system is shown in Figure 6.

Coating microhardness is equal to 11.33, 10.64, 10.27 and 10.1 GPa at Al content of 0.5, 1, 2, 3 % in the powder, respectively. Coating hardness somewhat decreases with increase of Al powder content in the coating, which is attributable to phase composition of the coatings, as phase hardness is of the following order: Cr–C > (Cr, Al)C_x > Cr_2AlC.

The coefficient of coating crack resistance is equal to 2.37, 2.5, 2.6 and 2.4 MPa·$m^{1/2}$ at Al content in the powder of 0.5, 1, 2 and 3 %, respectively. Coating strength is ensured by microlamellarity of the structure (Figure 7) which consists of alternating layers of carbides and MAX phase. As MAX phase proper has a nanolayered structure, its presence in the coatings prevents crack propagation, leading to increase of the coating strength as a whole.

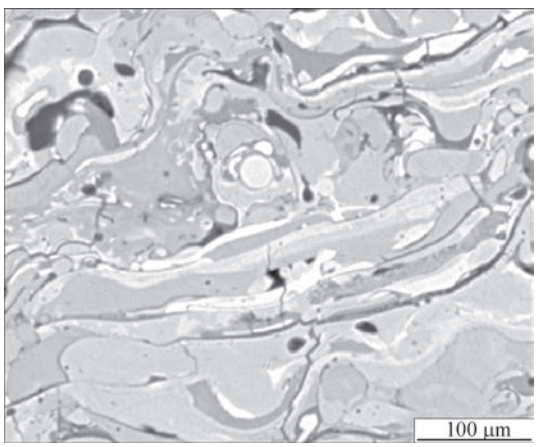

Figure 7. Microstructure of plasma coating of Cr_3C_2–Al–Cr system

FORMATION OF COATINGS CONTAINING Cr_2AlC MAX PHASE, UNDER THE CONDITIONS OF HIGH-VELOCITY OXY-FUEL SPRAYING (HVOF)

The influence of addition of Cr_2AlC MAX phase powder on formation and properties of NiMoAl based coatings produced by HVOF-spraying method was studied [32]. A mechanical mixture of Ni–Mo–Al powder with addition of Cr_2AlC MAX phase powder in the amount of 10, 20 and 50 wt.% was used for spraying. Cr_2AlC powder was produced in several stages: sintering of chromium and graphite powders (Cr:C = 2:1 at 1550 °C for 1 h in argon atmosphere), grinding of CrC_x powder (x = 0.5) for 15 h and subsequent sintering of CrC_x and Al powders (CrC_x:Al = 2:1.4) at 800 °C for 2 h in argon atmosphere) [39]. The powder consists of >99 % Cr_2AlC phase with a small additive of chromium carbide (<1 %). Characteristics of spraying powder are given in Table 4.

It is shown that no decomposition or oxidation of powders takes place as a result of HVOF-spraying, and the coating phase composition corresponds to phase composition of the powders. At the same time, at deposition of the same compositions by plasma spraying method [31] Cr_2AlC MAX phase is absent in the coatings, and oxides (Al_2O_3 and Cr_2O_3) and carbides (Cr_7C_3 and Cr_3C_2) form as a result of decomposition and oxidation. This is associated with a higher temperature of the jet at plasma spraying than at HVOF-process. In other works [33] it is reported that during HVOF-spraying partial decomposition of Cr_2AlC MAX phase takes place with formation of Cr_7C_3 chromium carbide. In this study it was possible to minimize the process of oxidation and ensure preservation of MAX phase in the coating by conducting the process of HVOF-spraying at lower oxygen flow rate (250 l/min) and 0.24 ratio of propane/oxygen flow rates.

Produced composite coatings of NiMoAl–Cr_2AlC system have a dense layered structure; coating porosity decreases compared to NiMoAl coatings from 4.6 to 3.6, 2.13 and 1.95 % when using powders with addition of 10, 20 and 50 wt.% of Cr_2AlC powder, respectively.

Table 4. Characteristics of powders of NiMoAl–Cr_2AlC system for HVOF-deposition

Powder name	Element composition, wt.%					Phase composition	Average particle size, μm
	Ni	Mo	Cr	Al	C		
NiMoAl	54	44	–	2	–	Ni, Mo	70.98 ± 1.5
NiMoAl–10 wt.% Cr_2AlC	48.3	39.3	5.43	5.54	1.43	Ni, Mo, Cr_2AlC	69.54 ± 3.5
NiMoAl–20 wt.% Cr_2AlC	43.2	35.2	11.2	7.5	2.9	Ni, Mo, Cr_2AlC	68.12 ± 4.0
NiMoAl–50 wt.% Cr_2AlC	27	22	27.96	15.99	7.05	Ni, Mo, Cr_2AlC	79.38 ± 5.0
Cr_2AlC	–	–	55.99	29.98	14.03	Cr_2AlC	66.34 ± 1.5

Formation of a denser microstructure can be the consequence of addition of fine Cr_2AlC particles to NiMoAl matrix and their uniform distribution in the coating structure, which leads to their densification.

Addition of Cr_2AlC powder to NiMoAl alloy powder leads to increase of both the coating hardness and modulus of elasticity. Average nanohardness of NiMoAl, NiMoAl–10 % Cr_2AlC, NiMoAl–20 % Cr_2AlC, NiMoAl–50 % Cr_2AlC and Cr_2AlC coatings is equal to 390 ± 20, 446 ± 20, 501 ± 20, 637 ± 20 and 663 ± 20 $VHN_{0.001}$, respectively; modulus of elasticity is 193 ± 4.201, 201 ± 5, 209 ± 3, 221 ± 6 and 264 ± 5 GPa, respectively.

Among the studied composite coatings NiMoAl-20 wt.% Cr_2AlC coating has the lowest friction coefficient and highest wear resistance under the conditions of sliding friction, which was determined by pin-on-disk procedure. Increase of the strengthening phase amount to 50 wt.% Cr_2AlC leads to lowering of the tribological properties, because of poor cohesion strength of the coating.

FORMATION OF COATINGS CONTAINING Cr_2AlC MAX PHASE UNDER THE CONDITIONS OF COLD GAS-DYNAMIC SPRAYING

Investigations of formation of coatings containing Cr_2AlC MAX phase under the conditions of cold gas-dynamic spraying were conducted in work [34]. Spraying was performed using powder of Sandvik Company (Sweden), which was ground prior to that to particle size d_{10} = 2 μm, d_{50} = 9 μm, d_{90} = 23 μm. Spraying was conducted using Impact 5/11 System of Impact Innovations Company (Rattenkirchen, Germany). Nitrogen at the pressure of 50 bar and 1000 °C temperature was used as the carrier and working gas.

In the produced coating, similar to the powder, the main phase is Cr_2AlC MAX phase (approximately 68 % in the powder and 79 % in the coating); secondary phases are chromium carbides, such as Cr_7C_3 (approximately 17 % in the powder and 10 % in the coating) and Cr_3C_2 (approximately 16 % in the powder and 12 % in the coating). It is noted that as the phase content in the coatings and powder was determined by comparing the peak height on the roentgenograms, the obtained data on their amount are of a tentative nature.

It is shown that at collision of Cr_2AlC MAX phase particles with the substrate, their plastic deformation and spreading take place, resulting in formation of a dense microstructure of the coating (porosity <3 %) and an interface with the steel base (Figure 8, *a*). Coating thickness is nonuniform and varies from 200 to 320 μm. Coatings are characterized by local heterogeneity of the microstructure and presence of cracks and delaminations (Figure 8, *b*), which is caused by insufficient strength of cohesion between the particles. Availability of such coating defects is attributable to nonuniform powder feeding, because of its low flowability and vibration mode of operation of the

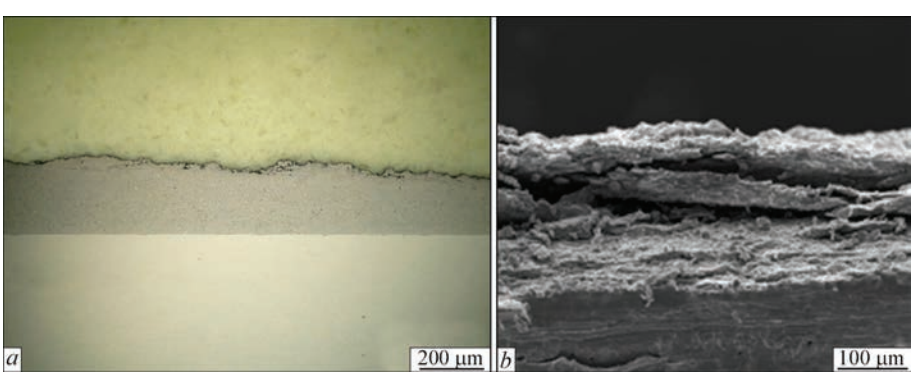

Figure 8. Cr_2AlC coating produced by the method of cold gas-dynamic spraying: *a* — microstructure; *b* — appearance of coating cracking

Table 5. Technological parameters of cold gas-dynamic deposition of powder based on MAX phase Cr_2AlC

Gas pressure (N_2), bar	Spraying distance, mm	Number of passes	Gas temperature (N_2), °C
40	60	10	650
			750
			950

powder feeder, which may lead to power fraction separation into particles of different size. It is noted that increasing the coating quality required performance of further investigations on improvement of technological properties of the powders and optimization of cold spraying parameters.

Coating microhardness is equal to 585 ± 63 $HV_{0.1}$, nanohardness is 1153 ± 321 $HV_{0.001}$. The difference in micro- and nanohardness values is attributable to the difference in measurement procedures. Loading at nanoindentation is much smaller, and, thus the indentations are limited to the plane of one deformed coating particle and reflect its properties. Results of microindentation reflect the averaged value of microhardness of the entire coating and they largely depend on cohesion between the particles and presence of pores in the coatings. Proceeding from photos of indentations from nanoindenter, the measured nanohardness corresponds to hardness of chromium carbide and hardness of the interface between the carbide particles and Cr_2AlC inclusions.

In work [35] the method of cold gas-dynamic spraying was used to produce relatively dense (9 % porosity) of the coating with up to 98 % MAX phase content. Powder produced by sintering a mixture of Cr_3C_2, Cr, Al powders (in the ratio of 1:1:2.05) at 1300 °C in argon atmosphere for 2 h with subsequent grinding in a planetary mill for 2 h was used as the spraying material. The produced powder has high purity, its main phase (>98 %) being Cr_2AlC MAX phase with admixtures of Cr_7C_3 carbide, Cr_2Al aluminide and Al_2O_3 oxide. Particle size is equal to: d_{10} = 4.1 μm, d_{50} = 7.6 μm, d_{90} = 13.2 μm.

Spraying was conducted onto a stainless steel substrate using Kinetiks 8000 system (Oerlikon Metco, Switzerland) with application of technological parameters, shown in Table 5.

Coatings of 40–100 μm thickness were formed as a result of spraying. The coating phase composition corresponds to that of the powder, which is indicative of absence of particle oxidation during spraying and degradation of Cr_2AlC MAX phase.

It is shown that at increase of gas temperature from 650 to 950 °C denser coatings are formed (porosity decreases from 12.4 to 9.1 %, respectively) and the number of cracklike defects is reduced. This is attributable to increase of temperature and velocity of the sprayed particles and degree of their deformation at collision with the base. It results in greater cohesion between the particles and formation of coatings with a smaller number of defects. No cracks or delaminations were observed on the interface of the coating–steel substrate, which is indicative of a good strength of cohesion with the substrate. At the same time, it is noted that at increase of working gas temperature from 650 to 950 °C the value of residual stresses in the coatings increases from 200 up to 310 MPa, respectively, and it may lead to coating delamination during operation.

The possibility of using a coating with Cr_2AlC MAX phase as a bond coat in the thermal barrier coating system of a bond coat–main thermal barrier layer of ZrO_2–Y_2O_3 was considered. A Cr_2AlC bond coat was deposited on the steel substrate by cold spraying and a ZrO_2–Y_2O_3 coating was applied over it by the plasma method. No spallations, delaminations or secondary phase formation as a result of the reaction on the bond coat–main layer interface are observed. This is indicative of the potential for application of Cr_2AlC coating produced by the method of cold gas-dynamic spraying, as a bond coat in thermal barrier coating systems.

CONCLUSIONS

Based on the conducted analysis of the specialized scientific literature, the possibility was shown of producing coatings, containing Cr_2AlC MAX phase, by the methods of thermal spraying, using both synthesized powders with a high content of the MAX phase, and a mechanical mixture of individual elements.

One of the most critical aspects during the process of thermal spraying of coatings containing Cr_2AlC MAX phase, is particle oxidation and running of undesirable reactions with MAX phase decomposition and reduction of its amount in the coatings. These decompositions are caused by noncongruent melting of MAX phases, which, certainly, is one of the main difficulties of their spray deposition.

When deposition is performed using powders, where the main phase is Cr_2AlC MAX phase, it is rational to apply high-velocity thermal spraying methods, such as high-velocity plasma, high-velocity flame and cold gas-dynamic spraying. Owing to high velocities of particle flight, the time of interaction with oxygen and high-temperature jet is reduced, which allows producing coatings, where the phase composition corresponds to that of the deposited powder. However, coatings based on Cr_2AlC MAX phase produced by the method of cold gas-dynamic spraying, are characterized by presence of cracks and inner delaminations, considering their low cohesive strength.

Powders of a mechanical mixture of (Cr + Al + graphite, Cr_3C_2 + Al + Cr) initial components are used in plasma spraying. In this case, Cr_2AlC MAX phase synthesis occurs directly during deposition and formation of the coating layer at interaction of the initial components. Increase of MAX phase content in these coatings can be achieved through their further heat treatment.

Under the conditions of the above-mentioned deposition methods dense coatings with <9 % porosity and dense interface with the steel substrates are formed. Coating hardness depends mainly on their phase composition, and it varies from 5 to 11 GPa.

On the whole, the need for further development of materials for deposition and optimisation of the processes of producing the coatings is stated in the works devoted to investigations of formation of thermal coatings containing Cr_2AlC MAX phase.

REFERENCES

1. Sokol, M., Natu, V., Kota, S., Barsoum, M.W. (2019) On the chemical diversity of the MAX phases. *Trends in Chemistry*, 1(**2**), 210–223. DOI: https://doi.org/10.1016/j.trechm.2019.02.016
2. Gonzalez□Julian, J. (2021). Processing of MAX phases: From synthesis to applications. *J. of the American Ceramic Society*, 104(**2**), 659–690. DOI: https://doi.org/10.1111/jace.17544
3. Lin, Z.J., Li, M.S., Wang, J.Y., Zhou, Y.C. (2007) High-temperature oxidation and hot corrosion of Cr_2AlC. *Acta Materialia*, 55(**18**), 6182–6191. DOI: https://doi.org/10.1016/j.actamat.2007.07.024
4. Barsoum, M.W., Radovic, M. (2011) Elastic and mechanical properties of the MAX phases. *Annual Review of Materials Research*, **41**, 195–227. DOI: https://doi.org/10.1146/annurev-matsci-062910-100448
5. Tian, W., Wang, P., Zhang, G. et al. (2006) Synthesis and thermal and electrical properties of bulk Cr_2AlC. *Scripta Materialia*, 54(**5**), 841–846. DOI: https://doi.org/10.1016/j.scriptamat.2005.11.009
6. Tian, W.B., Wang, P.L., Zhang, G.J. et al. (2007) Mechanical properties of Cr_2AlC ceramics. *J. of the American Ceramic Society*, 90(**5**), 1663–1666. DOI: https://doi.org/10.1111/j.1551-2916.2007.01634.x
7. Li, S.B., Yu, W B., Zhai, H.X. et al. (2011) Mechanical properties of low temperature synthesized dense and fine-grained Cr_2AlC ceramics. *J. of the European Ceramic Society*, 31(**1–2**), 217–224. DOI: https://doi.org/10.1016/j.jeurceramsoc.2010.08.014
8. Tian, W., Wang, P., Zhang, G. et al. (2007) Effect of composition and processing on phase assembly and mechanical property of Cr_2AlC ceramics. *Materials Sci. and Eng.: A*, **454**, 132–138. DOI: https://doi.org/10.1016/j.msea.2006.11.032
9. Ying, G., He, X., Li, M. et al. (2011) Synthesis and mechanical properties of high-purity Cr_2AlC ceramic. *Materials Sci. and Eng.: A*, 528(**6**), 2635–2640. DOI: https://doi.org/10.1016/j.msea.2010.12.039
10. Manoun, B., Gulve, R.P., Saxena, S.K. et al. (2006) Compression behavior of M_2AlC (M = Ti, V, Cr, Nb, and Ta) phases to above 50 GPa. *Physical Review B*, 73(**2**), 024110. DOI: https://doi.org/10.1103/physrevb.73.024110
11. Tian, W., Sun, Z., Du, Y., Hashimoto, H. (2009) Mechanical properties of pulse discharge sintered Cr_2AlC at 25–1000 °C. *Materials Letters*, 63(**8**), 670–672. DOI: https://doi.org/10.1016/j.matlet.2008.12.024
12. Panigrahi, B.B., Chu, M.C., Kim, Y.I. et al. (2010) Reaction synthesis and pressureless sintering of Cr_2AlC powder. *J. of the American Ceramic Society*, 93(**6**), 1530–1533. DOI: https://doi.org/10.1111/j.1551-2916.2009.03560.x
13. Xiao, L.O., Li, S.B., Song, G., Sloof, W.G. (2011) Synthesis and thermal stability of Cr_2AlC. *J. of the European Ceramic Society*, 31(**8**), 1497–1502. DOI: https://doi.org/10.1016/j.jeurceramsoc.2011.01.009
14. Tian, W., Sun, Z., Du, Y., Hashimoto, H. (2008) Synthesis reactions of Cr_2AlC from Cr–Al_4C_3–C by pulse discharge sintering. *Materials Letters*, 62(**23**), 3852–3855. DOI: https://doi.org/10.1016/j.matlet.2008.05.001
15. Yeh, C.L., Kuo, C.W. (2011) Effects of Al and Al_4C_3 contents on combustion synthesis of Cr_2AlC from Cr_2O_3–Al–Al_4C_3 powder compacts. *J. of Alloys and Compounds*, 509(**3**), 651–655. DOI: https://doi.org/10.1016/j.jallcom.2010.09.169
16. Duan, X., Shen, L., Jia, D. et al. (2015) Synthesis of high-purity, isotropic or textured Cr_2AlC bulk ceramics by spark plasma sintering of pressure-less sintered powders. *J. of the European Ceramic Society*, 35(**5**), 1393–1400. DOI: https://doi.org/10.1016/j.jeurceramsoc.2014.11.008
17. Yeh, C.L., Yang, W.J. (2013) Formation of MAX solid solutions (Ti, V)$_2$AlC and (Cr, V)$_2$AlC with Al_2O_3 addition by SHS involving aluminothermic reduction. *Ceramics Inter.*, 39(**7**), 7537–7544. DOI: https://doi.org/10.1016/j.ceramint.2013.03.005
18. Yembadi, R., Panigrahi, B.B. (2017) Thermodynamic Assessments and mechanically activated synthesis of ultrafine Cr_2AlC MAX phase powders. *Advanced Powder Technology*, 28(**3**), 732–739. DOI: https://doi.org/10.1016/j.apt.2016.11.020
19. Li, J.J., Qian, Y.H., Niu, D. et al. (2012) Phase formation and microstructure evolution of arc ion deposited Cr_2AlC coating after heat treatment. *Applied Surface Sci.*, **263**, 457–464. DOI: https://doi.org/10.1016/j.apsusc.2012.09.082
20. Mockute, A., Persson, P.O., Magnus, F. et al. (2014) Synthesis and characterization of arc deposited magnetic (Cr, Mn)$_2$AlC MAX phase films. *Physica Status Solidi (RRL)–Rapid Research Letters*, 8(**5**), 420–423. DOI: https://doi.org/10.1002/pssr.201409087
21. Wang, Z., Ma, G., Liu, L. et al. (2020) High-performance Cr_2AlC MAX phase coatings: Oxidation mechanisms in the 900–1100 °C temperature range. *Corrosion Sci.*, **167**, 108492. DOI: https://doi.org/10.1016/j.corsci.2020.108492
22. Stevens, M., Pazniak, H., Jemiola, A. et al. (2021) Pulsed laser deposition of epitaxial Cr_2AlC MAX phase thin films on MgO (111) and Al_2O_3 (0001). *Materials Research Letters*, 9(**8**), 343–349. DOI: https://doi.org/10.1080/21663831.2021.1920510
23. Lange, C., Hopfeld, M., Wilke, M. et al. (2012) Pulsed laser deposition from a pre-synthesized Cr_2AlC MAX phase target with and without ion-beam assistance. *Physica Status Solidi (A)*, 209(**3**), 545–552. DOI: https://doi.org/10.1002/pssa.201127537
24. Li, Y., Zhao, G., Qian, Y. et al. (2018) Deposition of phase-pure Cr_2AlC coating by DC magnetron sputtering and post annealing using Cr–Al–C targets with controlled elemental composition but different phase compositions. *J. Mater. Sci. & Technol.*, 34(**3**), 466–471. DOI: https://doi.org/10.1016/j.jmst.2017.01.029
25. Qureshi, M.W., Ma, X., Tang, G. et al. (2021) Fabrication and mechanical properties of Cr_2AlC MAX phase coatings on TiBw/Ti6Al4V composite prepared by HiPIMS. *Materials*, 14(**4**), 826. DOI: https://doi.org/10.3390/ma14040826

26. Naveed, M., Obrosov, A., Zak, A. et al. (2016) Sputtering power effects on growth and mechanical properties of Cr_2AlC MAX phase coatings. *Metals*, 6(**11**), 265. DOI: https://doi.org/10.3390/met6110265
27. Liu, J., Zuo, X., Wang, Z. et al. (2018) Fabrication and mechanical properties of high purity of Cr_2AlC coatings by adjustable Al contents. *J. of Alloys and Compounds*, **753**, 11–17. Doi: 10.1016/j.jallcom.2018.04.100.
28. Gonzalez□Julian, J., Mauer, G., Sebold, D. et al. (2020) Cr_2AlC MAX phase as bond coat for thermal barrier coatings: Processing, testing under thermal gradient loading, and future challenges. *J. of the American Ceramic Society*, 103(**4**), 2362–2375. DOI: https://doi.org/10.1111/jace.16935
29. Zhang, F., Yan, S., Li, C. et al. (2019) Synthesis and characterization of MAX phase Cr_2AlC based composite coatings by plasma spraying and post annealing. *J. of the European Ceramic Society*, 39(**16**), 5132–5139. DOI: https://doi.org/10.1016/j.jeurceramsoc.2019.08.039
30. Zhang, F., Yu, G., Yan, S. et al. (2023) Characterization and reaction mechanism of in-situ micro-laminated Cr_2AlC coatings by plasma spraying Cr_3C_2/Al/Cr powder mixtures. *Surf. and Coat. Technol.*, **456**, 129271. DOI: https://doi.org/10.1016/j.surfcoat.2023.129271
31. Davis, D., Srivastava, M., Malathi, M. et al. (2018) Effect of Cr_2AlC MAX phase addition on strengthening of Ni–Mo–Al alloy coating on piston ring: Tribological and twist-fatigue life assessment. *Applied Surface Sci.*, **449**, 295–303. DOI: https://doi.org/10.1016/j.apsusc.2018.01.146
32. Davis, D., Singh, S., Chakradhar, R.P.S., Srivastava, M. (2020). Tribo-mechanical properties of HVOF-sprayed Ni-MoAl–Cr_2AlC composite coatings. *J. Thermal Spray Technol.*, **29**, 1763–1783. DOI: https://doi.org/10.1007/s11666-020-01069-8
33. Chen, Y., Chu, M., Wang, L. et al. (2012) Microstructure and performance of Cr(2)AlC coatings deposited by HVOF spraying. *Chinese J. of Rare Metals*, 36(**4**), 568–573. DOI: https://doi.org/10.3969/j.issn.0258-7076.2012.04.011
34. Elsenberg, A., Busato, M., Gärtner, F. et al. (2021) Influence of MAX phase deformability on coating formation by cold spraying. *J. Thermal Spray Technol.*, **30**, 617–642. DOI: https://doi.org/10.1007/s11666-020-01110-w
35. Go, T., Sohn, Y.J., Mauer, G. et al. (2019) Cold spray deposition of Cr_2AlC MAX phase for coatings and bond-coat layers. *J. of the European Ceramic Society*, 39(**4**), 860–867. DOI: https://doi.org/10.1016/j.jeurceramsoc.2018.11.035
36. Zhang, Z., Lim, S.H., Chai, J. et al. (2017) Plasma spray of Ti_2AlC MAX phase powders: Effects of process parameters on coatings' properties. *Surf. and Coat. Technol.*, **325**, 429–436. DOI: https://doi.org/10.1016/j.surfcoat.2017.07.006
37. Zhang, Z., Lai, D.M.Y., Lim, S.H. et al. (2018) Isothermal oxidation of the Ti_2AlC MAX phase coatings deposited by kerosene-fuelled HVOF spray. *Corrosion Sci.*, **138**, 266–274. DOI: https://doi.org/10.1016/j.corsci.2018.04.022
38. Gutzmann, H., Gärtner, F., Höche, D. et al. (2013) Cold spraying of Ti_2AlC MAX phase coatings. *J. Thermal Spray Technol.*, **22**, 406–412. DOI: https://doi.org/10.1007/s11666-012-9843-1
39. Rajkumar, Y., Rahul, B.M., Ananth Akash, P., Panigrahi, B.B. (2017) Nonisothermal sintering of Cr_2AlC powder. *Inter. J. of Applied Ceramic Technology*, 14(**1**), 63–67. DOI: https://doi.org/10.1111/ijac.12617

ORCID

N.V. Vihilianska: 0000-0001-8576-2095,| D.V. Filonenko: 0009-0004-9021-2425,
A.O. Yushchenko: 0009-0005-6636-8275,
C. Senderowski: 0000-0002-0331-3702,
J.-C. Grivel: 0000-0001-7835-9054

CONFLICT OF INTEREST

The Authors declare no conflict of interest

CORRESPONDING AUTHOR

N.V. Vihilianska
E.O. Paton Electric Welding Institute of the NASU
11 Kazymyr Malevych Str., 03150, Kyiv, Ukraine.
E-mail: pewinataliya@gmail.com

SUGGESTED CITATION

N.V. Vihilianska, D.V. Filonenko, A.O. Yushchenko, C. Senderowski, J.-C. Grivel (2024) Thermal spraying of coatings, containing Cr_2AlC MAX phase (Review). *The Paton Welding J.*, **3**, 24–32.

JOURNAL HOME PAGE

https://patonpublishinghouse.com/eng/journals/tpwj

Received: 16.11.2023
Received in revised form: 26.12.2023
Accepted: 03.04.2024

DOI: https://doi.org/10.37434/tpwj2024.03.05

PRODUCING ADVANCED ALLOYS BASED ON TITANIUM ALUMINIDES FOR MODERN AIRCRAFT ENGINE MANUFACTURING

O.V. Ovchinnikov[1], **S.V. Akhonin**[2], **V.O. Berezos**[2], **A.Yu. Severin**[2], **O.B. Galenkova**[3], **V.G. Shevchenko**[4]

[1]JSC "Titanium Institute"
180 Sobornyy Prosp., 69035, Zaporizhzhia, Ukraine
[2]E.O. Paton Electric Welding Institute of the NASU
11 Kazymyr Malevych Str., 03150, Kyiv, Ukraine
[3]SE "Ivchenko-Progress"
2 Ivanova Str., 69068, Zaporizhzhia, Ukraine
[4]Zaporizhzhia Polytechnic National University
64 Zhukovskoho Str., 69063, Zaporizhzhia, Ukraine

ABSTRACT

Works have been performed on optimization of the technological scheme of producing ingots for consumable electrodes with a stable chemical composition and properties. The paper presents the results of studying an ingot of 195 mm diameter from a titanium aluminide-based alloy of Ti–28Al–7Nb–2Mo system, made by double electron beam remelting. Further ingot remelting in the arc furnace was performed, which allowed producing a homogeneous and defect-free ingot of an optimal composition of Ti–28Al–7Nb–2Mo–0.3 (Y, Re, B). The influence of modifying on the structure and properties was studied. It was determined that addition of surfactants promotes refining of the structural components and improvement of the alloy mechanical properties.

KEYWORDS: electron beam melting, vacuum-arc melting, ingot, titanium aluminide, modifying, structure, mechanical properties

INTRODUCTION

The development of modern aircraft engine manufacturing requires the use of new materials with enhanced properties and functional characteristics, which are ensured by the stability of chemical composition and structure and depend on the manufacturing technology [1]. Technological aspects, including optimization of technological parameters, repeatability of the obtained results and shaping are interrelated. The impact of technology on the properties of aircraft materials requires process regulation, for example, the use of vacuum-arc remelting in the production of titanium alloys [2, 3].

Titanium aluminide-based alloys, whose properties depend on the parameters of technological processes, are among the advanced materials for the aircraft industry. These alloys are an important class of structural materials with a unique set of physical and mechanical properties. Intermetallic alloys based on titanium aluminides are characterised by low density, high heat strength, heat resistance, and thermal stability. They have a high potential for replacing nickel-based alloys designed for operation at temperatures of up to 850 °C [4].

Heat-strength titanium aluminide-based alloys are characterised by a multicomponent chemical composition. The individual alloying elements of these alloys differ significantly in thermal and physical properties and density. Therefore, it is necessary to provide a uniform distribution of alloy components at the nominal level throughout the whole ingot volume, as macrosegregations may cause arising of different microstructures and, consequently, high anisotropy of mechanical properties.

The industrial development of titanium aluminide-based alloys involves the production of high-quality semi-finished ingots with a uniform distribution of elements and a homogeneous structure with stable physical, mechanical and operational characteristics.

Mechanical properties largely depend on the ultimate shaping technology for which the optimal chemical composition was developed.

When developing the alloy composition, it is necessary to focus on the peculiarities of the technological process of manufacturing stator and rotor engine parts, such as turbine blades. Motor Sich enterprise uses consumable electrodes of its own production for the smelting vacuum-arc furnace to produce titanium alloy shaped castings [5–7].

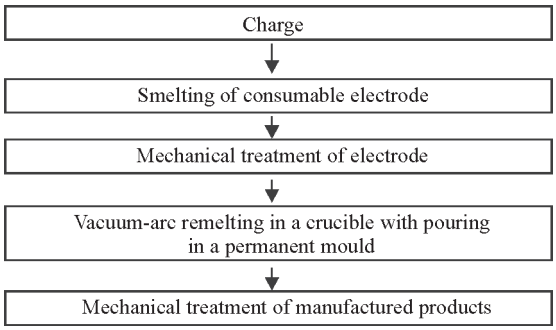

Figure 1. Scheme of the technological process for manufacturing titanium aluminide products

To introduce new titanium aliminide-based alloys for advanced engines, it is necessary to develop the entire technological process, taking into account the ultimate shaped casting technology and ensuring the chemical composition and mechanical properties of the alloy.

Taking into account the serial technological process of casting from the consumable electrode with a diameter of more than 200 mm, the aim of the work is to produce industrial ingots for consumable electrodes from titanium aluminide with stable chemical composition and properties.

RESEARCH PROCEDURE, EQUIPMENT AND MATERIALS

The object of the research was the technological processes of casting, which included the operations of producing a consumable electrode, remelting of the electrode in a crucible and pouring of metal from a crucible in a permanent mould (Figure 1). As a product, a turbine blade of the last stage made of a nickel-based VZhL12E-VI alloy was chosen. Taking into account earlier research works [8, 9], to ensure service properties, the following composition of the alloy based on titanium aluminide Ti–28Al–7Nb–2Mo–0.3 (Y, Re, B) was substantiated.

To smelt ingots from the charge, well-optimized technologies [10–12] for manufacturing aircraft materials by electron beam melting (EBM) of charge in the UE-208M unit were used [13] (Figure 2).

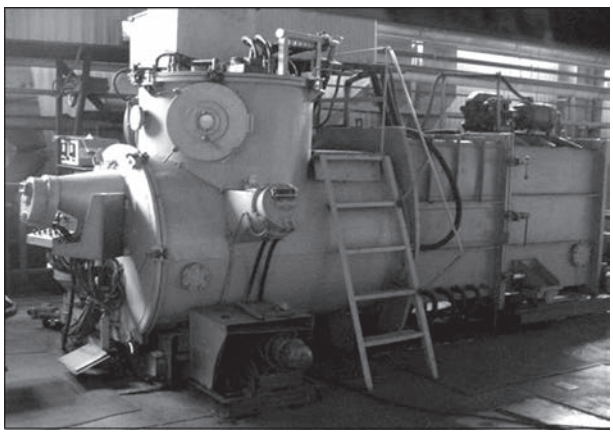

Figure 2. Appearance of electron beam unit UE-208M

For the studies, the ingot of the basic composition Ti–28Al–7Nb–2Mo was melted using the EBR method, which made it possible to correct the chemical composition and additional charging.

Stability of the chemical composition of the base alloy was achieved by double remelting. During the first remelting, refractory alloying elements such as niobium and molybdenum were introduced into the alloy. During the second remelting, aluminium was added to the ingot to account for evaporation losses. This allowed minimising aluminium losses and ensured that refractory alloying elements were dissolved and unifromly distributed over the length and cross-section of the ingot.

Ingot smelting was carried out in accordance with the capacities and configuration of ingot surface heating in the mould built in accordance with the calculated mathematical models [14].

The melting parameters of an ingot with a diameter of 195 mm from titanium aluminide Ti–28Al–7Nb–2Mo are as follows:

total power of EB heating, kW	60
power in the mould, kW	18
melting rate, kg/h	60

After loading the charge (Figure 3, *a*), the unit was pumped down to a residual pressure of 10^{-2} Pa in the gun chamber and 10^{-1} Pa in the melting chamber. Then the billet was melted in a cold hearth until it was filled and the liquid metal was periodically poured in a copper water-cooled mould (Figure 3, *b*). The first portions of the discharge were used to form the dummy bar for the future ingot to a height equal to the inner diameter of the mould, at which, according to mathematical calculations, the melting transfers to a quasi-stationary mode. The ingot of the required height was smelted at the achieved technological mode.

The composition of the charge for smelting basic and modified ingots: aluminium of A5 grade according to GOST 11069–2001, titanium billet (remelting of initial charge of titanium sponge of grade TG-100) according to DSTU 3-25-22–94; niobium (rods); master alloy (93 % Ti–7 % Mo); master alloy Al–Re, Al–Y, aluminoboron. The master alloys were produced by melting pieces of sponge titanium and aluminium with the corresponding elements Y, Re and B in the form of powders in a vacuum in a copper mould using a nonconsumable tungsten electrode. In such a way, master alloys with the content of modifying elements of 5, 10 and 15 % each, for example, Ti–5 % Y, A1–5 % Y, Ti–10 % Re, etc. were produced to ensure

Figure 3. Charge billet (*a*) and electron beam melting process (*b*) of titanium aluminide ingot Ti–28Al–7Nb–2Mo

the required concentration of elements in the composition of the experimental alloy.

To produce an ingot of a specified composition with modifiers Y, Re, B, to determine the transition coefficients of alloying elements and to model the processes occurring in electron beam melting, the alloy of the base composition was remelted in an arc furnace with a nonconsumable electrode with a controlled atmosphere (Figure 4) [15, 16].

To determine the chemical composition of the base alloy, samples in the form of a chip were taken from the melted ingot. Samples for analysis were taken from the head, middle and bottom parts of the ingot along its length. The content of alloying elements was determined by the method of inductively coupled plasma of optical emission spectrometry (ICP-OES) using an ICP spectrometer ICAP 6500 DUO. To determine the content of oxygen, nitrogen, and hydrogen, the ELTRA gas analyser was applied with the use of cylindrical samples of 3 mm in diameter and length. The essence of determining gas mixtures consisted in burning the mentioned samples and determining the volume of gaseous chemical elements that have been released.

The chemical composition of the alloy was analysed on the samples taken along the entire length of the ingot using a spectral reference-free method in an Expert 3L energy dispersive X-ray fluorescence analyser.

The etching of the samples for metallographic examinations was performed in the Titan etchant with the composition $HF:HNO_3:H_2O = 1:2:6$.

The macrostructure of the template was evaluated by the naked eye over the ingot thickness. The microstructure of the ingot material was examined with the use of the AxioObserver 5 optical microscope at magnifications from 25 to 200.

Tensile mechanical properties were determined in accordance with DSTU ISO 6892-1:2019. The samples for testing were cut out transversely to the ingot axis.

During the statistical processing of the experimental data, the dispersion and standard deviation were determined.

RESEARCH RESULTS AND DISCUSSION

As a result of the research, an ingot Ti–28Al–7Nb–2Mo with a diameter of 195 mm and a mass of 106 kg was produced (Figure 5, *a*). The ingot had no external coarse defects (tears and cold laps), the surface was satisfactory with small corrugations.

To eliminate cast defects in the form of corrugations, the ingot surface was subjected to turning to a depth of 5 mm (Figure 5, *b*).

Figure 4. Arc furnace with nonconsumable electrode

Figure 5. Appearance of the base composition ingot before (*a*) and after mechanical treatment (*b*)

Table 1. Chemical composition of the ingot with a diameter of 195 mm, wt.%

Alloy	Sample, sampling location	Ti	Al	Nb	Mo	O	N	H
Ti–28Al–7Nb–2Mo (without modifiers)	1 (top)	Base	26.6	7.6	2.0	0.13	<0.01	<0.005
	2		27.4	7.5	–»–			
	3		27.2	–»–	2.1			
	4		31.0	7.2	1.9			
	5 (bottom)		30.5	7.3	2.2			

From the produced ingot without modifiers, the samples for ICP analysis were taken according to the scheme shown in Figure 6. The data of chemical analysis are presented in Table 1.

The deviation in the aluminium content in the head and bottom parts is explained by nonstationary melting modes at the beginning and end of melting during the dummy bar formation and removal of the shrinkage cavity, respectively. The levelling of the content by alloying elements and the achievement of the required chemical composition were further planned with the use of an arc furnace.

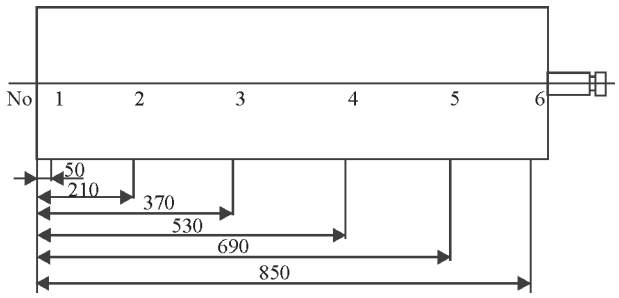

Figure 6. Scheme of sampling (1–6) from the ingot with a diameter of 195 mm

To provide the optimal chemical composition, parts were cut off from an ingot of 195 mm diameter, which were additionally charged with modifiers and remelted with the use of a small-scale furnace shown in Figure 4. The vacuum-arc remelting of the electrode was performed in a graphite MPG-7 crucible, and the metal was poured in a permanent mould (Figure 7).

The chemical composition of the alloy was analysed on the samples taken along the entire length of the ingot from the upper, middle and lower parts (Table 2).

Due to the fact that when smelting titanium alloys in a graphite crucible, the carbon content does not exceed the admissible limits of 0.10–0.15 %, the carbon content for experimental melting was not studied.

Figure 7. Appearance of graphite crucible (*a*) and permanent mould (*b*) for vacuum-arc remelting

The results of studying chemical composition of the metal showed a uniform distribution of alloying elements along the length of the melted ingots.

Transverse templates were cut out from the ingots and macrosections were made to control the structure. It was found, that in the ingots, a homogeneous and dense structure was formed. No defects in the form of pores, cavities or cracks visible to the naked eye were detected.

The macrostructure of the ingot without modifiers is characterised by grains close to equilibrium. The grain size corresponds to 8-9 numbers of the 10-number scale of titanium alloys' macrostructures (Figure 8, *a*).

The macrostructure of the ingot with modifiers contains smaller grains corresponding to 2–3 numbers of the macrostructure scale (Figure 8, *b*).

No difference in the grain size number in the central part of the ingot and on the periphery was found.

During a metallographic examination of the produced ingots, a significant effect of modifiers on the morphology of the alloy structure was revealed. Thus, the microstructure of the alloy without modifiers was characterised by a coarse-grained structure, in the middle of which there are colonies of light and dark coloured plates of 100–350 μm in size, disoriented within one grain (Figure 9, *a*). The combined effect of the three modifiers in the amount of 0.1 % each led to the formation of a fine-grained duplex ($\alpha_2+\gamma$)-structure with the sizes of plate colonies of not more than 30 μm (Figure 9, *b*).

The main mechanical properties of the Ti–28Al–7Nb–2Mo (Y, Re, B) alloy are as follows: σ_t, MPa – 800–870; δ, % — 0.8–1.3.

As is known, cast titanium aluminide-based alloys have almost zero ductility, which makes it very difficult to conduct standard tensile tests, but the analysis of literature data showed that the tensile strength of cast alloys of a similar composition is at a level of 500 MPa [17], while with the combined introduction of modifiers, an increase in strength of up to 800 MPa is achieved, i.e. almost 2 times compared to the initial one.

Based on the results of the carried out research, a scheme was developed that corresponds to the industrial technology and includes the manufacture of a consumable electrode by double remelting, its additional charging with modifiers to provide the optimal chemical composition in an arc furnace with a controlled atmosphere and subsequent pouring of metal in a permanent mould.

For this scheme, optimal melting modes have been calculated and proven, that ensure the absence of anisotropy of properties both when introducing refractory elements in the ingot of the basic composition, as well as when producing a consumable electrode of a modified composition during smelting in a permanent mould.

Table 2. Chemical composition of the ingot with modifiers, wt.%

Alloy	Sampling location	Ti	Al	Nb	Mo	Modifiers		
						Y	Re	B
Ti–28Al–7Nb–2Mo–0.3 (Y, Re, B)	Top	Base	28.3	7.5	2.0	0.13	0.09	0.10
	Middle		28.7	7.6	1.8	0.09	0.12	–»–
	Bottom		29.4	7.5	2.1	0.08	0.08	0.12

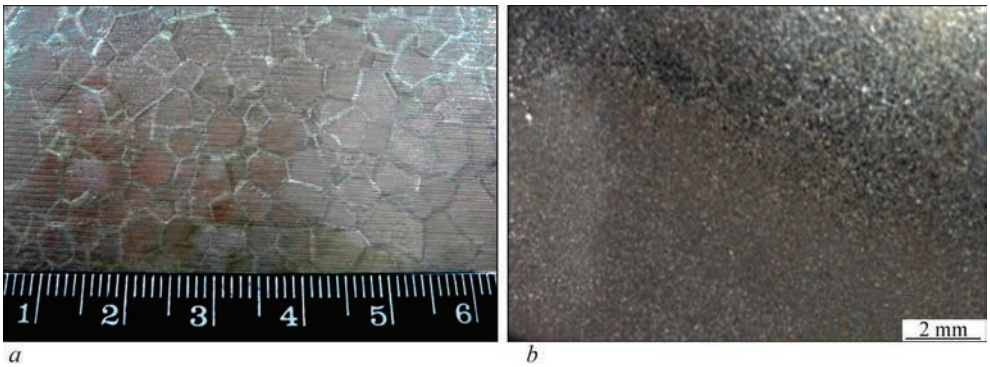

Figure 8. Macrostructure of ingots after etching: *a* — without modifiers; *b* — with modifiers

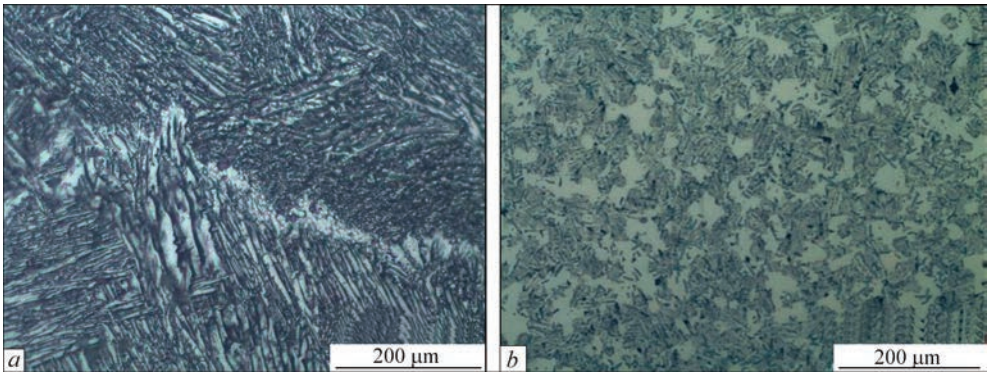

Figure 9. Microstructure of ingots after etching: *a* — without modifiers; *b* — with modifiers, ×200

It was established that in the end product, due to the uniform distribution of alloying and modifying elements and the absence of a gradient of elements' concentrations, the structure was significantly refined from 8–9 to 2–3 numbers of the macrostructure grain, which is an important parameter for ensuring the quality of casting products.

The grain refinement of the cast structure was achieved by introducing modifiers Y, Re, and B, which contribute to a reduction in grain size, lead to a change in phase morphology, refine grain boundaries from impurities, delay the development of diffusion processes at the boundary interface and inhibit the processes of growth of structural components. This, in turn, made it possible to improve the mechanical characteristics of the material, including strength and ductility.

The tensile strength of the experimental alloy was 800–870 MPa, the relative elongation was 0.8–1.3 % at the tensile strength of the serial VZhL12E-VI alloy at a level of ≥ 830 MPa.

Thus, it is shown that the technological process with the established modes makes it possible to manufacture serial products of the experimental alloy from titanium aluminide instead of a serial nickel-based alloy. The reduction in weight of one blade, taking into account the density of experimental and serial alloys, amounts to 34 % and is a significant advantage of the experimental alloy for rotor parts operating at high temperatures.

CONCLUSIONS

1. Technological scheme for smelting titanium aluminide ingots of the Ti–28Al–7Nb–2Mo system by the EBR method with the use of certain technological modes is proposed. The use of double remelting provided a uniform distribution of refractory elements and elements with a high vapour pressure along the ingot length and cross-section.

2. Further remelting of titanium aluminide ingot in an arc furnace with a controlled atmosphere was carried out, the transition coefficients of alloying elements were determined, and a homogeneous and defect-free ingot of the composition Ti–28Al–7Nb–2Mo (Y, Re, B) was produced.

3. In the end product, the structure of the cast metal was significantly refined — from 8–9 to 2–3 numbers of macrostructure grains. The grain refinement of the cast structure was caused by the introduction of surface-active elements in the alloy, namely Y, Re, B. The microstructure of the alloy without modifiers was characterised by a coarse-grained structure, in the middle of which there were collonies of plates of 100–350 μm in size, disoriented within the same grain. The combined effect of three modifiers in the amount of 0.1 % each resulted in obtaining a fine-

grained duplex structure with the size of the plate colonies not exceeding 30 μm.

4. The tensile strength of the alloy of the optimal composition was 800–870 MPa, which is 1.7 times higher than the properties of the alloy of the base composition, and corresponded to the tensile strength of the serial VZhL12E-VI alloy.

5. The calculated reduction in weight of the blade when using the experimental alloy instead of a serial one amounts to 34 %, which is a significant advantage of the experimental alloy for rotor parts operating at high temperatures, rotation speeds and dynamic loads.

REFERENCES

1. Clemens, H., Mayer, S. (2016) Intermetallic titanium aluminides in aerospace applications — processing, microstructure and properties. *Mater. High Temp*., **33**, DOI: http://dx.doi.org/10.1080/09603409.2016.1163792
2. Chuchuryukin, A.D. (1991) Vacuum in titanium melting. In: *Physical metallurgy and processing of titanium and heat-resistant alloys.* Moscow, VILS, 159–163 [in Russian].
3. Sobolevskaya, T.D., Gishkina, V.I., Kovalenko, T.A. (2009) Influence of sponge titanium quality on presence of defects in semi-finished products and parts from titanium alloys. *Novi Materialy i Tekhnologii v Metalurgii ta Mashynobuduvanni,* **2**, 50–54 [in Russian].
4. Appel, F., Paul, J.D.H., Oehring, M. (2011) *Gammatitanium aluminide alloys: Science and Technology*. Weinheim, Wiley-VCH VerlagGmbH&Co. KGaA.
5. Ivchenko, Z.A., Lunyov, V.V. (2008) Manufacture of shaped castings and consumable electrodes from titanium alloys. *Metallovedenie i Termich. Obrab. Metallov,* **1**, 33–36 [in Russian].
6. Ivchenko, Z.A., Lunyov, V.V. (2010) Investigation of properties of castings produced by second remelting electrodes of VT5L alloy of domestic manufacture. *Protsessy Litiya,* **4**, 73–78 [in Russian].
7. Ivchenko, Z.A., Lunyov, V.V. (2010) Manufacture of consumable titanium electrodes by vacuum-arc melting from sponge titanium extruded briquettes. *Teoriya i Praktika Metallurgii,* **3–4**, 21–25 [in Russian].
8. Grigorenko, G.M., Akhonin, S.V., Severin, A.Yu. et al. (2014) Effect of alloying with boron and lanthanum on structure and properties of alloy on base of intermetallic compound TiAl. *Sovrem. Elektrometall.,* **2**, 15–20 [in Russian].
9. Akhonin, S.V., Severin, A.Yu., Berezos, V.O. et al. (2022) Producing ingots of Ti–28Al–7Nb–2Mo–2Cr titanium aluminide by electron beam melting. *Suchasna Elektrometal.,* **1**, 11–15 [in Ukrainian]. DOI: https://doi.org/10.37434/sem2022.01.01
10. Akhonin, S.V., Severin, A.Yu., Berezos, V.O. et al. (2020) Producing large-sized ingots of titanium aluminides by EBM method. *Suchasna Elektrometal.,* **2**, 18–22 [in Ukrainian]. DOI: https://doi.org/10.37434/sem2020.02.03
11. Akhonin, S.V., Severin, A.Yu., Berezos, V.O. (2015) Development of technology of adding the refractory alloying elements into alloys on the base of Ti_2AlNb intermetallic in electron beam melting. *Sovrem. Elektrometall.,* **3**, 12–15 [in Russian]..
12. Akhonin, S.V., Severin, A.Yu., Berezos, V.O. (2022) Mathematical modeling of evaporation processes at EBM of alloys based on titanium aluminide of Ti–Al–Nb–Cr–Mo alloying system. *Suchasna Elektrometal.,* **2**, 10–16 [in Ukrainian]. DOI: https://doi.org/10.37434/sem2022.02.02.
13. Akhonin, S.V., Pikulin, A.N., Berezos, V.A. et al. (2019) Laboratory electron beam unit UE-208M. *Sovrem. Elektrometall.,* **3**, 15–22 [in Russian]. DOI: http://dx.doi.org/10.15407/sem2019.03.03
14. Akhonin, S.V., Gorislavets, Yu.M., Glukhenkiy, A.I. et al. (2019) Modeling hydrodynamic and thermal processes in the mould in cold-hearth electron beam melting. *Suchasna Elektrometal.,* **4**, 9–17 [in Ukrainian]. DOI: https://doi.org/10.15407/sem2019.04.02
15. Ovchinnikov, A.V., Teslevich, S.M., Tizenberg, D.L., Efanov, V.S. (2019) Technology of melting ingots of cobalt alloy by the arc remelting method. *Sovrem. Elektrometall.,* **1**, 23–27 [in Russian]. DOI: http://dx.doi.org/10.15407/sem2019.01.03
16. Ovchynnykov, O.V., Kapustian, O.E. (2020) Technology for smelting zirconium alloy ingots by vacuum arc remelting with a nonconsumable electrode in a skull furnace. *Suchasna Elektrometal.,* **4**, 32–38 [in Ukrainian]. DOI: https://doi.org/10.37434/sem2020.04.06
17. Firstov, S.A., Gornaya, I.D., Podrezov, Yu.N. et al. (2018) Properties of alloys on titanium aluminide γ-TiAl/α_2–Ti_3Al base at complex alloying. *Sovrem. Elektrometall.,* **3**, 32–38 [in Russian]. DOI: http://dx.doi.org/10.15407/sem2018.03.05

ORCID

O.V. Ovchinnikov: 0000-0002-5649-1094,
S.V. Akhonin: 0000-0002-7746-2946,
V.O. Berezos: 0000-0002-5026-7366,
A.Yu. Severin: 0000-0003-4768-2363,
O.B. Galenkova: 0009-0008-6007-1931,
V.G. Shevchenko: 0000-0001-9037-6367

CONFLICT OF INTEREST

The Authors declare no conflict of interest

CORRESPONDING AUTHOR

V.O. Berezos
E.O. Paton Electric Welding Institute of the NASU
11 Kazymyr Malevych Str., 03150, Kyiv, Ukraine
E-mail: titan.paton@gmail.com

SUGGESTED CITATION

O.V. Ovchinnikov, S.V. Akhonin, V.O. Berezos, A.Yu. Severin, O.B. Galenkova, V.G. Shevchenko (2024) Producing advanced alloys based on titanium aluminides for modern aircraft engine manufacturing. *The Paton Welding J*., **3**, 33–39.

JOURNAL HOME PAGE

https://patonpublishinghouse.com/eng/journals/tpwj

Received: 22.12.2023
Received in revised form: 14.02.2024
Accepted: 03.04.2024

DOI: https://doi.org/10.37434/tpwj2024.03.06

ELECTROSLAG REMELTING OF TITANIUM UNDER VACUUM CONDITIONS

I.V. Protokovilov[1], **T. Beinerts**[2], **V.B. Porokhonko**[1], **D.A. Petrov**[1]

[1]E.O. Paton Electric Welding Institute of the NASU
11 Kazymyr Malevych Str., 03150, Kyiv, Ukraine
[2] Institute of Physics, University of Latvia
32 Miera Str., Salaspils LV-2169, Latvia

ABSTRACT

The results of experimental studies of the process of electroslag remelting of titanium in a chamber furnace at different values of pressure in the melting space, from vacuum to excess pressure, are given. Experiments were carried out during the melting of ingots with a diameter of 85 and 105 mm from titanium alloys VT1-0 and VT22 using fluoride-chloride flux AN-T4. The pressure of the inert gas in the furnace chamber was varied from 20 to 300 kPa. It is shown that in the entire studied range of pressures, the electroslag process proceeded stably with the formation of ingots with a high-quality side surface and a dense structure, without pores, slag inclusions and other internal defects. Experimental data on the effect of pressure in the melting space on the gas composition and structure of titanium ingots are given. The possibility of reducing the hydrogen content in titanium alloys by carrying out the electroslag process in vacuum conditions is shown. It was also established that the VT1-0 titanium ingot, melted under vacuum conditions, is characterized by a larger grain size compared to the ingot obtained under excess pressure.

KEYWORDS: electroslag remelting, chamber furnace, vacuum, titanium, gas composition, ingot, structure

INTRODUCTION

Due to the high chemical activity of titanium, in particular its interaction with atmospheric gases at temperatures above 400–450 °C, electroslag remelting (ESR) of titanium alloys should occur exclusively in chamber furnaces in a protective inert atmosphere [1–3]. Usually, in the ESR of titanium, the melting space is pre-vacuumed, and then filled with an inert gas (argon). The melting process is carried out under excess pressure of argon (120–140 kPa), which prevents air inflow in the event of leaks in the furnace units. At the same time, the melting process can be carried out both in a stagnant argon atmosphere and in a flowing one.

Such a scheme provides a reliable protection of the molten metal and consumable electrode heated to high temperatures from interaction with the air atmosphere and also prevents the evaporation of alloying components with high vapor elasticity. However, it also has certain disadvantages compared to melting under vacuum conditions.

It is known that hydrogen, which belongs to the category of harmful impurities because it causes hydrogen embrittlement of titanium alloys, has a reversible solubility in titanium. As the temperature increases and the pressure decreases, the solubility of hydrogen in titanium decreases significantly. Because of this, when remelting titanium in a vacuum, it is refined from hydrogen. This happens, for example, with vacuum-arc remelting (VAR) and electron beam melting of titanium alloys [4, 5]. When remelting titanium under excess pressure, hydrogen removal occurs to a much lesser extent or does not occur at all.

In addition, the remelting of titanium under conditions of excess pressure creates, unfavorable conditions for the removal of moisture, which can be adsorbed by the material of the consumable electrode, salt residues on the inner surface of the furnace chamber, etc. To a greater extent, this applies to the remelting of electrodes pressed from spongy titanium (or titanium shavings). This is due to the fact that in the process of storing the titanium sponge, during the production of consumable electrodes from it, their transportation and storage, physical adsorption of moisture by the developed surface of the sponge titanium (and residual chlorine salts which were not completely removed from the sponge titanium) is possible. It should be noted that atmospheric gases physically adsorbed on the surface of the sponge are not dissolved in titanium. Therefore, during further metallurgical processing, in conditions of high temperatures and vacuum, they are removed by a vacuum system. In the case of remelting of spongy titanium electrodes under conditions of excess pressure, residual moisture can cause an increased content of hydrogen and oxygen in titanium.

The authors of works [6, 7] also point to the possibility of grinding the microstructure of ingots melted by vacuum ESR. This effect is explained by a more uniform temperature distribution in the molten slag pool, alignment of the crystallization front, and an

increase in the local rate of solidification caused by the intensification of the hydrodynamic flows of the slag as a result of the evaporation of fluorides and the emission of CO.

In view of the above, it is of some interest to study the process of ESR of titanium under vacuum conditions. Vacuum ESR can combine the advantages of ESR and VAR processes, in particular, to ensure high quality of the ingot surface formation, dense and homogeneous metal structure, reliable gas protection and hydrogen removal.

The aim of this work was to study the technological features of the ESR process of titanium under vacuum conditions, to determine its effect on the gas composition and features of the structure formation of the ingot metal.

EXPERIMENTAL PROCEDURE

Experimental studies were carried out in the equipment for chamber ESR of highly reactive materials developed in the E.O. Paton Electric Welding Institute (Figure 1). The installation is equipped with a chamber that ensures complete sealing of the melting space, a vacuum system, an inert gas supply system and pressure monitoring devices. The installation allows the remelting process both under conditions of excess pressure up to 500 kPa, and under conditions of vacuum, when melting ingots with a diameter from 60 to 260 mm.

Experimental melting was performed by remelting pressed consumable electrodes with a diameter of 50 and 75 mm under fluoride-chloride AN-T4 flux, in copper water-cooled moulds with a diameter of 85 and 105 mm. Electrodes of two compositions were used: made of spongy titanium TG 110, for titanium VT1-0 (commercially pure titanium); made of spongy titanium TG 130 and K-5-1 master alloy (TU 48-4-306–88) for VT22 alloy (Ti–5Al–5V–5Mo–1Fe–1Cr, wt.%). Before melting, the melting space was evacuated to a pressure of 2.6 Pa ($2 \cdot 10^{-2}$ mm Hg), then filled with argon. Experiments were performed at different values of argon pressure, from a vacuum of 20 kPa to an excess pressure of 300 kPa. Acceptable pressure values were chosen taking into account the results of work [8].

According to the results of the experiments, the stability of the electroslag process was evaluated, the gas composition and features of the structure formation of the ingot metal were investigated. The gas composition was determined by the method of reductive melting of samples in a flow of inert carrier gas [9]. For this purpose, samples of a cylindrical shape with a diameter of 3 mm and a length of 3 mm (type MI-99) were produced.

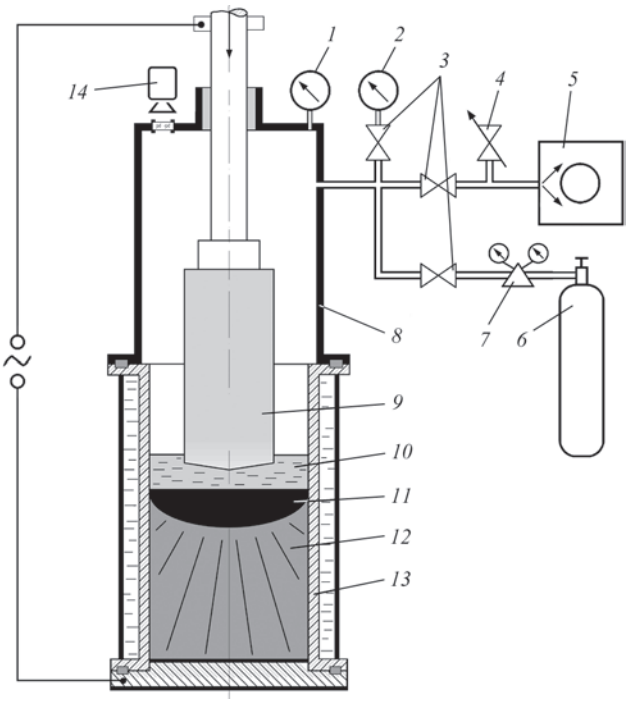

Figure 1. Schematic of the experimental installation for the ESR in a vacuum condition: *1* — vacuum/pressure gauge; *2* — ionization vacuum gauge; *3* — vacuum valves; *4* — inlet valve; *5* — vacuum pump; *6* — argon cylinder; *7* — pressure regulator with rotameter; *8* — furnace chamber; *9* — consumable electrode; *10* — slag pool; *11* — metal pool; *12* — ingot; *13* — water-cooled mould; *14* — camcorder

RESULTS AND DISCUSSION

The results of the experiments are presented in the Table 1 and in Figures 2–7. In the entire studied range of pressures, from vacuum to excess pressure, the electroslag process was stable. This confirms the results of research presented in [8], where acceptable ranges of low pressure were established when using AN-T4 flux.

The melted ingots had a good quality of side surface formation. For comparison, Figure 2 shows the appearance of VT1-0 ingots obtained at pressures of 25 and 160 kPa. When melting under vacuum conditions, the side surface turned out to be a little rougher (Figure 2, *a*) than under excess pressure (Figure 2, *b*). This can be

Table 1. The gas composition of titanium ingots obtained by ESR at different pressures in the melting space, wt.%

Alloy	Pressure, kPa	Content weight, %		
		[O]	[N]	[H]
VT1-0	25	0.074	0.0060	0.0034
	160	0.070	0.0056	0.0052
VT22	25	0.13	0.015	0.0052
	50	0.14	0.027	0.0053
	75	0.09	0.022	0.0065
	100	0.14	0.020	0.0076
	150	0.14	0.025	0.0068
	200	0.14	0.027	0.0064
	250	0.13	0.014	0.0070
	300	0.13	0.015	0.0064

Figure 2. VT1-0 titanium ingots melted at a pressure of 25 kPa (*a*) and 160 kPa (*b*)

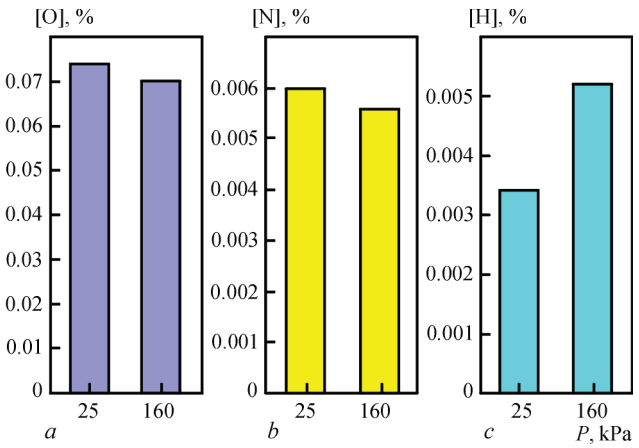

Figure 3. The content of oxygen (*a*), nitrogen (*b*) and hydrogen (*c*) in VT1-0 titanium ingots, depending on the inert gas pressure in the melting space of the ESR furnace

explained by an increase in the hydrodynamic activity of slag and metal pools during melting in a vacuum, which, in turn, leads to a periodic change in the thickness of the slag skull on the surface of the ingot. However, in both cases no surface defects were found.

The results of gas analysis of the ingots metal are given in Table 1 and in Figures 3, 4. The analysis of the obtained data indicates the absence of a clear regularity regarding the effect of pressure on the content of oxygen and nitrogen in the metal of ingots. In VT1-0 titanium ingots, a slight (by 5–7 %) increase in the content of oxygen and nitrogen was observed in the metal melted under vacuum conditions (25 kPa) compared to the metal obtained under excess pressure (160 kPa) (Figure 3 *a*, *b*). However, the difference in the content of elements is within the measurement error, which does not give grounds to assert a certain regularity.

The absence of regularity in the effect of pressure (in the studied range of 25–300 kPa) on the content of oxygen and nitrogen was also observed during the smelting of the VT22 alloy. In this case, the oxygen and nitrogen content in the experiments ranged from 0.09 to 0.14 and 0.014 to 0.027 %, respectively, without increasing or decreasing trends (Figure 4 *a*, *b*). Obviously, such results are related to various random factors that influenced the obtained data (measurement errors, impossibility to maintain absolutely identical conditions for different experimental melting, etc.). This suggests the need for further statistical supplementation of the obtained results. Nevertheless, it can be stated that in the studied range, the pressure level in the melting space has no effect on the content of oxygen and nitrogen in titanium ingots.

As for the hydrogen content, a certain regularity was established in this case, both for ingots of commercially pure VT1-0 titanium and for ingots of titanium VT22 alloy. It manifests itself in a decrease in the presence of hydrogen when conducting the ESR process under vacuum conditions (Figures 3, *c*, 4, *c*). When smelting VT1-0 ingots, a decrease in the pressure in the melting space from 160 to 25 kPa led to a decrease in the hydrogen content in the metal from 0.0052 to 0.0034 wt.%., i.e. by 35 %. Similar results were obtained for VT22 alloy ingots. When the pressure decreased from 100–300 kPa (overpressure range) to 25 kPa, there was a regular decrease in the hydrogen content in the ingot metal from 0.0064–0.0076 to 0.0052 wt.% (by 25 % on average).

Thus, the data obtained give grounds to assert that it is possible to reduce the hydrogen content in titanium alloys by 20–35 % by carrying out the ESR process under vacuum conditions (20–25 kPa).

Figure 5 shows the cross-sectional macrostructures of VT1-0 titanium ingots obtained by ESR at an inert gas pressure in the melting space of 25 and

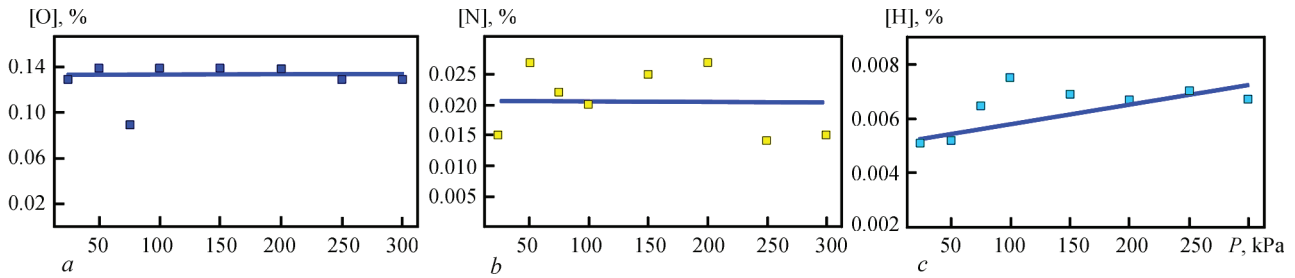

Figure 4. The content of oxygen (*a*), nitrogen (*b*) and hydrogen (*c*) in ingots of the VT22 alloy, depending on the inert gas pressure in the melting space of the ESR furnace

160 kPa. In both cases, the metal structure is dense, without pores, non-metallic inclusions and other internal defects.

Figures 6–7 present the results of metal macrostructure analysis using the MIPAR software. The average grain size (equivalent diameter) in the ingot melted at a pressure of 25 kPa was 2.07 mm, and at 160 kPa – 1.26 mm. That is, the ingot smelted under excess pressure had a finer-grained structure than the ingot smelted in a vacuum. On the one hand, this coincides with the data given in [10], where it is noted that the ingots of ESR under pressure have a more dispersed structure, compared to the ingots of traditional ESR. On the other hand, it contradicts the data of the work [6], where the grain grinding of ESR ingots melted under vacuum conditions was found.

The effect of excessive pressure on the nature of structure formation can be explained by known factors: an increase in the degree of supercooling and the crystallization rate, a decrease in the size and more uniform formation of crystal nuclei, a decrease in the energy of interphase interaction at the melt-crystal interface, etc. [11].

In our case, the influence of pressure on the formation of the structure of ingots can also be explained by its influence on the modes of ESR. Thus, it was shown in [8] that a decrease in the pressure in the melting space below the atmospheric pressure leads to a decrease in the melting current. In turn, this causes a decrease in heat generation in the slag pool (without a forced increase in the melting current due to the electrode feed rate), which affects the nature of metal structure formation, the local rate of hardening and the size of the grains of the cast metal.

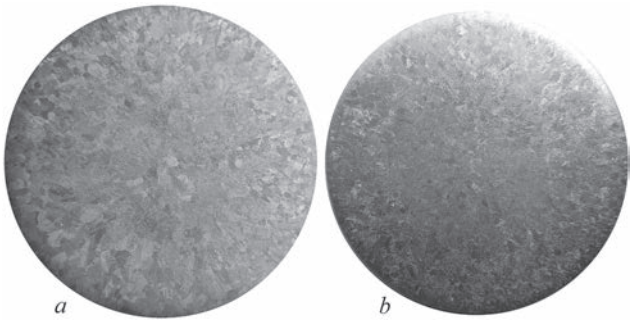

Figure 5. Macrostructure of the cross-section of titanium ingots with a diameter of 80 mm, obtained by ESR at an inert gas pressure of 25 (*a*) and 160 kPa (*b*)

Figure 7 shows the microstructure of VT1-0 titanium ingots obtained at different pressure values. Defects in the form of microporosity, cracks, non-metallic inclusions were not detected. The metal is char-

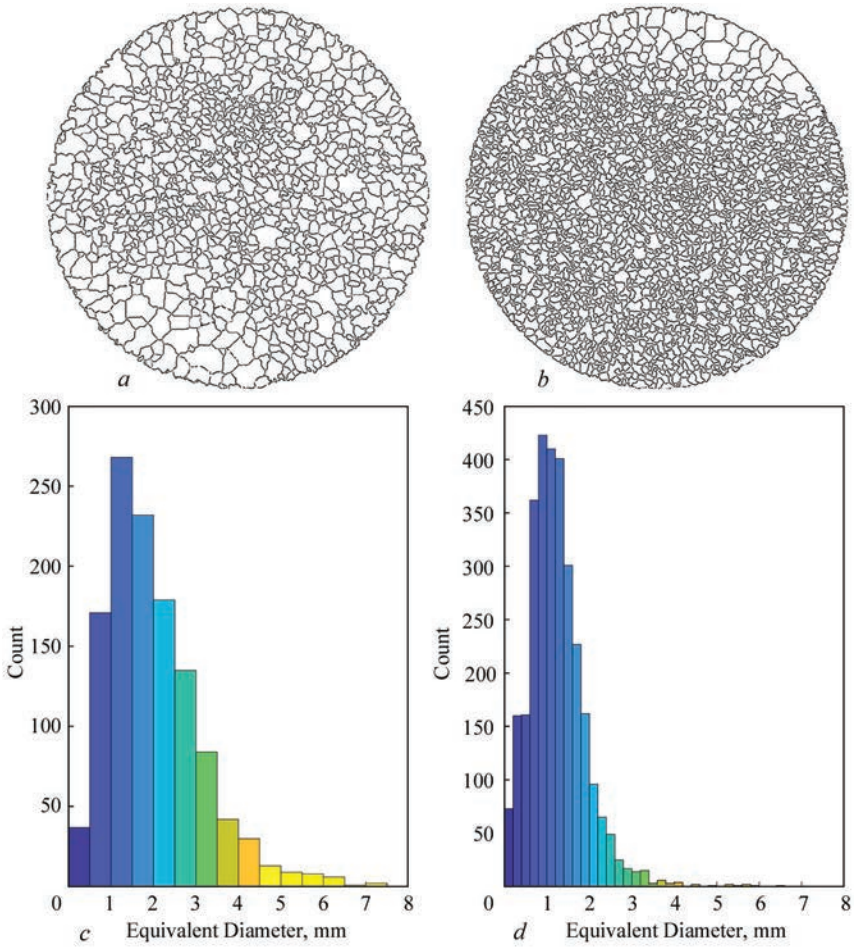

Figure 6. Grain structure (*a*, *b*) and grain size distribution (*c*, *d*) in VT1-0 ingots obtained at pressure: *a*, *c* — 25 kPa; *b*, *d* — 160 kPa

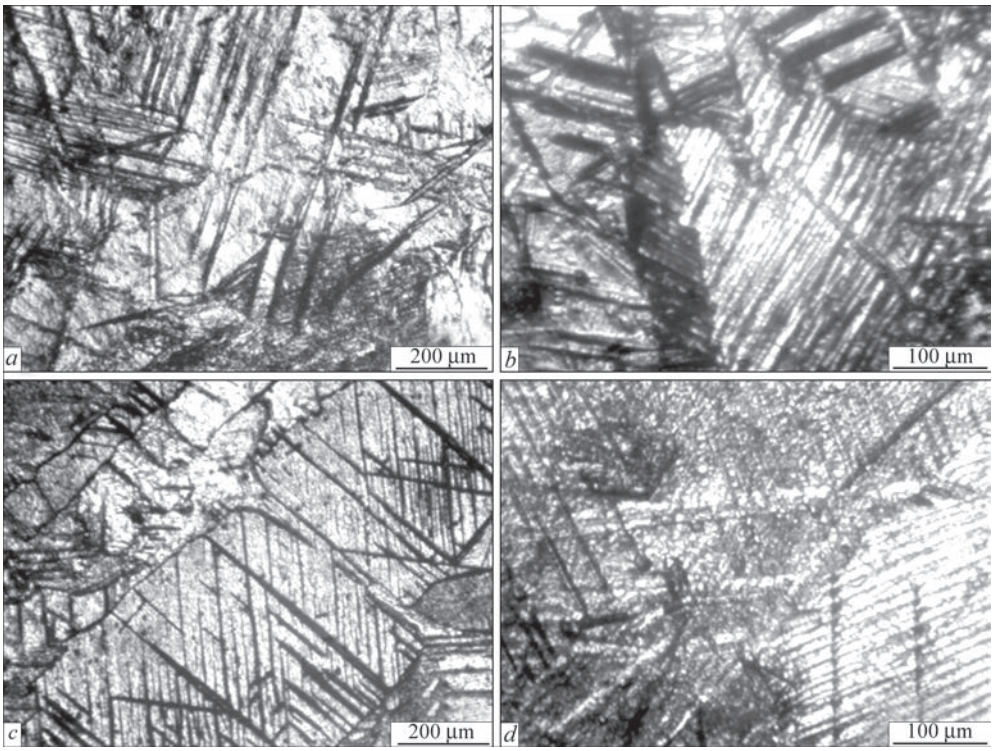

Figure 7. Microstructure of the titanium ingots, obtained by ESR at an inert gas pressure of 25 (*a*, *b*) and 160 kPa (*c*, *d*)

acterized by a coarse lamellar (acicular) structure with a disoriented intra-grain structure. The thickness of α-plates is on average 8–15 μm. This structure is typical for titanium in the cast state and is formed due to high overheating of the melt and low crystallization rates. Fundamental differences in the microstructure of ingots obtained under vacuum conditions (25 kPa) and under excess pressure (160 kPa) were not found.

CONCLUSIONS

1. Ingots of titanium alloys VT1-0 and VT22 were obtained by the ESR method in a chamber-type furnace at different values of pressure in the melting space, from vacuum to excess pressure. It is shown that in the entire investigated pressure range of 20–300 kPa, the electroslag process was stable with the formation of ingots with a high-quality side surface and a dense structure, without pores, slag inclusions and other internal defects.

2. Experimental data on the influence of the pressure in the melting space of the ESR furnace in the range of 20–300 kPa on the gas composition of titanium ingots were obtained. The possibility of reducing the hydrogen content in titanium alloys by 20–35 % by carrying out the ESR process under vacuum conditions (20–25 kPa) has been established. At the same time, a regular influence of the pressure in the melting space on the content of oxygen and nitrogen in titanium ingots in the investigated range was not found.

3. It was established that the VT1-0 titanium ingot, melted under vacuum conditions of 25 kPa, is characterized by a larger grain size compared to the ingot obtained at an excess pressure of 160 kPa. At the same time, the average equivalent diameter of the grains was 2.07 mm and 1.26 mm, respectively.

REFERENCES

1. Protokovilov, I.V., Petrov, D.A., Porokhonko, V.B., Nazarchuk, A.T. (2018) Technological and metallurgical peculiarities of melting of titanium alloy ingots in chamber-type electroslag furnaces. *Suchasna Elektrometal.*, **2**, 45–51 [in Russian]. DOI: http://dx.doi.org/10.15407/sem2018.02.06.
2. Kompan, Y.Y., Protokovilov, I.V. (2002) Some technological aspects of magnetically-impelled electroslag melting (MEM) of titanium alloys. In: *Proc. of Int. Conf. on Special Metallurgy: Yesterday, Today, Tomorrow (8–9 October 2002, Kyiv)*, 256–262 [in Russian].
3. Protokovilov, I.V., Porokhonko, V.B. (2014) Methods to control metal solidification in ESR. *Sovrem. Elektrometall.*, **3**, 7–15 [in Russian].
4. Anoshkin, N.F., Glazunov, S.G., Morozov, E.I., Tetyukhin, V.V. (1978) *Melting and casting of titanium alloys*. Ed. by V.I. Dobatkin. Moscow, Metallurgiya [in Russian].
5. Paton, B.E., Trigub, N.P., Kozlitin, D.A. et al. (1997) *Electron beam melting*. Kyiv, Naukova Dumka [in Russian].
6. Yu, Liu, Xijie, Wang, Guangqiang, Li et al. (2020) Cleanliness improvement and microstructure refinement of ingot processed by vacuum electroslag remelting. *J. of Materials Research and Technology*, 9(**2**), 1619–1630. DOI: https://doi.org/10.1016/j.jmrt.2019.11.087
7. Yu, Liu, Xijie, Wang, Guangqiang, Li et al. (2018) Role of vacuum on cleanliness improvement of steel during electroslag remelting. *Vacuum*, **154**, 351–358. DOI: https://doi.org/10.1016/j.vacuum.2018.05.032
8. Protokovilov, I.V., Petrov, D.A., Porokhonko, V.B. (2020) Investigation of the technological features and admissible pressures of the process of vacuum ESR. *Suchasna Elektro-*

metal. **2**, 3–9 [in Russian]. DOI: https://doi.org/10.37434/sem2020.02.01
9. Kalyniuk, N. (2014) Arrangement of the process for titanium alloys analysis on content of oxygen, nitrogen, hydrogen and carbon impurities. *Metrologiya ta Prylady*, **2**, 50–57 [in Russian].
10. Rashev, Ts. (1995) *High-nitrogen steels. Metallurgy under pressure*. Sofia. Publ. House of the Bulgarian Academy of Sci. [in Russian].
11. Batyshev, A.I. (1990) *Crystallization of metals and alloys under pressure*. 2nd ed. Moscow, Metallurgiya [in Russian].

ORCID
I.V. Protokovilov: 0000-0002-5926-4049
T. Beinerts: 0000-0001-7616-0025
V.B. Porokhonko: 0000-0002-6490-7221
D.A. Petrov: 0000-0003-2937-9299

CONFLICT OF INTEREST
The Authors declare no conflict of interest

CORRESPONDING AUTHOR
I.V. Protokovilov
E.O. Paton Electric Welding Institute of the NASU
11 Kazymyr Malevych Str., 03150, Kyiv, Ukraine.
E-mail: lab38@paton.kiev.ua

SUGGESTED CITATION
I.V. Protokovilov, T. Beinerts, V.B. Porokhonko, D.A. Petrov (2024) Electroslag remelting of titanium under vacuum conditions. *The Paton Welding J*., **3**, 40–45.

JOURNAL HOME PAGE
https://patonpublishinghouse.com/eng/journals/tpwj
Received: 09.01.2024
Received in revised form: 14.02.2024
Accepted: 03.04.2024

DOI: https://doi.org/10.37434/tpwj2024.03.07

RESEARCH OF THE RESIDUAL MAGNETIZATION OF STEEL STRUCTURES AFTER LOCAL MAGNETIZATION WITH AN ATTACHABLE MAGNETIC TRANSDUCER

V.M. Uchanin[1], **S.M. Minakov**[2], **R.M. Solomakha**[3]

[1]G.V. Karpenko Physico-Mechanical Institute of the NASU
5 Naukova Str., 79060, Lviv, Ukraine
[2]National Technical University of Ukraine "Igor Sikorsky Kyiv Polytechnic Institute"
37 Prospect Beresteiskyi (former Peremohy), 03056, Kyiv, Ukraine
[3]CM DIAGNOSTICS sp. z o.o., ul. Przemiarki 23, lokal 8, Krakow, Poland

ABSTRACT

The general problem of residual magnetization of steel products and a typical case of its formation after cyclic magnetization by an attachable type magnetic transducer in the process of magnetic structural analysis by hysteresis loop parameters determination is highlighted. The importance of reliable assessment of residual magnetization, including for quality control of demagnetization of steel products, is emphasized. The method of determining the residual magnetization and evaluating the quality of the demagnetization procedures of steel products by measuring the residual magnetic field is presented. Residual magnetization of 09G2C type steel specimen after hysteresis loop parameters measuring using a magnetic analyzer of the KRM-Ts-MA type, depending on the number of magnetization cycles and its distribution in the area of application of the attachable type magnetic transducer was investigated. It is shown that after multiple magnetization the level of residual induction in 09G2C type steel products does not exceed 0.75 mT, which allows welding without additional demagnetization operations. The tasks of further research on the influence of residual magnetization of steel products made of different steels on their further use and the formation of additional noise during eddy current testing are formulated. It was shown that the presence of residual magnetization after multiple measurements of hysteresis loop parameters does not affect the accuracy of their repeated measurement, which confirmed the stability of the measurement procedure with a KRM-Ts-MA type magnetic analyzer with respect to the residual magnetization created by it.

KEYWORDS: residual magnetization, magnetic structural analysis, attachable magnetic transducer, parameters of the magnetic hysteresis loop, demagnetization

INTRODUCTION. STATE OF THE PROBLEM

Magnetization, including to the technical saturation state, is often used during performance of magnetic and eddy current testing of structures from ferromagnetic materials. After termination of the external magnetic field, the material preserves a certain state of magnetization, which is characterized as residual magnetization. In engineering the term "residual magnetic induction" is sometimes used, although at closer consideration these characteristics differ by a magnetic constant. Residual magnetization depends both on the material magnetic properties and on the previous impact of the magnetic field on it. Moreover, residual magnetization of the products essentially depends on their shape, because of the action of the demagnetization factor, as well as on the impact of mechanical stresses and strains. Therefore, the respective changes in the residual magnetic field on the surface of the object of inspection from ferromagnetic steels are used for their diagnostics [1].

The inadmissibly high level of residual magnetization forms, in particular, after conducting magnetic particle inspection, which necessitates performance of additional demagnetization operations [2, 3]. The need for demagnetization is especially urgent for parts and elements of structures from alloyed steels, characterized by a high remanence level. For this reason, all the instructions on magnetic particle inspection envisage performance of mandatory demagnetization operations. Residual magnetization of a local zone of steel structures can also be the result of cyclic magnetization up to the state of technical saturation by attachable magnetic transducers (MT) during performance of magnetic structural analysis based on measurements of the parameters of magnetic hysteresis loop (MHL) [4–8]. This has not been given enough attention for a long time, and the level of residual magnetization after magnetic structuroscopy has not been studied.

The high level of residual magnetization has a negative effect on the welded structure quality, because of violation of optimal welding conditions. The welding arc instability and its deviations often are the cause of porosity and lacks-of-penetration, which may significantly limit the possibility of welding application in technological processes. It is known that the level

of the magnetic field at the pipe edges after magnetic flaw detection reaches 25 mT. This level, however, can rise significantly (up to 120 mT) after abutment of the pipe edges for subsequent welding. Here, the level of the residual magnetic field in the welding gap, at which sound welding can be performed, cannot exceed 6–8 mT. However, it is better when the magnetic field at the pipe edges does not exceed 1.5 mT, which requires high quality and controlled demagnetization [9]. Moreover, residual magnetization influences the machining quality, because of chips sticking.

Depending on the part shape and dimensions, demagnetization can be performed by such most common methods:

- moving the part through the solenoid, to which alternating current is supplied, and removing it to a distance equal to five solenoid diameters (diagonals);
- reducing to zero the alternating current in the solenoid with the demagnetized part placed into it (solenoid length here should be greater than the part length);
- removing the part from the electric magnet, to which alternating current is supplied (or removing the electric magnet from the part);
- reducing to zero the alternating current in the electric magnet, in the interpolar zone of which the demagnetized part region is located.

Leading companies propose special devices for demagnetization of ferromagnetic products. In particular, a device for demagnetization of rods and pipes of EMAG M type (manufacturer is Institut Dr. Foerster GmbH, Germany) uses feed-through coils, powered by an alternating magnetic field of industrial frequency, which limits the possibility of demagnetization of products of the diameter and wall thickness of more than 30 and 5 mm, respectively [10]. A demagnetization device EMAG F, which ensures demagnetization of rods of more than 240 mm diameter and pipes with more than 25 mm wall thickness, has better characteristics. This device uses a solenoid with two demagnetization coils, where the frequency of the alternating magnetic field is regulated in the range of 5–100 Hz [10]. Known is a series of publications, dealing with development of improved methods of demagnetization of ferromagnetic assemblies and structures [9, 11–14]. Here, a low-informative method is often recommended to control the demagnetization quality, using small ferromagnetic parts [3]. More reliable are the procedures of demagnetization quality control, when the instruments for magnetic field measurement are used to conduct quantitative analysis of the residual magnetic field on the structure surface [9, 11].

The **objective** of the work is analyzing the influence of magnetization during performance of magnetic structural analysis by attachable MT on residual magnetization of the specimens and accuracy of magnetic parameter measurement.

EXPERIMENTAL PROCEDURE, SPECIMENS AND RESEARCH EQUIPMENT

Residual magnetization in the specimen local zone was created using a П-shaped magnetization system of the attachable MT from the set of magnetic analyzer KRM-Ts-MA (Figure 1, *a*), developed by SPF "Spetsialni naukovi rozrobky" (Kharkiv) [4–7]. Attachable MT with the generalized circuit of the magnetic analyzer is shown in Figure 1, *b*.

Experimental specimens of 460.0×60.0×4.00 mm size (Figure 1, *a*) were produced in the form of plates from low-carbon steel of 09G2S type (German analogs are 13MN6 or 9MnSi5), chemical composition of which corresponds to DSTU 8541:2015 (%): ≤0.12 C; 0.5–0.8 Si; 1.3–1.7 Mn; ≤0.3 Ni; ≤0.04 S; ≤0.035 P; ≤0.3 Cr; ≤0.12 N; ≤0.12 Cu. The studied steel is widely used, in particular, in production of pipes for oil and gas transportation.

Measurement of the vertical component of the residual magnetic field on the specimen surface was conducted, using a universal milliteslameter of MTU-1 type (SPF "Spetsialni naukovi rozrobky") with magnetically sensitive transducer based on Hall sensor (Figure 1, *c*), which ensures magnetic field measurement with 3 % error at measurement limit of 20 mT.

To create residual magnetization, magnetic analyzer MT was installed on the specimen surface. After that, 15 cycles of MHL parameter measurement were conducted. Evaluation of residual magnetization of the specimens was performed by measurement of residual magnetic field H_r on the specimen surface after 1, 3, 6, 8, 12 and 15 cycles of measurement in 5 zones of the specimen relative to poles of the П-shaped magnetization system of attachable MT (Figure 2, *a*), where: MT center and pole centers are designated by letters *A*, *B* and *C*, respectively, and side zones are designated by letters *E*, *D*. Measurement of the distribution of vertical component of residual magnetic field H_r on the specimen surface was conducted by the scheme as in Figure 2, *b*. Dotted lines in Figure 2 designate the places of MT pole mounting. After 15 cycles of MHL parameter measurement, specimen demagnetization was conducted by slowly moving it into the demagnetization coil and its subsequent removal. The demagnetization coil is made in the form of 560 turns of enamel wire of 0.95 mm diameter, with outer and inner diameter of 200 and 170 mm, respectively, and 46 mm height. Resistance of demagnetization coil at direct current is equal to 9 Ohms. Demagnetization

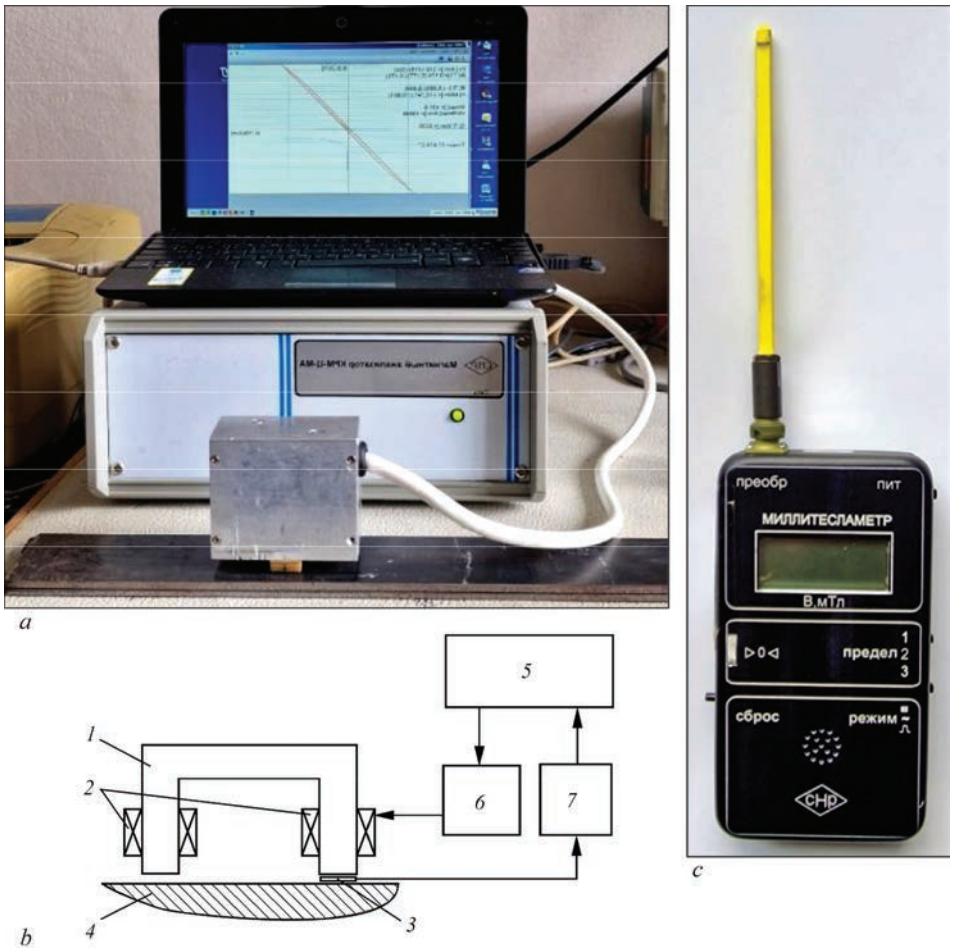

Figure 1. Magnetic analyzer of KRM-Ts-MA type with attachable MT on the studied specimen (*a*), design of attachable MT with the generalized diagram of magnetic analyzer (*b*), all-purpose milliteslameter of MTU-1 type (*c*); *1* — П-shaped core; *2* — magnetization reversal windings; *3* — Hall sensor for magnetic flux measurement in the magnetic circuit; *4* — object of control; *5* — circuit of control, measurement and indication; *6* — circuit of generation of currents of attachable MT winding; *7* — circuit of magnetic flux measurement

coil was connected to standard 220 V network, which created a demagnetization alternating electromagnetic field of 50 Hz 34.5 mT magnitude in its center.

Moreover, to determine the influence of residual magnetization on measurement accuracy, MHL parameter measurement was also performed after the measurement cycles without shifting the MT position on the specimen. Obtained values were compared with the values of the specimen coercive force in as-delivered condition and after demagnetization.

RESULT ANALYSIS

Dependence of residual magnetic field H_r on the specimen surface in zones *A* (×), *B* (●), *C* (○), *D* (▲) and *E* (▼) of MT application (Figure 2, *a*) on the number of measurement cycles *N* is given in Figure 3, *a*. One can see that residual magnetic field H_r on the specimen surface in the central and lateral zones of MP application is close to zero, which was anticipated, taking into account the zero value of the vertical component of primary magnetic field in these zones. The

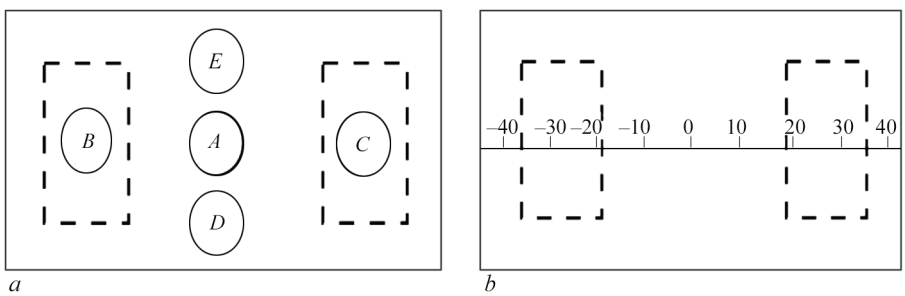

Figure 2. Zones of measurement of residual magnetic induction in MT action zone (*a*) and schemes of measurement of residual magnetic induction distribution

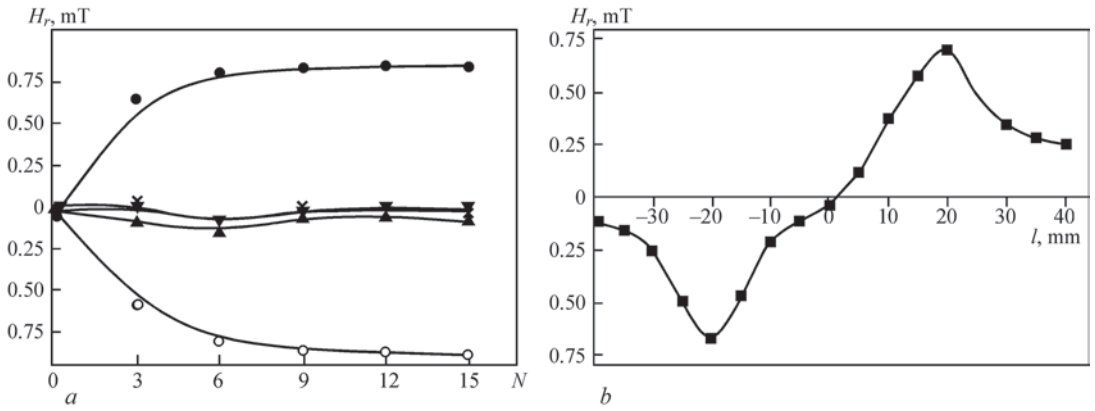

Figure 3. Changes of vertical component of residual magnetic field H_r in the zone of MT action, depending on the number of magnetization cycles in zones *A* (×), *B* (●), *C* (○), *D* (▲) and *E* (▼) (*a*) and its distribution in the zone of MT action after 3 measurement cycles (*b*)

values of the vertical component of residual magnetic induction H_r of the specimen in the centers of location of MT poles (zones *B* and *C*) are of different sign and they grow gradually with increase of the number of measurement cycles *N*. However, already after 6 measurement cycles residual magnetic field H_r on the specimen surface becomes close to the maximal value, and furtheron it practically does not change with increase of the number of measurement cycles ($N > 9$).

Distribution of the vertical component of residual magnetic field H_r after 3 measurement cycles (Figure 3, *b*) shows the presence of two maximums of different sign, which correspond to the centers of MT magnetic pole location. Here, even at multiple magnetization, the level of residual magnetic field H_r in specimens of steel of 09G2s type does not exceed 0.75 mT, which allows welding structures from this steel without conducting additional demagnetization operations, when the level of the residual magnetic field below 1.5 mT is believed to be optimal [9]. This, however, does not mean that such a conclusion can be made as regards other steels, particularly those, which are characterized by higher coercive force values. More over, it does not mean that even such a low level of residual magnetic field will not affect further performance of the steel products, for instance because of metal chips sticking, or it will not create significant noise, which often limits the possibility of application of eddy current flaw detection of ferromagnetic steels without stabilizing magnetization [15]. Thus, additional studies in these areas are also relevant.

Results of repeated measurements of MHL parameters of specimens with different residual magnetization showed that it did not affect the measurement accuracy which confirmed the stability of the procedure of measurements by magnetic analyzer of KRM-Ts-MA type. At the same time, it should be noted that the induced level of residual magnetization can have a more significant influence on the results of dynamic MHL parameter measurement by local MT, where significantly smaller values of primary magnetic field are used [16].

If it is necessary to reduce the residual magnetization after conducting magnetic structural analysis, we proposed complementing the cycle of MHL parameter measurement by an additional operation of demagnetization, using a series of pulses of different polarity alternating magnetic field, where the amplitude decays to a zero value (Uchanin V.M., Solomakha R.M. Method for determination of the magnetic and mechanical characteristics of ferromagnetic materials and monitoring the technical state of structures. Patent of Ukraine No. 154135. Publ. 11.10.2023, Bul. 41). To reduce the error of MHL parameter measurement, it is also proposed to apply alternating magnetic field pulses to the control zone, before conducting the measurement cycle of magnetization. Pulses of different polarity alternating magnetic field, the amplitude of which decays to zero, can be generated by windings of the electric magnet of П-shaped MT, used to realize the cycle of MHL parameter measurement.

CONCLUSIONS

1. The general problem of residual magnetization of steel products and the characteristic case of its formation after cyclic magnetization by an attachable MT during magnetic structural analysis by MHL parameters is highlighted. The importance of reliable evaluation of residual magnetization is emphasized, in particular for quality control of demagnetization of steel products. A procedure is presented for determination of residual magnetization and evaluation of the quality of the procedures of steel product demagnetization by measurement of the residual magnetic field.

2. Residual magnetization of specimens from steel of 09G2S type was studied after conducting measurements of MHL parameters, using a magnetic analyzer

of KRM-Ts-MA type, depending on the quantity of magnetization cycles and its distribution in the zone of application of an attachable MT. It is shown that at multiple magnetization the residual induction level in the products from steel of 09G2S type is not higher than 0.75 mT, that allows performance of welding without conducting the additional demagnetization operations.

3. The tasks of further studies on the influence of residual magnetization of steel products from different steels on their further application and generation of additional noise during performance of eddy current testing are formulated.

4. It is shown that presence of residual magnetization after multiple measurements of MHL parameters does not influence the accuracy of their repeated measurement, which confirmed the stability of the procedure of measurement by magnetic analyzer of KRM-Ts-MA type as to residual magnetization generated by it.

REFERENCES

1. Roskosz, M, Bieniek, M. (2012) Evaluation of residual stress in ferromagnetic steels based on residual magnetic field measurements. *NDT& E International*, 45(**1**), 55–62. DOI: https://doi.org/10.1016/j.ndteint.2011.09.007
2. Ostash, O.P., Fedirko, V.M. (2007) *Fracture mechanics and strength of materials*: Refer. Book, Vol. 9*: Strength and service life of aircraft materials and structure elements.* Lviv, Spolom [in Ukrainian].
3. Kuts, Yu., Protasov, A., Tsapenko, V. et al. (2012) *Magnetic non-destructive testing.* Kyiv, NTUU KhPI [in Ukrainian].
4. Bezlyudko, G. (2003) Operational control of fatigue condition and residual life of metal structures by nondestructive (coercimetric) method. *Tekh. Diagnost. i Nerazrush. Kontrol,* **2**, 20–26 [in Russian].
5. Lobanov, L.M., Bondarenko, A.Yu., Bondarenko, Yu.K. (2004) Evaluation of welded joints of structures by magnetic (coercimetric) for forecasting individual residual life. *Tekh. Diagnost. i Nerazrush. Kontrol,* **1**, 3–8 [in Russian].
6. Bezlyudko, G.Ya. (2004) Practical evaluation of the condition of welds by measuring the magnetic characteristic — coercive force of the metal. *Tekh. Diagnost. i Nerazrush. Kontrol,* **1**, 20–22 [in Russian].
7. Uchanin, V., Ostash, O., Nardoni, G., Solomakha, R. (2020) *Coercive Force Measurements for Structural Health Monitoring, The Fundamentals of Structural Integrity and Failure* (Ed. R.M. Wilcox), Nova Science Publishers, New York, USA, 163–192.
8. Rybachuk, V.G., Uchanin, V.M. (2021) Coercive force of two-layer ferromagnetic materials. *Vidbir i Obrobka Informatsii,* 125(**49**), 3–8. DOI: https://doi.org/10.15407/vidbir2021.49.003 [in Ukrainian].
9. Dobrodeev, P.N. (2014) Study of methods of demagnetization of pipe ends in repair of main pipelines. *Elektrotekhnika i Elektromekhanika,* **3**, 50–54 [in Russian].
10. https://www.foerstergroup.com/en/usa/products/emag/
11. Rozov, V., Pilyugina, O., Lupikov, V. et al. (2006) Introduction into demagnetization of technical objects. *Elektrotekhnika i Elektromekhanika,* **4**, 55–59 [in Russian].
12. Volokhov, S.A., Dobrodeyev, P.N., Mamin, G.I. (2012) Integrated demagnetization of pipes in electric arc welding. *Tekhnichna Elektrodynamika,* **4**, 19–24 [in Russian].
13. Oxley, P. (2009) Apparatus for magnetization and efficient demagnetization of soft magnetic materials. *IEEE Transact. on Magnetics*, 45(**9**), 3274–3283.
14. Shelikhov, G.S. (2010) Experience in the demagnetization of large objects. *Rus. J. of Nondestr. Testing*, 46(**5**), 315–323.
15. Deng, Z., Yu, Z., Yuan, Z. et al. (2022) Mechanism of magnetic permeability perturbation in magnetizing-based eddy current nondestructive testing. *Sensors*, **22**, 2503. DOI: https://doi.org/10.3390/s22072503
16. Minakov, S.M., Uchanin, V.M., Minakov, A.M. et al. (2023) Determining the parameters of the dynamic magnetic hysteresis loop of the structural materials by attachable primary transducers. *Vidbir i Obrobka Informatsii,* 127(**51**), 12–18 [in Ukrainian]. DOI: https://doi.org/10.15407/vidbir2023.51.012

ORCID

V.M. Uchanin: 0000-0001-9664-2101,
S.M. Minakov: 0000-0001-8607-4120

CONFLICT OF INTEREST

The Authors declare no conflict of interest

CORRESPONDING AUTHOR

V.M. Uchanin
G.V. Karpenko Physico-Mechanical Institute of the NASU
5 Naukova Str., 79060, Lviv, Ukraine.
E-mail: vuchanin@gmail.com

SUGGESTED CITATION

V.M. Uchanin, S.M. Minakov, R.M. Solomakha (2024) Research of the residual magnetization of steel structures after local magnetization with an attachable magnetic transducer. *The Paton Welding J.*, **3**, 46–50.

JOURNAL HOME PAGE

https://patonpublishinghouse.com/eng/journals/tpwj

Received: 03.01.2024
Received in revised form: 23.02.2024
Accepted: 03.04.2024

SUCCESSFUL CERTIFICATION. DNIPROMETYZ TAS IS PREPARING FOR NEW CHALLENGES

Dniprometyz TAS is a market leader in manufacturing hardware products, specializing in the production of low- and high-carbon wire.

In 2023, the plant produced and sold more than 1,000 tons of welding wire and took one of the leading positions among manufacturers in Ukraine.

During Russian aggression, the Dniprometyz TAS plant continues to develop and increase its production, despite the difficult situation.

The year 2023 for Dniprometyz TAS is a year of significant changes and achievements. The plant is constantly developing, building new production sites to meet the growing demand for its products. The company's export activities are also growing rapidly, which indicates strong competition in international markets.

Projects have been implemented to modernize production, aimed at solving environmental problems, as well as expanding the range of products and increasing production volumes. The production base has been improved by purchasing modern equipment for the production of welding wire from the leading Swedish manufacturer Lämneå Bruk AB. Welding wire is widely used in metal structures, mechanical engineering, carriage building, defense industry and other industries.

The plant's product range includes a wide range of diameters of copper-plated welding wire, as well as uncoated and polished welding wire. The G3Si1 and G4Si1 wire is manufactured according to the international standard EN ISO 14341 (national standard DSTU EN ISO 14341). According to the results of the carried out procedure to confirm the compliance of the welding wire and the weld metal deposited by the method of arc welding in the shielding gas environment with the requirements of DB, the designations of the wire and the weld metal were confirmed: **EN ISO 14341 - A - G 46 4 M21 G3Si1 and EN ISO 14341 - A - G 46 4 M21 G4Si1**. Wire of the G3Si1 and G4Si1 brands occupies a large part in the total production of welding wire. Copper-plated welding wire of a solid section with diameters of 0.8 mm, 1.0, 1.2, 1.4, 1.6, 2.0 mm is produced on cassettes of 15, 5, 2.5, 1 kg with precision winding. The range of welding wire packages now includes 250 kg tubs for robotic welding complexes. This improves productivity and ensures the continuous operation of robotic machinery, as well as reducing wire loss and simplifying the welding process.

Welding wire produced by Dniprometyz TAS has established itself as a reliable and high-quality product used in industrial enterprises. In view of this, the plant has expanded its product line with the most popular brands of electrodes

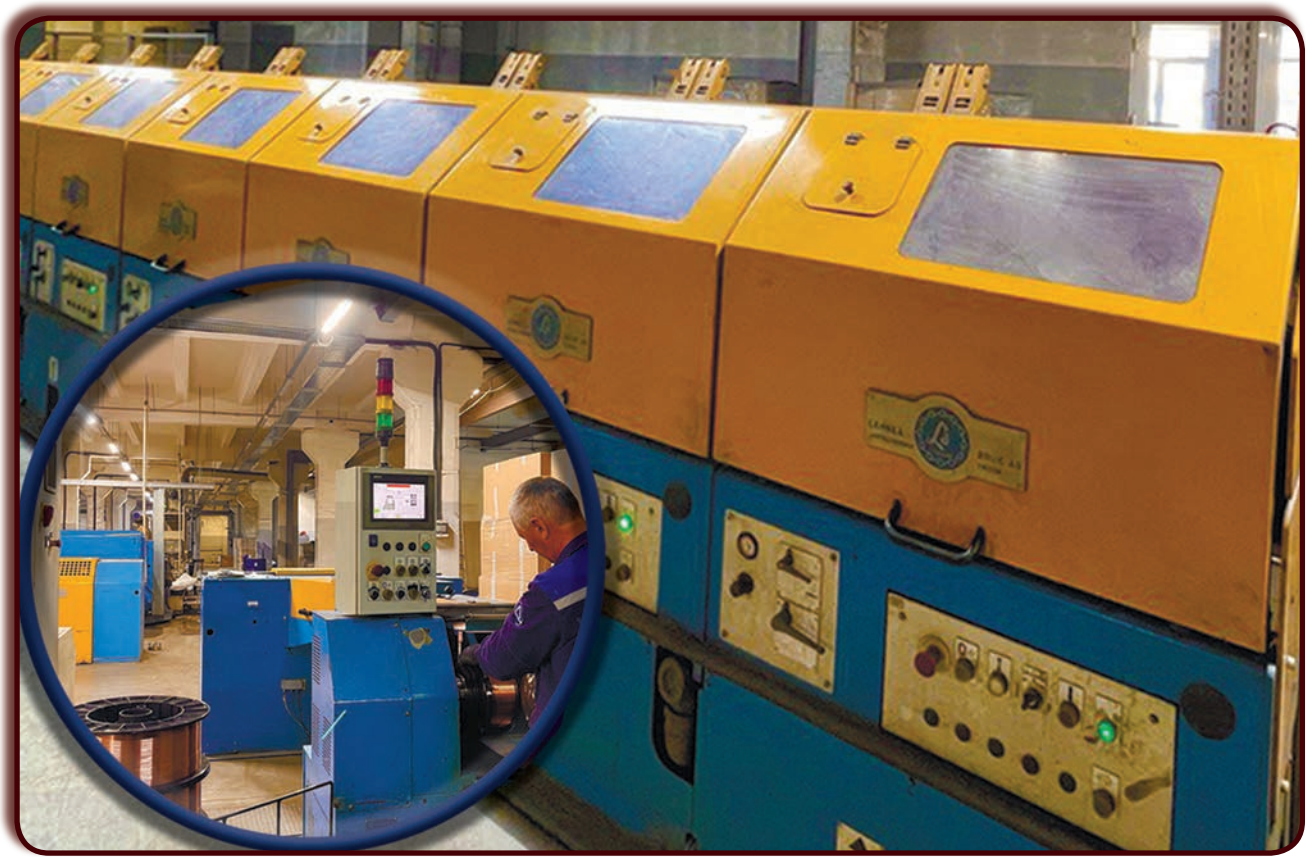

for manual arc welding of structures made of carbon steel grades.

The central factory laboratory Dniprometyz TAS is one of the few that have been accredited and confirmed their technical competence. Based on the research results, the laboratory issues an expert opinion, which is an official document. The laboratory is equipped with instruments and testing equipment for chemical analysis, mechanical tests, as well as welding and technological tests. A modern in-house laboratory guarantees the highest standards at every stage of production. Given the various wire applications, mechanical and process requirements, thorough testing is important to ensure reliability and safety. To effectively study the microstructure and mechanical properties of wire rod and wire, the plant invested in advanced equipment — a ZEISS Axiovert 5 digital inverted microscope and a Micro-Vickers hardness tester. This innovative approach ensures the compliance of products with the highest international standards.

In January 2024, G4Si1 wire produced by Dniprometyz TAS was successfully tested at the E.O. Paton Electric Welding Institute of the NAS of Ukraine and is ready for use in the production and erection of steel bridge structures. After intensive testing, positive results have been obtained indicating high efficiency and excellent quality of the welding wire. The use of G4Si1 wire is very important during the erection of steel bridges, ensuring the strength and reliability of structures. There is no doubt that the Dniprometyz TAS welding wire will help to improve the quality and duration of operation of bridge structures.

Dniprometyz TAS is one of the first Ukrainian manufacturers to successfully pass the certification of welding wire in accordance with the requirements of Deutsche Bahn.

In February 2024, the Dniprometyz TAS plant underwent a factory production audit, which was carried out by qualified specialists from Deutsche Bahn AG. The result of the audit was the completion of qualification tests of copper-bonded alloyed welding wire grades 3Si1 and 4Si1, with a diameter of 0.6–1.6 mm, as well as obtaining a certificate of conformity from Deutsche Bahn.

This certificate opens up wide opportunities for the plant to enter the European market. It confirms that the welding wire produced by Dniprometyz TAS meets the requirements of Deutsche Bahn. The presence of such a certificate is a mandatory condition for participation in tenders of one of the demanding Deutsche Bahn companies, as well as other enterprises in the field of carriage building, locomotive building and mechanical engineering.

Deutsche Bahn is a powerful manufacturer in the field of carriage and locomotive construction, has authority in the field of passenger and freight transportation by rail and road transport in Germany and abroad. As one of the largest transport operators in Europe and the world, Deutsche Bahn is an important player in the field of mobility and has authority and significant influence on the development and forming of the transport sector.

The certified welding wire produced by Dniprometyz TAS has a number of advantages that distinguish it from its competitors:

❖ **Credibility and reliability**. Certification of Deutsche Bahn products confirms their compliance with high European standards of quality and safety. This increases confidence in the products on the part of the company's customers and partners.

❖ **Market access**. Confirmation of product compliance with Deutsche Bahn standards opens access to the field of railway engineering, allowing Dniprometyz TAS to participate in tenders and enter into contracts with Deutsche Bahn and other European railway operators that comply with similar standards.

❖ **Security and compatibility**. The welding wire certified by Deutsche Bahn meets the safety requirements and is compatible with the railway network infrastructure, which is important for ensuring reliable and safe operation of trains.

❖ **Reputation and brand.** Certification of Deutsche Bahn products indicates a high level of quality and compliance with international standards. This strengthens the company's reputation and brand as a reliable and innovative supplier of welding consumables.

The high quality and reliability of welding wire produced by Dniprometyz TAS contributes to its successful competition with the products of European manufacturers in international markets.